SKB

# TECHNICAL REPORT 95-01

## Biotite and chlorite weathering at 25°C

Maria Malmström[1], Steven Banwart[1], Lara Duro[2], Paul Wersin[3], Jordi Bruno[3]

[1] Royal Institute of Technology, Department of Inorganic Chemistry, Stockholm, Sweden

[2] Universidad Politécnica de Cataluña, Departmento de Inginería Química, Barcelona, Spain

[3] MBT Technología Ambiental, Cerdanyola, Spain

January 1995

**SVENSK KÄRNBRÄNSLEHANTERING AB**
*SWEDISH NUCLEAR FUEL AND WASTE MANAGEMENT CO*
BOX 5864 S-102 40 STOCKHOLM
TEL 08-665 28 00 TELEX 13108 SKB
TELEFAX 08-661 57 19

# BIOTITE AND CHLORITE WEATHERING AT 25°C

## THE DEPENDENCE OF pH AND (BI)CARBONATE ON WEATHERING KINETICS, DISSOLUTION STOICHIOMETRY, AND SOLUBILITY; AND THE RELATION TO REDOX CONDITIONS IN GRANITIC AQUIFERS

*Maria Malmström[1], Steven Banwart[1], Lara Duro[2], Paul Wersin[3], Jordi Bruno[3]*

1 **Royal Institute of Technology, Department of Inorganic Chemistry, Stockholm, Sweden**
2 **Universidad Politécnica de Cataluña, Departmento de Inginería Química, Barcelona, Spain**
3 **MBT Tecnología Ambiental, Cerdanyola, Spain**

January 1995

# BIOTITE AND CHLORITE WEATHERING AT 25 °C:

## The dependence of pH and (bi)carbonate on weathering kinetics, dissolution stoichiometry, and solubility; and the relation to redox conditions in granitic aquifers.

Maria Malmström[1], Steven Banwart[1], Lara Duro[2], Paul Wersin[3], Jordi Bruno[3]

[1]Royal Institute of Technology, Department of Inorganic Chemistry, Stockholm, Sweden
[2]Universidad Politécnica de Cataluña, Departmento de Inginería Química, Barcelona, Spain
[3]MBT Tecnología Ambiental, Cerdanyola, Spain

January 1995

Keywords:

Groundwater, Dissolution kinetics, Biotite, Chlorite, Solubility, Clay minerals , Redox potentials, Oxygen reduction, Canister stability

**Abstract** (english)

We have studied the kinetics and thermodynamics of biotite and chlorite weathering in the pH range $2<pH<10$ at 25 °C. The dissolution is highly non-stoichiometric and pH dependent in the whole pH region. By XPD we have identified a clay mineral to be the main weathering product formed. A model of biotite dissolution and the formation of secondary solubility controlling minerals, such as Fe(III)-hydroxide, Na-clay, quartz and gibbsite is used to explain experimental equilibrium concentrations of silicon, iron, aluminium and magnesium. The model predicts redox potentials in the range of -200--400 mV at neutral pH and qualitatively agrees with field data reported in the literature. We use observed iron release rates to make conservative estimates of timescales of 1) the depletion of molecular oxygen from deep aquifers ($10^1$-$10^2$ years); and 2) the development of characteristic Fe(II) concentrations ($10^{-5}$ M in $10^{-1}$ years).

The Fe(II)-bearing clay minerals formed during these experiments are similar to the fracture-filling-material observed at the Äspö Hard Rock Laboratory. Such clays can provide reducing capacity to a repostory. They can help maintain anoxic conditions by consuming oxygen that enters the repository during the construction and operation phases thereby helping maintain the redox stability of the repository regarding canister corrosion. The half-life of oxygen trapped in the repository at the time of closure depends on the rate of oxygen uptake by Fe(II) minerals, sulfide minerals and organic carbon. Fe(II)-caly minerals are important to the redox stability of a repository, as well as providing a sorption barrier to radionuclide migration.

**Abstract** (Swedish).

Vi har studerat jämvikt och kinetik av biotit och klorit vittring i pH intervallet $2<pH<10$ vid 25 °C. Upplösningsreaktionerna är icke-stökiometriska och vittringshastigheten såväl som jämviktskoncentrationerna av kisel, järn, aluminium och magnesium är starkt pH beroende. Vi modellerar jämvikts koncentrationerna med hjälp av lösligheten av sekundära faser såsom ett Fe(II)-lermineral, kvarts och gibbsit. Modellen ger redoxpotentialer mellan -200--400 mV vid neutralt pH vilket överenstämmer med fältstudier. Vi använder data från försöken till att göra konservativa uppsakttningar av tidskalor för 1) omsättning av löst syre ($10^{1}$-$10^{2}$ år); och 2) ackumulering av Fe(II) i djupa grundvatten ($10^{-5}$ M inom $10^{-1}$ år).

De Fe(II)-haltiga lermineral som bildats under dessa försök liknar de sprick mineral som observerats på Äspö Hard Rock Laboratory. Sådana lermineral kan tillföra reducerande buffert kapacitet till ett slutförvar och på detta sätt positivt bidra till slutförvarets kemiska korrosions stabilitet. Halveringstiden för kvarvarande syre då slutförvaret stängs beror av hastigheten av reaktioner mellan syre coh Fe(II)-mineral, sulfidmineral samt organiskt kol. Fe(II)-lermineral är därför viktiga för redox stabiliteten av ett slutförvar och tjänar också som en sorptions barriär mot radionuklid migration.

## Summary and conclusions

During the construction and operation of a deep repository the groundwater system will be open to oxic conditions. There is a concern that, once the repository has been closed, residual molecular oxygen will accelerate canister corrosion and enhance the mobility of redox sensitive radionuclides. The release and oxidation of structural Fe(II) in silicates, such as biotite and chlorite, is one of several processes that will serve to deplete oxygen from the deep aquifer.

We have studied the kinetics and thermodynamics of biotite and chlorite weathering in the pH range $2<pH<10$ at 25 °C. The elemental release rates at a specified condition are highly non-stoichiometric, with preferential release of Fe, Mg and Al at low pH and of Si at higher pH on the time scale of our experiments ($\sim$1 month). We postulate that, due to diffusion through depletion layers, the long-term dissolution will be congruent and limited by the lowest elemental release rate. The Fe, Al, Si and Mg release rates are pH dependent and resemble the behaviour of FeOOH, $Al_2O_3$ and $SiO_2$ respectively. We use a combination of the surface complexation/activated complex theory to model the observed behaviour. The accumulated release of potassium increases parabolically with time suggesting a diffusion controlled release mechanism for potassium. The dissolution rate and stoichiometry are not influenced by (bi)carbonate.

Speciation calculations indicate that equilibrium data of biotite dissolution obtained from batch and titration experiments are best explained by 1) the dissolution of biotite; 2) the formation of secondary solubility controlling minerals (i.e Na-clay, Fe(III)-(hydr) oxide, gibbsite and quartz); and 3) an ion-exchange reaction. This model predicts redox potentials that agree with field data reported in the literature and indicates the importance of Fe(II)-clays for redox potentials in deep groundwaters.

Mössbauer analyses indicate that there is an increase in the Fe(III)/Fe(total) ratio in the mineral phase during biotite weathering. XPD reflections show an expansion, typical for a clay formation, of the mineral structure at $pH>2$ and indicate the formation of kaolinite in some samples below pH 4.6.

In the pH range $2<pH<4$ we measured redox potentials, using redox electrodes, in the range of 350-650 mV. We model these observed redox potentials by the following equilibrium reaction:

$$Fe^{2+} + 3\,H_2O \rightarrow Fe(OH)_3(s) + 3\,H^+ + e^-$$

At higher pH we did not obtain reliable redox potentials due to the very low Fe(total) concentration.

We use observed Fe release rates to make conservative estimates of timescales of 1) the depletion of molecular oxygen from deep aquifers ($10^1$-$10^2$ years); and 2) the development of characteristic Fe(II) concentrations ($10^{-5}$ M in $10^{-1}$ years). We use literature data on $O_2$-consumption by Fe(II)-silicates to estimate the redox capacity ($10^{-5}$-$10^{-4}$ moles/$m^2$) of common granitic minerals.

In the final section we show that there is a optimal redox potential region where the canister is chemically stable towards corrosion by molecular oxygen (to copper oxide) and where sulfate reduction is prevented, thereby stabilizing the copper towards corrosion to copper sulfide. We define redox capacities with respect to these reactions, and conclude that the evaluation of these equations for repositories requires site specific data such as abundance of redox active compounds and flow parameters. We present a conceptual model for evolution of oxidizing capacity with time during the life-time of a repository, and a methodology for estimating the half-life of oxygen in the post-closure period. The model emphasizes the importance of chemical kinetics for depletion of molecular oxygen and other redox reactions.

TABLE OF CONTENTS


| | | |
|---|---|---|
| 1. | INTRODUCTION | 1 |
| 1.1 | BACKGROUND | 1 |
| 1.2 | OBJECTIVES | 1 |
| 1.3 | BIOTITE AND CHLORITE STRUCTURE AND WEATHERING | 3 |
| 1.3.1 | Structure of Biotite and Chlorite | 3 |
| 1.3.2 | Biotite and Chlorite Weathering | 4 |
| 2. | EXPERIMENTAL METHODS AND MINERAL CHARACTERIZATION | 7 |
| 2.1 | MINERAL CHARACTERIZATION AND SAMPLE PREPARATION | 7 |
| 2.1.1 | Mineral Preparation | 7 |
| 2.1.2 | Mineral Characterization | 7 |
| 2.2 | EXPERIMENTAL METHODS | 10 |
| 2.2.1 | Equilibrium Experiments | 11 |
| 2.2.2 | Kinetic Experiments | 13 |
| 3. | RESULTS AND DISCUSSION | 15 |
| 3.1 | RESULTS FROM KINETIC EXPERIMENT | 15 |
| 3.1.1 | Wet Chemistry Results | 15 |
| 3.1.2 | XPD -Results | 22 |
| 3.1.3 | SEM/Micro Probe Results (Biotite) | 24 |
| 3.1.4 | Mössbauer Results | 26 |
| 3.1.5 | Discussion (Biotite) | 26 |
| 3.1.6 | Conclusions | 31 |
| 3.2 | RESULTS FROM EQUILIBRIUM EXPERIMENT | 33 |
| 3.2.1 | Wet-Chemistry Results | 33 |
| 3.2.2 | XPD Results (Biotite) | 37 |
| 3.2.3 | SEM/Micro Probe Analysis | 37 |
| 3.2.4 | Discussion (Biotite) | 40 |
| 3.2.5 | Conclusions | 49 |
| 4. | IMPLICATIONS FOR THE PERFORMANCE OF A DEEP REPOSITORY | 51 |
| 4.1 | TECHNICAL BACKGROUND | 51 |
| 4.2 | CONSUMPTION OF MOLECULAR OXYGEN | 52 |
| 4.2.1 | The Capacity of Minerals for Uptake of Molecular Oxygen | 52 |
| 4.2.2 | Time-Scale for Depletion of Molecular Oxyg3n | 52 |
| 4.3 | ACCUMULATION OF Fe(II) IN SOLUTION | 56 |
| 4.4 | AN EQUILIBRIUM MODEL FOR THE REDOX POTENTIALS IN DEEP GROUND WATERS | 57 |

| | | |
|---|---|---|
| 4.5 | APPLICATION TO THE REDOX BUFFER CAPACITY OF A DEEP REPOSITORY | 58 |
| 4.5.1 | Redox Scales | 58 |
| 4.5.2 | Redox Capacities | 59 |
| 4.5.3 | Conceptual Model for Evolution of Redox Capacity in the Repository | 62 |
| 4.5.4 | A Methodology for Calculating the Half-Life of Dissolved Oxygen in the Closed Repository | 64 |
| 5. | ACKNOWLEDGEMENTS | 66 |
| 6. | REFERENCES | 67 |
| 7. | APPENDIX | 74 |
| 7.1 | APPENDIX: Kinetic data from the biotite-$H_2O$-system | 74 |
| 7.2 | APPENDIX: Kinetic data from the biotite-$H_2O$-$CO_2$(g)-system | 82 |
| 7.3 | APPENDIX: Kinetic data from the chlorite-$H_2O$-$CO_2$(g)-system | 86 |
| 7.4 | APPENDIX: Equilibrium data from the biotite-$H_2O$-system | 91 |
| 7.5 | APPENDIX: Equilibrium data from the biotite-$H_2O$-$CO_2$-system | 93 |
| 7.6 | APPENDIX: Equilibrium data from the chlorite-$H_2O$-$CO_2$(g)-system | 94 |
| 7.7 | APPENDIX: Estimation of solubility-product of phyllosilicates | 95 |
| 7.8 | APPENDIX: Acid-base equilibrium at mineral surfaces | 97 |
| 7.9 | APPENDIX: XPD patterns | 98 |

# 1. INTRODUCTION

## 1.1 BACKGROUND

During the construction and operation of a deep repository the ground water system will be open to surface water inflow and oxic conditions. The presence of molecular oxygen is expected to have adverse effects on the repository safety by a) accelerating canister corrosion; and b) increasing the mobility of redox sensitive radionuclides, which form sparingly soluble (hydr)oxides under reducing conditions but are highly soluble in their higher valence state (e.g. U. Np, Pu, Tc and, Am). Therefore it is important to quantify the rate of oxygen depletion when the repository has been closed to the atmosphere. In principal oxygen reduction will occur by respiration of organic carbon and oxidation of reduced minerals (Grenthe et al., 1992).

Fe(II)-silicates can contribute to the reduction of oxygen by oxidation of a) Fe(II)-sites at the mineral surface; and/or b) dissolved Fe(II) subsequent to release from the mineral (White and Yee, 1985). Biotite is the main Fe(II)-bearing mineral in granite. Banwart et al. (1992) showed that in a granitic fracture zone at the Äspö Hard Rock Laboratory, biotite is the most important Fe(II) mineral in the unaltered host rock. At the fracture surface chlorite is the dominating reduced mineral.

## 1.2 OBJECTIVES

In order to estimate the rate and extent of oxygen depletion by Fe(II) silicates we studied the kinetics and thermodynamics of biotite and chlorite weathering. Specific objectives were to:

1) determine the extent and rate of iron release from biotite and chlorite

2) measure the $E_h$ developed during biotite weathering

3) determine saturation with respect to some secondary minerals, and identify solubility controlling phases

4) determine the rate and stoichiometry of biotite and chlorite dissolution at different pH ($2 < pH < 10$).

5) assess the effect of the (bi)carbonate ligand on the biotite dissolution.

We have used batch and titration experiments to study the equilibrium concentration of elements released to solution during biotite

weathering. In the near neutral to basic pH region the solution composition is highly non-stoichiometric and the elemental concentrations can be explained by equilibrium with secondary phases like gibbsite, quartz, Fe(III)-(hydr)oxide and a clay mineral. At lower pH the equilibrium composition is more closely stoichiometric and the solubility is consistent with equilibrium with Fe(III)-(hydr)oxide, and an Fe(II)-clay. XPD-patterns of reacted solids indicates an expansion, typical for a clay transformation, of the silicate structure. We identify kaolinite as a secondary weathering product at low pH.

Redox measurements, using redox electrodes, indicates the preference of Fe(II) in solution at pH <4. We show that the Fe(III)-concentrations are consistent with the solubility of an Fe(III)-(hydr)oxide. At higher pH we have not been able to measure $E_h$.

The kinetics of biotite dissolution have been studied using a continuous flow through reactor (Bruno et al., 1991). The dissolution reaction is highly non-stoichiometric in the whole pH region ($2 < pH < 10$) studied. The release rate of Fe, Mg, Si and Al are highly pH dependent showing a minimum around neutral pH. We show that potassium release is diffusion controlled whereas the release of the other elements are surface-reaction controlled on the time-scale of the experiment. We propose that at longer time-scales the release rate of elements will be limited by the slowest elemental release rate. Our experiments indicate that iron has the slowest release rate and is surface reaction controlled. We do not observe any effects of (bi)carbonate concentrations on Fe-release rates. XPD-patterns again indicate expansion of the structure. Mössbauer analysis show a higher percentage of Fe(III) in the weathered than in the fresh biotite.

Comparative experiments show similar dissolution behaviour for chlorite and biotite.

We estimate a timescale of $10^1$-$10^2$ years to reach anoxic conditions for a fracture zone initially saturated with oxygen. In contrast, the time scale to develop Fe(II) concentrations characteristic for deep ground water is $10^{-1}$ years.

We show that there is an optimal redox potential region where the canister is chemically stable towards corrosion by molecular oxygen (to copper oxide) and where sulfate reduction is prevented, thereby stabilizing the copper towards the formation of copper sulfide. We define redox capacities with respect to these reactions, and conclude that the evaluation of these equations for repositories requires site specific data such as abundance of redox active compounds and flow parameters. We present a conceptual model for evolution of oxidizing capacity with time during the life-time of a repository, and a methodology for estimating the half-life of oxygen in the post-closure

period. The model emphasizes the importance of chemical kinetics for depletion of molecular oxygen and other redox reactions.

## 1.3 BIOTITE AND CHLORITE STRUCTURE AND WEATHERING

### 1.3.1 Structure of Biotite and Chlorite

Biotite and chlorite are both phyllosilicates, eg. they have an infinite two-dimensional silicate-structure (Fig 1-1). The basic structural feature (Newman and Brown, 1987; Biotite: Fanning et al., 1989; chlorite: Barnhisel and Bertsch, 1989) of these two minerals is the sheet structure with octahedrally coordinated cations sandwiched between two layers of tetrahedrally coordinated cations. The octahedra are occupied by $Mg^{2+}$, $Al^{3+}$, $Fe^{2+}$ and $Fe^{3+}$. The tetrahedra are mainly occupied by Si and Al, Al giving a charge deficiency to the tetrahedra and a negative charge to the sheet. Biotite maintains charge balance with $K^+$ ions in the silicate interlayers whereas chlorite has brucite/gibbsite-like hydroxy-interlayers.

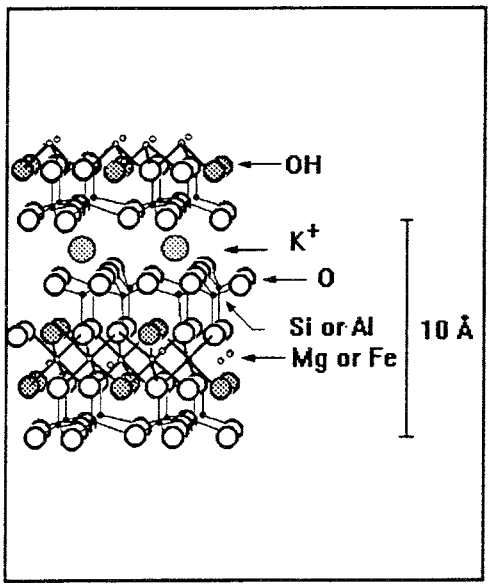


Figure 1-2a

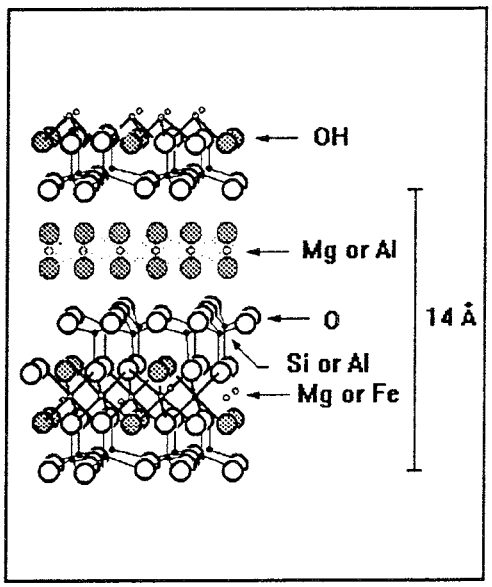


Figure 1-2b

Figure 1-2.
Idealized crystal structure (modified from Barnhisel and Bertsch (1989)) of a) biotite and b) chlorite . An octahedral sheet of cations lies between by two tetrahedral sheets of silicon and aluminium. Biotite maintains charge balance by $K^+$-ions whereas chlorite has a hydroxy-interlayer.

Phyllosilicates are usually subdivided into two groups. Dioctahedral minerals have two trivalent ions in the octahedral sites for each 10 oxygens in the mineral. Trioctahedral minerals keep the same total

charge, having three divalent ions for each such unit (Fanning et al., 1989).

### 1.3.2 Biotite and Chlorite Weathering

Allen and Hajek (1989) concluded that biotite and chlorite are unstable under earth-surface conditions. They also pointed out that the "stability" is dependent on specimen composition and the weathering environment.

#### 1.3.2.1 Biotite

The weathering of biotite (see review by Fanning et al., 1989; and Scott and Amonette, 1988) is usually regarded as an alteration process where the sheet structure is transformed. Kaolinite (Grant, 1964; Rausell-Colom et al., 1965; Wilson, 1966; Stoch and Sikora, 1976; Banfield and Eggelton, 1988; Fordham, 1990), amesite (Grant, 1964), smectite (Fordham, 1990), gibbsite (Wilson, 1966; Fordham, 1990) and goethite (Walker, 1949; Banfield and Eggelton, 1988) are considered to be the final weathering products. The transformation of the sheet structure and the formation of meta-stable intermediates, for example vermiculite (Walker, 1949; Bassett, 1959; Norrish, 1973; Banfield and Eggelton, 1988; Fordham, 1990); and interstratified minerals (biotite-vermiculite (Banfield and Eggelton, 1988), hydro-biotite (Bassett, 1959; Wilson, 1970; Yassoglou et al., 1972; Fordham, 1990) vermiculite-chlorite (Wilson, 1966,1970)), are considered to be dependent on the weathering situation and specimen (Wilson, 1975). Generally the following alterations of the mineral can be observed during weathering:

* Expansion of the interlayer distance due to exchange of non-hydrated $K^+$ by hydrated ions or formation of hydroxy-polymer interlayers of units such as $Al_n(OH)_m$.

* Increasing Si/Al ratios in the tetrahedral layer (reducing the layer charge.)

* Oxidation of octahedral iron

* Enhanced cation exchange capacity (CEC) due to expansion of the sheet.

* Substitution of divalent for trivalent ions in the octahedral sheet.

There is no solubility product, or stability diagram valid under earth surface circumstances, published for biotite.

It is well known that the iron- content and oxidation state are of major importance for biotite weathering susceptibility (Fanning et al., 1989 and references therein), with decreasing stability with increasing iron content. Oxidation of structural iron destabilizes the mineral.

Previous laboratory investigations of biotite dissolution kinetics focused on the acid pH region (Schnitzer and Kodama, 1976; Trotignon and Turpault 1992,1994; Acker and Bricker, 1992 (up to pH 7)) or only on potassium release (Rausell-Colom et al., 1965). A few articles report laboratory studies of weathering kinetics of other micas (Clemency and Lin, 1981; Lin and Clemency, 1981a,b,c; Knauss and Wolery, 1989) at natural or near natural conditions.

Rausell-Colom et al. (1965) found that the kinetics of potassium release from biotite into salt solutions is controlled by diffusion. They concluded that the rate of diffusion is dependent on specimen and salt concentration and that the release stops at a certain solution concentration of potassium.

Acker and Bricker (1992) reported strongly pH dependent, incongruent dissolution of biotite ($3 < pH < 7$) with preferential release of magnesium and iron. They indicated the possibility of vermiculite formation during continuous-flow-experiments, but were unable to verify it by XPD.

### 1.3.2.2 Chlorite

The weathering of chlorite (See review by Barnhisel and Bertsch, 1989) results in a variety of different secondary minerals (vermiculite (Gilkes and Little, 1972; Ross and Kodama, 1974; Ross et al., 1982), goethite (Ross et al., 1982), interstratified minerals (chlorite-vermiculite (Johnson, 1964; Herbillon and Makumbi, 1975; Ross et al., 1982; Rabenhorst et al., 1982), corrensite (Post and Janke, 1972)), nontronite (Herbillon and Makumbi, 1975), hydroxy-interlayered minerals, smectite, goethite (Bain, 1977), Fe-oxyhydroxides (Cho and Mermut, 1992), halloysite (Cho and Mermut, 1992) and kaolinite (Herbillon and Makumbi, 1975; Cho and Mermut, 1992)). As in the case of biotite, the amount of Fe(II) and its oxidation play a significant role in the weathering susceptibility (Ross, 1975).

Commonly 1) oxidation of Fe(II); 2) loss of Fe and Mg; and 3) removal of the hydroxide sheet is observed during chlorite weathering

(Barnishel and Bertsch, 1989) . Ross and Kodama (1974) suggested the mechanistic interpretation that the irreversible oxidation of Fe(II) produces a structural disturbance, facilitating removal of the hydroxide sheet and thereby the weathering.

Ross (1969) reported stoichiometric release of metals from eight different chlorites during dissolution in Si-saturated 2 N HCl.

# 2. EXPERIMENTAL METHODS AND MINERAL CHARACTERIZATION

## 2.1 MINERAL CHARACTERIZATION AND SAMPLE PREPARATION

The natural mineral specimens used in this study (Biotite LK 5210, Chlorite 740665) were provided by Naturhistoriska Riksmuseet (Stockholm).

### 2.1.1 Mineral Preparation

Mineral powder was prepared by peeling small sheets from the mineral surface, size fractionating with sieves. The 53-75 $\mu$m, 75-125 $\mu$m, and 125-300 $\mu$m fractions were used in the experiments. The mineral powders used in the kinetic experiments were washed ultrasonically three times in ethanol to remove ultra fine particles (Schott et al., 1981).

### 2.1.2 Mineral Characterization

#### 2.1.2.1 Chemical Composition

The elemental composition of the minerals was determined by 1) dissolution by standard methods (Bock and Marr, 1979; Pirhonen and Pikänen, 1991) and determination by ICP-AES (see section 2.2); and 2) micro-probe analysis of mineral powder. Scanning Electron Microscopy (SEM) and micro probe analysis were made at the department of Physical Metallurgy and Ceramics, KTH, Stockhom. The Fe(II) /Fe(III) ratio was determined by spectrophotometric analysis after dissolution (Pirhonen and Pitkänen, 1991) and Mössbauer analysis of mineral powder. Mössbauer analysis was made at the department of Physics, SU, Stockholm. Table 2-1 lists characteristics of the mineral specimens.

Table 2-1
Mineralogical data for the specimens.

| | BIOTITE | CHLORITE |
|---|---|---|
| **ELEMENTAL** | **RATIO** | |
| Si | 3.81 ± 0.6 | 34.2 ± 6 |
| Fe | 1.65 ± 0.1 | 1 |
| Mg | 1 | 26.9 ± 9 |
| Al | 1.50 ± 0.04 | 6.7 ± 1 |
| K | 0.95 ± 0.1 | - |
| **Fe(II)/Fe(tot)** | [%] | |
| Spectrophotometric [a] | 74.9 ± 4.8 | 70.9 ± 5.3 |
| Mössbauer | 76.5 | 52.1 |
| **X-RAY d(001) SPACING [Å]** | 10.00 | 14.40 |
| **SPECIFIC** | **SURFACE** | [$m^2/g$] |
| 75-125 $\mu$m | 1.81 ± 0.1 [b] | 4.38 [c] |
| 125-300 $\mu$m | - | 3.36 [c] |

Error estimates are given as one standard deviation.
a) Method modified from Pirhonen and Pitkänen (1991)
BET-areas determined from b) krypton - and c) helium adsorption.

### 2.1.2.1.1 Biotite Stoichiometry

Based on the results in table 2-1, and making the assumption that the composition is given by $Y_pX_qZ_4O_{10}(OH)_2$ (Newman and Brown, 1987) where Z (Al,Si) denotes the tetrahedral, X (Mg,Fe,Al) the octahedral and Y (K) the interlayer position the biotite composition is:

$$K_{0.80}(Mg_{0.84}Fe^{II}_{1.10}Fe^{III}_{0.22}Al_{0.44})(Si_{3.18}Al_{0.82})O_{10}(OH)_2$$

This composition deviates from the ideal $(K(Mg,Fe^{II})_3(Si_3Al)O_{10}(OH)_2)$ by having lower layer charge and the presence of Fe(III). However, biotites (Deer et al., 1963) typically have down to 0.8 potassium atoms per formula unit and up to 55% of the total iron as Fe(III).

#### 2.1.2.1.2 Chlorite Stoichiometry

Based on the results in table 2-1, the correlation between X-ray diffraction d(001) spacing and silicon content of tetrahedral position recommended by Bailey (1972, p. 381, equation 1) and assignments to structural positions analogous as for biotite, the chlorite composition was calculated to be:

$$(Mg_{4.9}Al_{0.7}Fe^{II}_{0.1}Fe^{III}_{0.1})(Si_{3.5}Al_{0.5})O_{10}(OH)_8$$

According to the nomenclature given by Deer et al. (1963) this composition corresponds to a penninite/talc-chlorite.

### 2.1.2.2 BET - Surface Area

The specific surface area (table 2-1) of biotite (krypton adsorption Digisorb 2600 BET-analyzer) and chlorite (helium adsorption, Micromeretics Gemini 2370 BET-analyzer) samples was determined by the BET-method.

### 2.1.2.3 XPD

**X**-ray **P**owder **D**iffraction (XPD) was done using a Philips PW 1130/00 diffractometer, using a CoK$\alpha$ ($\lambda = 1.7902$ Å) target. The $2\theta$ scan-rate was 1°/min, the current 20 mA and the voltage 40 KV. The "low-angle-cut-off" for the instrument is $2\theta \approx 4°$ ($\sim 25$ Å). Scans were normally run in the region $4° \leq 2\theta \leq 100°$

Figure 2-1 shows the XPD-pattern of biotite and chlorite. The XPD-pattern confirmed the minerals to be mica and chlorite.

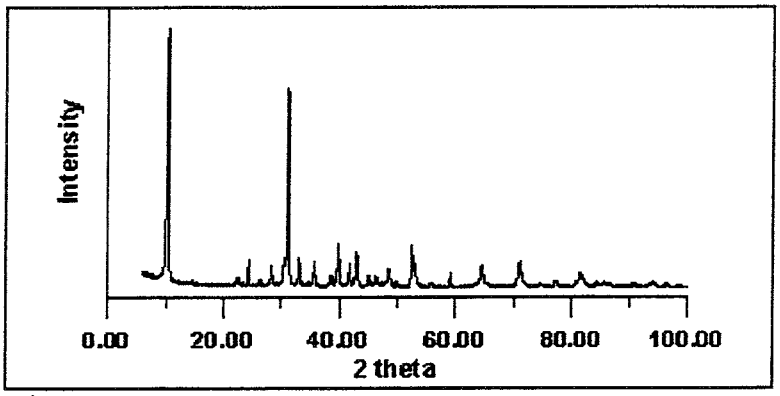


Figure 2-1a

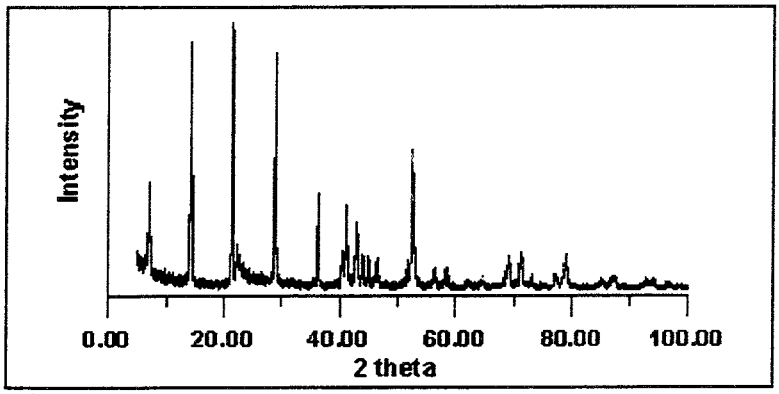


Figure 2-1b

Fig 2-1
The XPD pattern of a) biotite and b) chlorite.

## 2.2 EXPERIMENTAL METHODS

Experiments were carried out at 25 ± 1 °C, 1 atm pressure using the ionic medium: $[Na^+] + [H^+] = [HCO_3^-] + [ClO_4^-] + [OH^-] + 2[CO_3^{2-}]$ = 0.500 M. High purity chemicals (p.a or better) and gases (99.5% purity) were used. Gases were cleaned by bubbling through an oxygen trap (amalgamated zinc/vanadous solution) followed by ionic medium to remove traces of molecular oxygen and to saturate the gas stream with water vapour at the experimental conditions. Reacted solution samples were analyzed for Si, Mg, Al, total Fe, and K where applicable, using an ARL (Applied Research Laboratory) model 3520B ICP- (Inductively Coupled Plasma emission spectrometer) analyzer. Standards were prepared by dilution of Atomic Spectral Standards (Analytical Standards, Kungsbacka) into appropriate matrix solutions. Proton concentrations where determined using an electrochemical cell of the type:

glass electrode/test- solution//($AgNO_3$ or HCl), $NaClO_4$/AgCl(s), Ag(s)

The measuring cells were normally calibrated according to Gran (1981) before and after each experiment. Membrane filters used in the experiments were 0.2 $\mu$m pore size filters of PTFE-type (MFS J020A025A or Millex FG SLFG025BS).

## 2.2.1 Equilibrium Experiments

### 2.2.1.1 Batch Experiment

A known mass of mineral was placed in a teflon or polypropylene bottle. The bottle was filled with ionic medium at specified pH, sealed and placed onto a shaker table under $N_2(g)$ atmosphere. The system was left to equilibrate. The final pH was measured, the solid phase separated by membrane filtration and the filtrate acidified (to $pH < 1$ ) by a small volume of nitric acid.

### 2.2.1.2 Continuous Titration

Two experimental setups were used. In the conventional method (Figure 2-2a) a suspension of biotite in the ionic medium was titrated in a glass vessel coated with paraffin or in a teflon vessel. In the continuous-flow-through titration (figure 2-2b) the ionic medium was pumped through a filter holder containing the biotite during the titration. The titrations were carried out by consecutive additions of base (NaOH) or acid ($HClO_4$). After each addition, equilibrium was assumed when the potential drift in the glass electrode assembly was $< 10^{-4}$ mV/s. At equilibrium the solution was sampled by removal of some suspension/solution, separation of the solid phase by membrane filtration (conventional experiment) and acidification (to $pH < 1$) of the filtrate by a small volume of nitric acid. The titration vessel was maintained under $N_2(g)$ or Ar(g) ($N_2(g) + CO_2(g)$ mixtures for the $H_2O$-$CO_2$ systems) atmosphere. In the conventional titration the redox potential was measured electrochemically by a cell of the type:

indicator electrode/test- solution//($AgNO_3$ or HCl), $NaClO_4$/AgCl(s), Ag(s)

Two sheet-platinum, one sheet-gold and one glassy carbon electrode were used as indicator electrodes. The redox potential measurements were stable and the agreement between different electrodes was good in the low pH region (below pH 4). At higher pH both drift in the potentials and disagreement between electrodes make the interpretation of the measurements difficult. Grenthe et al. (1992) thoroughly discuss the necessary conditions for redox potential measurements in field and laboratory systems, namely 1) the

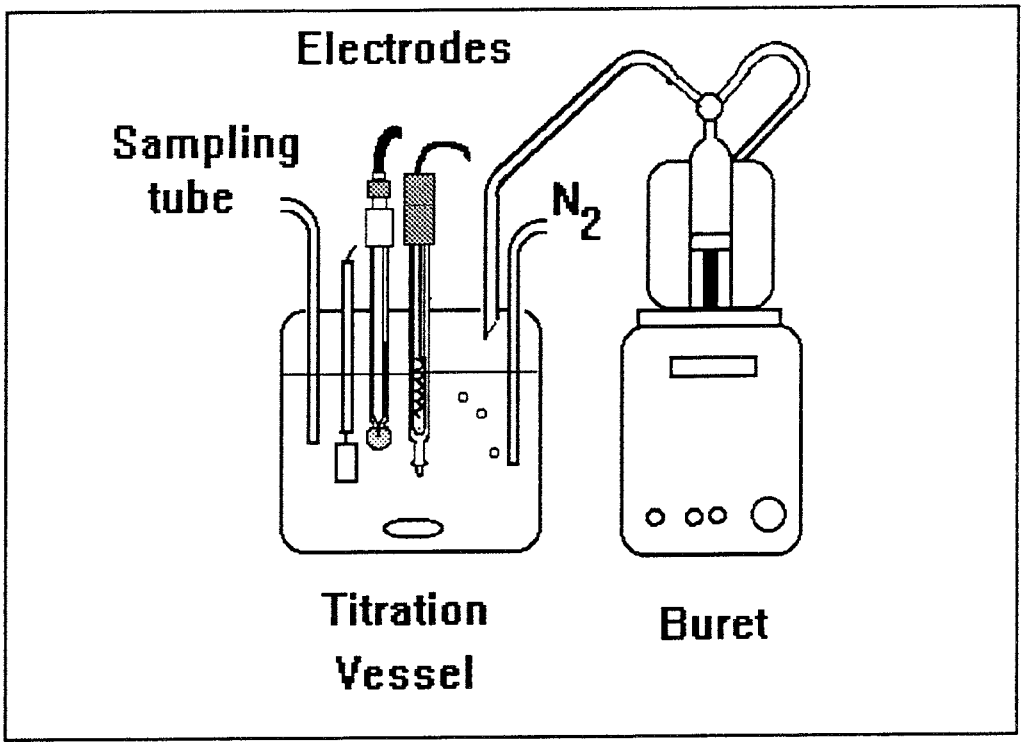


Figure 2-2a
Conventional continuous titration setup. A suspension of mineral is titrated.

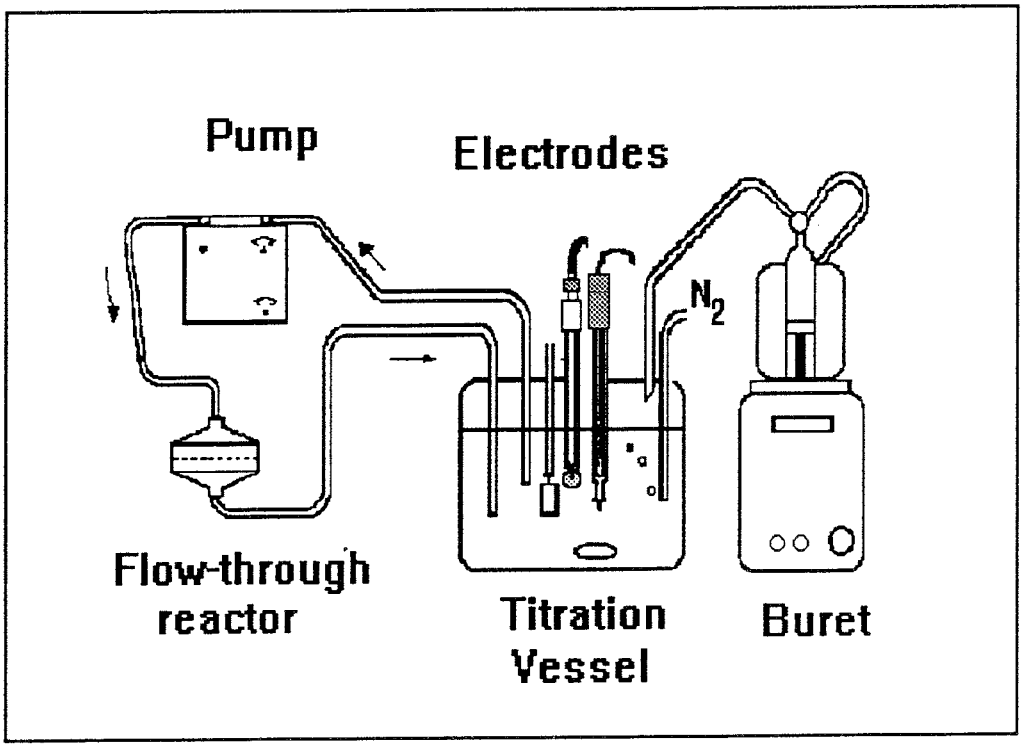


Figure 2-2b
Flow-through continuous titration setup.

presence of electrode-reactive species which are able to exchange electrons with the electrode; 2) redox reactions with one-electron transfers; 3) sufficient redox capacity in the system (for systems containing Fe(III) solid phases a minimum concentration of $10^{-6}$ M Fe(II) is needed). They conclude that the Fe(II)/Fe(III) redox couple can give reproducible (within 20 mV) redox potentials in natural and laboratory systems. Our experimental setup is open in the sense that it is flushed with argon. Although precautions were made to eliminate molecular oxygen from the system, an $E_h$ equal to -200 mV (obtained at near neutral pH in the simulated rock weathering experiment reported by Grenthe el al. (1992)) would require a partial oxygen pressure of maximum $10^{-16}$ atm which is not likely obtained in the experiment.

### 2.2.2 Kinetic Experiments

The experiments were performed using a continuous flow-through reactor (Bruno et al., 1991)(figure 2-3), consisting of a thin layer (<3mm) of mineral powder of known mass, held between two membrane filters, across which test solutions of known composition were pumped at specified rates. The pH of the reactor outflow was recorded continuously. Equation (2-1) calculates the surface area normalized mineral dissolution rate from concentration (C [moles/g solution]) of element j in sample i.

$$R_{i,j} = \frac{F_i C_{i,j}}{m A P_j} \quad [\frac{moles\ of\ mineral}{h\ m^2}] \qquad (2\text{-}1)$$

F is flow rate [g/h]; m, mass of mineral [g]; A, specific surface area [$m^2$/g]; and P, a stoichiometric factor [moles of element/moles of mineral].

Equation (2-2) calculates the accumulated release of element during an experiment:

$$a_j(t_i) = \sum_i R_{i,j}(t_i - t_{i-1}) \quad [\frac{moles\ of\ mineral}{m^2}] \qquad (2\text{-}2)$$

a denotes accumulated release [moles of mineral/$m^2$] and t the time [h] elapsed from the start of the experiment.

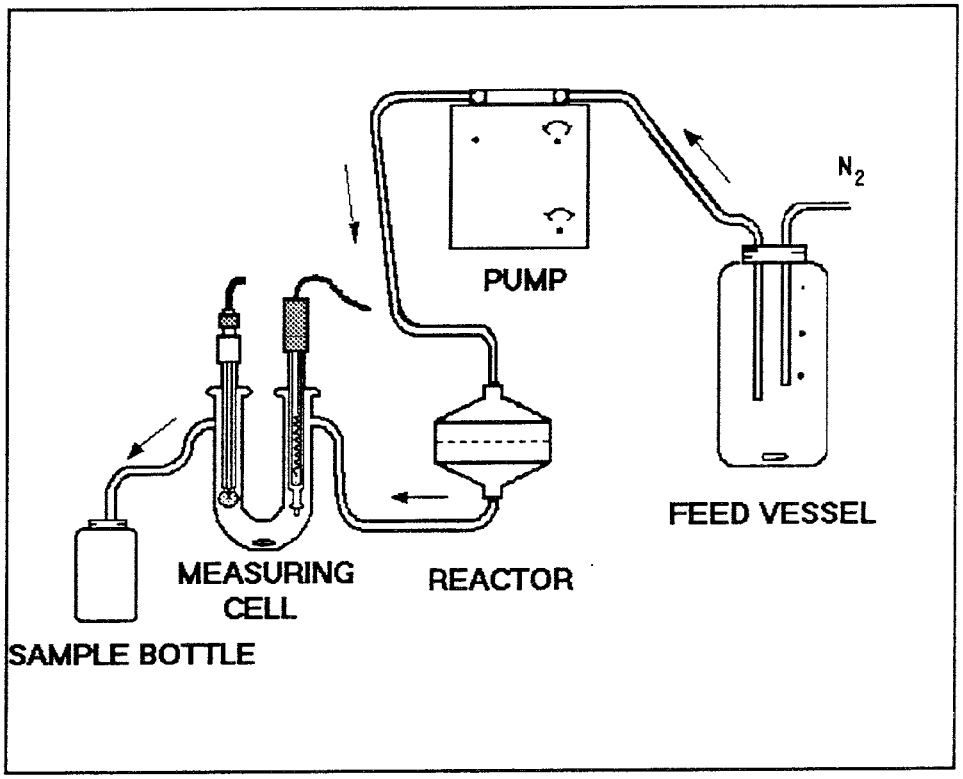


Figure 2-3

Figure 2-3. Experimental setup for the thin-film continuous flow-through system. Test solution of known composition is pumped through a thin-film reactor where the mineral powder is held between two membrane filters. The outflow solution passes a closed U-tube where pH is measured continuously. The reacted solution is collected in acid-containing polypropylene bottles.

In addition to continuously purging feed solutions with $N_2(g)$, the carbon dioxide-free experiments were carried out in a glove box under $N_2(g)$ atmosphere. In the $CO_2$-free experiments at near neutral pH the buffer capacity of the system was too low to give stable pH-measurements and the proton concentrations in these feed solutions were calculated from dilution of standard acid ($HClO_4$) or base (NaOH) solutions in $NaClO_4$. A fresh mineral sample was used for each experiment. Solution samples were collected in polypropylene, acid washed bottles, containing a small volume of concentrated $HNO_3$.

# 3. RESULTS AND DISCUSSION

The raw data from the solution analysis and the XPD analysis are given in appendix 7.1-7.6 and 7.9 respectively.

## 3.1 RESULTS FROM KINETIC EXPERIMENT

### 3.1.1 Wet Chemistry Results

#### 3.1.1.1 Biotite ($CO_2$-free system)

Figure 3-1 shows the accumulated release of biotite calculated (equation 2-2) from each element as function of time. The release of all elements is rapid at the beginning of the experiment and decreases to quasi steady-state rates with time. Such a decrease of dissolution rates with time is typical for dissolution kinetic experiments using fresh mineral samples (Furrer and Stumm, 1986; Caroll-Webb and Walther, 1988; Wieland and Stumm, 1992), and has been explained by dissolution of 1) ultrafine particles (Holdren and Berner, 1979; Schott et al., 1981); and 2) more reactive surface sites (Wherli, 1989). After an initial period of $<10$ days the accumulated release of Si, Fe, Mg and Al is directly proportional to time. Linear release, obtained at a fixed flow rate, reflects constant concentration in the outflow solution. The concentration in the outflow can be controlled by 1) equilibrium with a solid phase; 2) chemically kinetics; or 3) transport phenomena. If the system is operating at equilibrium the output concentration is independent of flow rate (C in equation 2-1 is constant). If the system is controlled by chemical kinetics the dissolution rate is independent of flow rate (R in equation 2-1 is constant and a decrease of F causes a corresponding increase of C). On the other hand if the overall reaction rate is controlled by transport phenomena Fick´s law of diffusion (equation 3-1) determines the concentration in the outflow solution:

$$|R_j| = \frac{D_L}{\Delta y}(C_{surface} - C_{out}) \qquad (3\text{-}1)$$

where $D_L$ is the diffusivity and $\Delta y$ is the diffusion path length. At steady-state $C_{surface}$ equals $C_{equil.}$. A combination of equation 2-1 and 3-1 shows that a decrease of F causes a non-proportional increase of $C_{out}$. At the end of the experiments at pH 2, 7 and 10 we ran the thin-film reactor at half the initial flow rate. In the experiments at pH 2

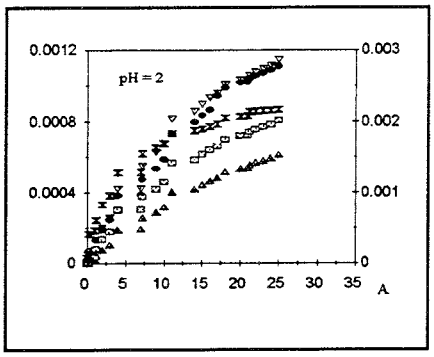


Figure 3-1a

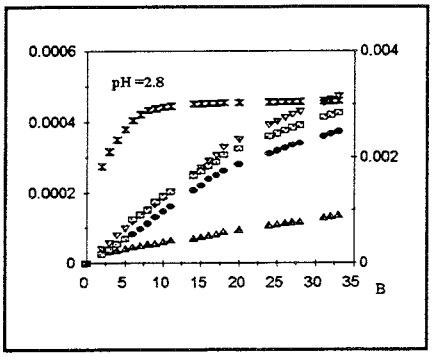


Figure 3-1b

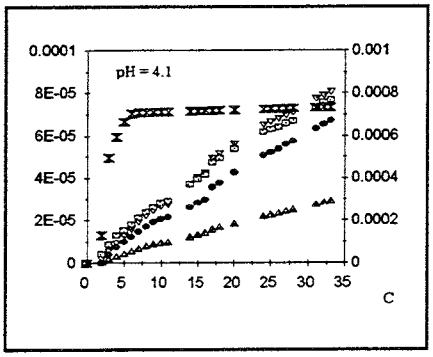


Figure 3-1c

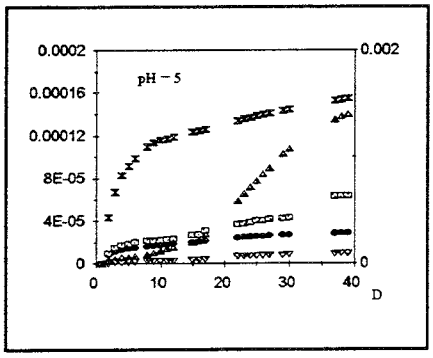


Figure 3-1d

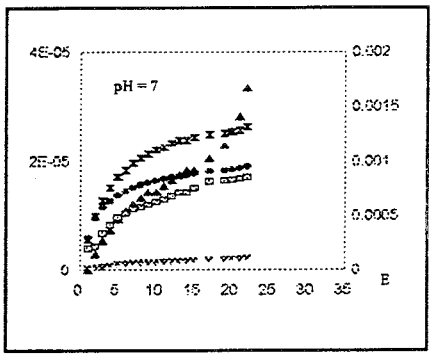


Figure 3-1e

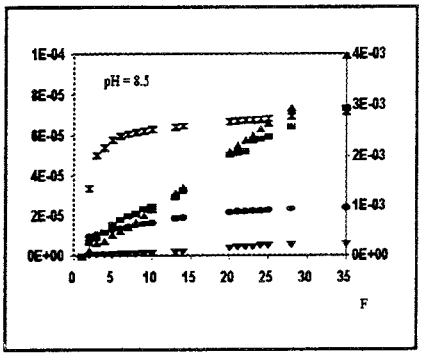


Figure 3-1f

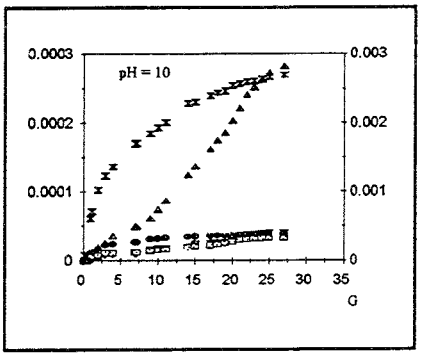


Figure 3-1g


Figure 3-1
Accumulated release [moles biotite/$m^2$] of elements from biotite in $CO_2$-free experiments at specified pH: a) 2; b)2.8; c) 4.1; d) 5; e) 7; f) 8.5; g) 10. Potassium scale on the vertical axis at right.

and 7 this yielded approximately double concentrations of iron, aluminium, and magnesium in the outflow solution. This excludes the possibility of equilibrium conditions or transport controlled release of these elements and indicates chemically kinetics control. Steady-state kinetics is expected for a surface-chemical-reaction-controlled dissolution mechanism with concentration of reactive surface sites at steady-state (Furrer and Stumm, 1986; Blum and Lasaga, 1988; Wieland et al., 1988; Stumm and Wieland, 1990; Stumm and Wollast, 1990). The uncertainty in the analyzed concentrations in the experiment at pH 10 makes interpretations impossible.

The steady-state rates (table 3-1, figure 3-2) of release of iron, magnesium and aluminium in the biotite/$H_2O$ system are highly pH dependent over the pH range 2-10 and in the case of iron and aluminium qualitatively similar to the simple end-member (hydr)oxides $Al_2O_3$ (Furrer and Stumm, 1986) and $\alpha$-FeOOH (Zinder et al., 1986). The release rate of silicon is only slightly dependent on pH in the range 3 - 8.5, with higher values below and above this region. The final release rate of potassium is only slightly dependent of pH.

Table 3-1
Biotite dissolution rate [moles mineral $m^{-2}$ $h^{-1}$] in the $CO_2$-free experiment as a function of pH.

| pH | Si | Fe | Mg | AL | K |
|---|---|---|---|---|---|
| 2 | $4.79*10^{-7}$ | $6.42*10^{-7}$ | $5.82*10^{-7}$ | $5.64*10^{-7}$ | $2.36*10^{-7}$ |
| 2.8 | $1.43*10^{-7}$ | $3.91*10^{-7}$ | $3.08*10^{-7}$ | $3.06*10^{-7}$ | $1.06*10^{-7}$ |
| 4.1 | $3.61*10^{-8}$ | $6.76*10^{-8}$ | $8.09*10^{-8}$ | $7.17*10^{-8}$ | $3.38*10^{-8}$ |
| 5 | $2.43*10^{-7}$ | $4.85*10^{-9}$ | $1.21*10^{-8}$ | $3.78*10^{-8}$ | $4.83*10^{-7}$ |
| 7 | $1.10*10^{-7}$ | $2.42*10^{-9}$ | $7.83*10^{-9}$ | $7.16*10^{-9}$ | $5.60*10^{-7}$ |
| 8.5 | $1.19*10^{-7}$ | $3.13*10^{-9}$ | $8.42*10^{-9}$ | $2.91*10^{-8}$ | $6.44*10^{-7}$ |
| 10 | $5.61*10^{-7}$ | $1.87*10^{-8}$ | $1.40*10^{-8}$ | $6.11*10^{-8}$ | $2*10^{-6}$ |
| 10 | $2.56*10^{-7}$ | $1.03*10^{-7}$ | $2.24*10^{-8}$ | $9.79*10^{-8}$ | $1*10^{-6}$ |

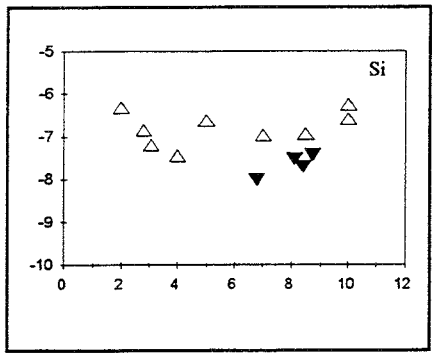


Figure 3-2a

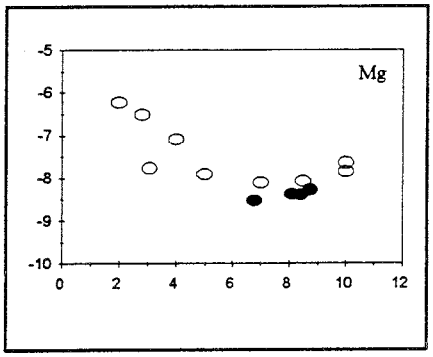


Figure 3-2c

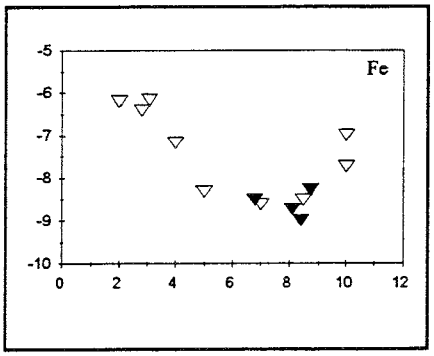


Figure 3-2b

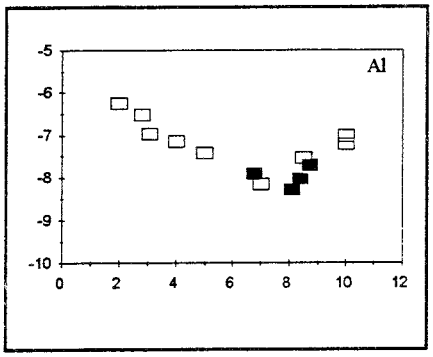


Figure 3-2d

Figure 3-2
Elemental release rates [moles biotite $m^{-2}$ $h^{-1}$] from biotite vs pH. Open symbols are for the $CO_2$-free system. Filled symbols are from the 1 % $CO_2$(g)-system. a) Si ;b) Fe; c) Mg; D) Al.

The steady-state dissolution rate is only stoichiometric with respect to iron, magnesium, aluminium and silicon near pH 4 - 5. Below this region the metals are preferentially released whereas at higher pH silicon is released faster (Fig 3-3) .

Potassium release is very fast at the beginning and apparently becomes diffusion controlled after approximately 1-2 days as indicated by a linear plot of accumulated release against $\sqrt{t}$ (Fig 3-4; Schott and Berner, 1985).

Figure 3-5 shows the dissolution of biotite under 0.01 atm $CO_2$(g). The behaviour of Fe, Mg, Al, and K, is similar to the $CO_2$-free experiments and shows no significant effect of (bi)carbonate on steady-state dissolution rate or stoichiometry (table 3-2, figure 3-2). The Si release rates are lower and more dependent on pH in the $CO_2$-system. In the literature both acceleration (Bruno et al., 1992a; Berg

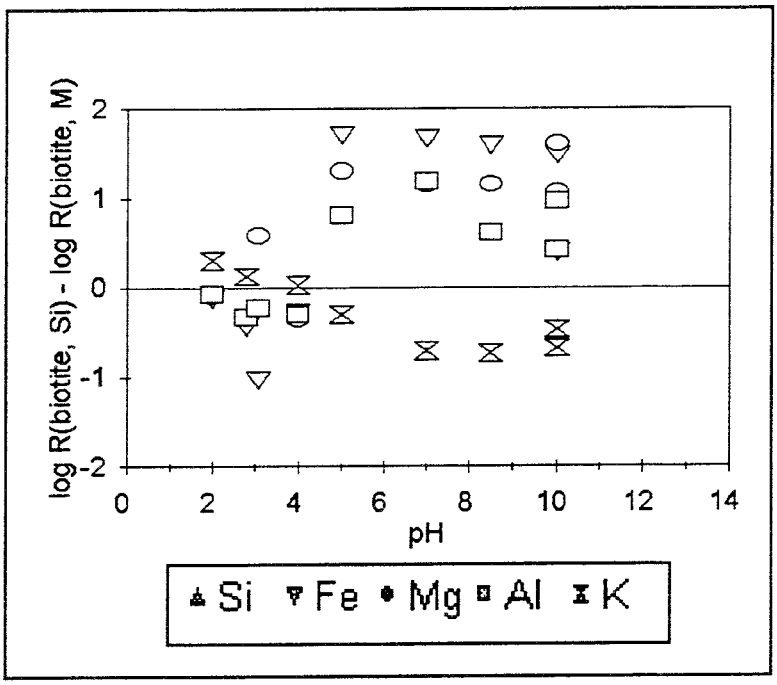


Figure 3-3
Release rates of elements compared to silicon release rates. Values above 0 mean that silicon is released faster.

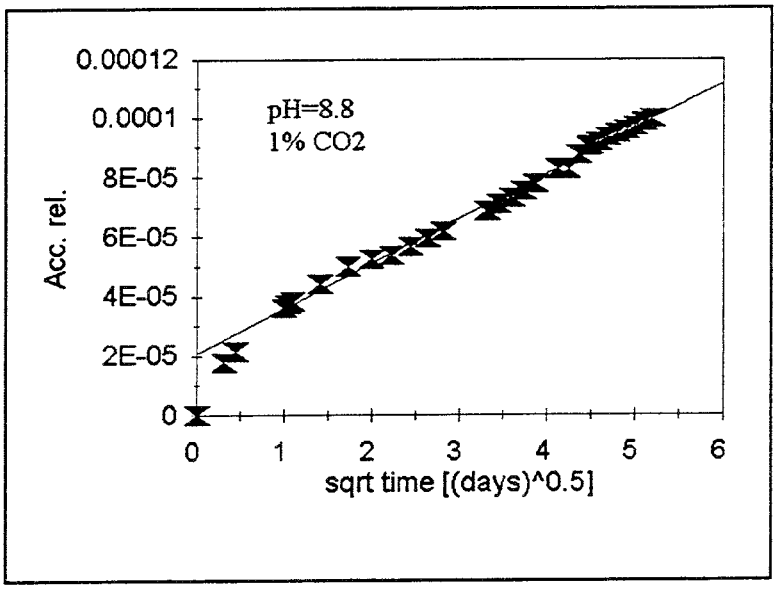


Figure 3-4
Accumulated release of potassium at pH 8.8, 1% $CO_2$ vs $\sqrt{}$time.

and Banwart, 1994a,b; Östhols and Malmström, 1994) and inhibition (Wogelius and Walther, 1991) of mineral dissolution by (bi)carbonate have been reported.

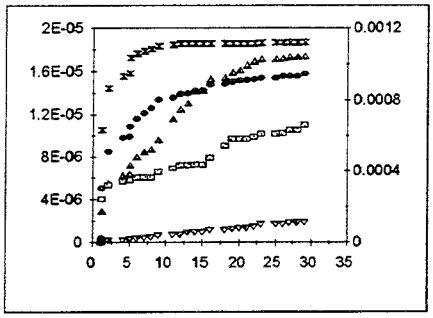


Figure 3-5a

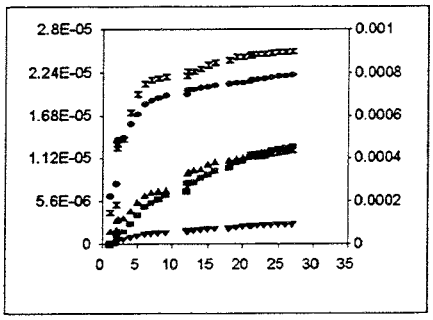


Figure 3-5c

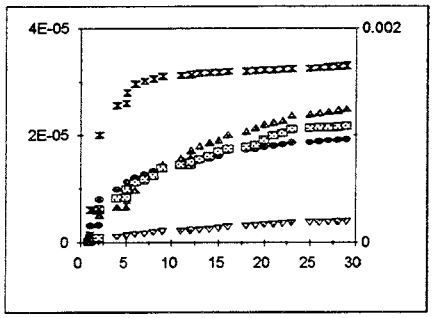


Figure 3-5b

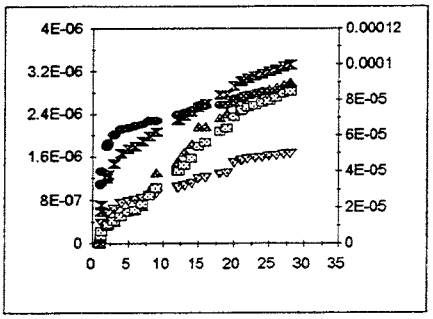


Figure 3-5d


Figure 3-5.
Accumulated release of elements [moles biotite $m^{-2}$] vs time [days] from biotite at specified pH and 1% $CO_2$. a) 6.8; b) 8.1; c) 8.4; d) 8.7. Potassium scale on the vertical axis at right.

Table 3-2
Biotite dissolution rate [moles mineral $m^{-2}$ $h^{-1}$] in the 1% $CO_2$ experiment as a function of pH.

| pH | SI | Fe | Mg | AL | K |
|---|---|---|---|---|---|
| 6.8 | $9.77*10^{-9}$ | $3.09*10^{-9}$ | $3.02*10^{-9}$ | $1.23*10^{-8}$ | $3.61*10^{-8}$ |
| 8.1 | $3.02*10^{-8}$ | $1.86*10^{-9}$ | $4.27*10^{-9}$ | $5.25*10^{-9}$ | $1.71*10^{-7}$ |
| 8.4 | $1.97*10^{-8}$ | $1.01*10^{-9}$ | $4.07*10^{-9}$ | $9.41*10^{-9}$ | $1.09*10^{-7}$ |
| 8.8 | $3.74*10^{-8}$ | $5.39*10^{-9}$ | $5.28*10^{-9}$ | $1.90*10^{-8}$ | $3.10*10^{-7}$ |

The (bi)carbonate concentration ranges between $10^{-3} \leq [HCO_3^-] \leq 10^{-1}$ and $10^{-7} \leq [CO_3^{2-}] \leq 10^{-3}$ M respectively.

### 3.1.1.2 Chlorite

Figure 3-6 shows the accumulated release of elements from chlorite at specified pH and $P_{CO2}$. The chlorite dissolution is less non-stoichiometric than the biotite dissolution. The steady-state dissolution rate is also much less pH dependent. The final accumulated release of elements is lower, mainly due to a lower initial dissolution. In the experiments at pH 7.1, 8.2 and 8.9 the solution concentration of aluminium and iron dropped below the detection limit of the ICP. However, in the near neutral pH region the final dissolution rate, calculated from silicon and magnesium release (table 3-3), is similar to the dissolution rate of biotite.

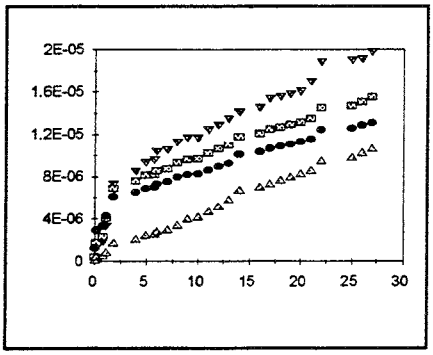


Figure 3-6a

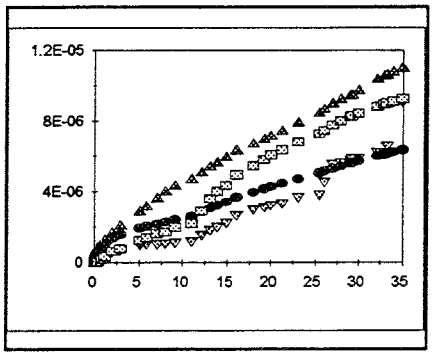


Figure 3-6b

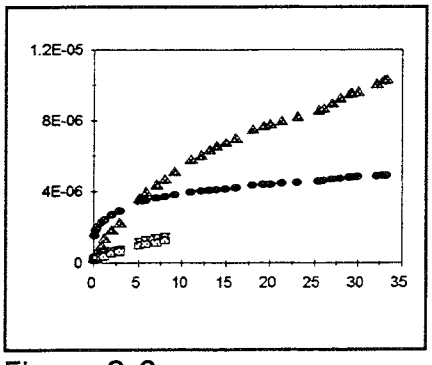


Figure 3-6c

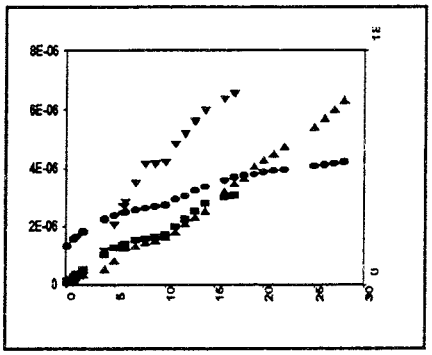


Figure 3-6d

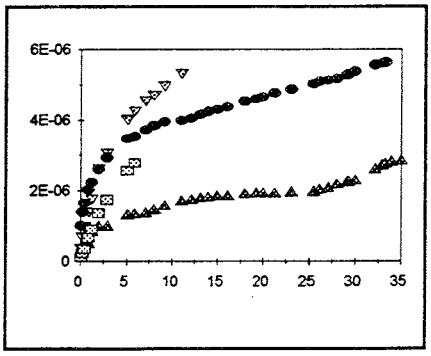


Figure 3-6e

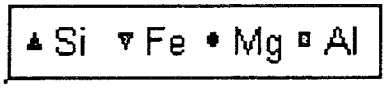


Figure 3-6. Accumulated release [moles of chlorite $m^{-2}$] vs time [days] of elements from chlorite at specified conditions: a) pH = 2.6 $CO_2$-free; b) pH = 3.8 100 % $CO_2$; c) pH = 7.1 100% $CO_2$; d) pH = 8.2 1% $CO_2$; e) pH = 8.9 1% $CO_2$.

Table 3-3
Chlorite dissolution rate [moles mineral $m^{-2}$ $h^{-1}$] at specified conditions

| pH | $CO_2$-condition | Si | Fe | Mg | Al |
|---|---|---|---|---|---|
| 2.6 | $CO_2$ -free | $1.34*10^{-8}$ | $1.92*10^{-8}$ | $9.82*10^{-9}$ | $1.31*10^{-8}$ |
| 3.8 | 100 % | $1.01*10^{-8}$ | $5.22*10^{-9}$ | $5.13*10^{-9}$ | $6.86*10^{-9}$ |
| 7.1 | 100 % | $7.90*10^{-9}$ | U.D. | U.D. | 3.98*10-9 |
| 8.2 | 1 % | 1.06*10-8 | U.D. | U.D. | 6.45*10-9 |
| 8.9 | 1 % | 3.87*10-9 | U.D. | U.D. | 3.98*10-9 |

U.D. means that the concentrations of elements in the outflow solution from the continuous flow-through reactor are under the detection limit of the ICP. The (bi)carbonate concentration ranges between $10^{-5} \leq [HCO_3^-] \leq 10^{-1}$ and $10^{-11} \leq [CO_3^{2-}] \leq 10^{-3}$ M respectively in the $CO_2$(g)-experiments.

### 3.1.2 XPD -Results

#### 3.1.2.1 Biotite

Figure 3-7 shows the XPD patterns of biotite and remaining solid phases from the thin-film-continuous flow-through reactor experiments run at specified pH. The most striking difference between the unreacted biotite and the remaining solid phases is the shift and splitting of the peak around 10 Å ($2\theta \approx 10.3$ deg). This peak d(001) corresponds to the basal spacing of the unit cell (inter-layer distance). At pH 2 this characteristic mica peak has totally disappeared in the favour of a peak around 12 Å ($2\theta \approx 8.4$ deg) reflecting an expansion of the crystal lattice. The inter-layer expands due to exchange of non-hydrated potassium ions for hydrated ions (eg Mg or Na) or hydrolysed ions (eg Fe, Mg or Al) (hydroxy inter-layers). A 12 Å peak has been ascribed to a sodium smectite (Brindley and Brown, 1980, table 5.18) or a interstratification of biotite and vermiculite ("hydro-biotite": Coleman, 1963; Farmer and Wilson, 1970).

The weak peak (figure 3-6 and appendix 6.9) around $2\theta \approx 14.7$ deg ($d \approx 7.00$ Å) together with the shoulder around $2\theta \approx 29.1$ deg ($d \approx 3.56$ Å) indicate the formation of kaolinite (Brindley and Brown, 1980 table 5.18). Kaolinite is often regarded as the final weathering product of biotite. Other minerals formed during the weathering are usually regarded as unstable intermediates. The formation of kaolinite during laboratory weathering has previously been proposed by several authors (see section 1.3.2.1).

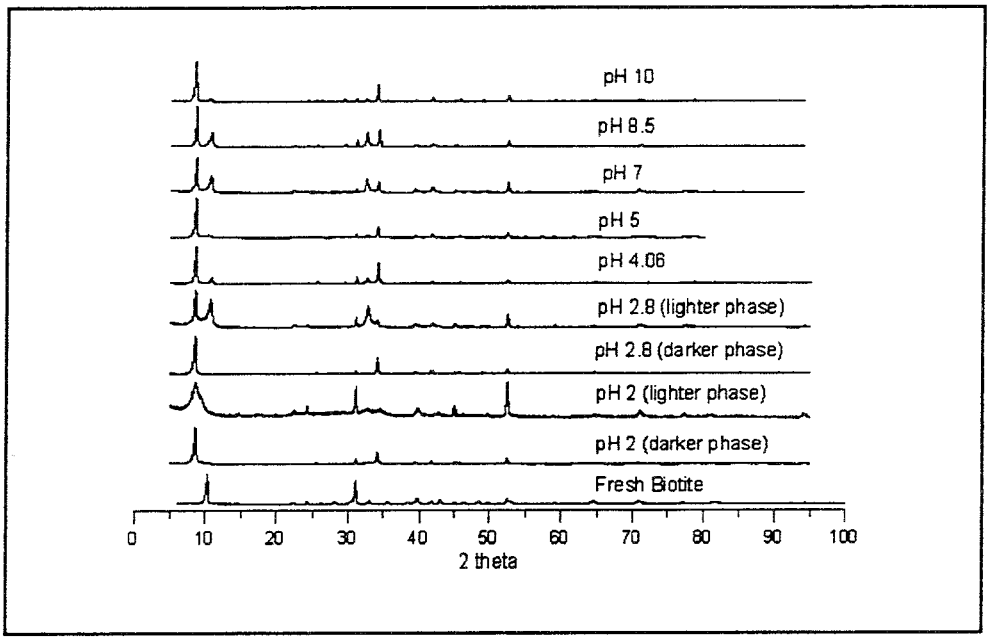


Figure 3-7
XPD reflections of minerals from the biotite kinetic experiment

There is no peak corresponding to formation of crystalline metal oxides or simple metal silicates in the XPD patterns of samples from the pH region $2 \leq pH \leq 10$. For a sample from an experiment run at pH slightly below 2, the typical d(001)-peak has totally disappeared. The remaining XPD-pattern corresponds to quartz. This does not conclusively indicate the formation of a silica phase because the quartz pattern is found as a part of the biotite pattern.

The location of the d(060) peak (1.51-1.56 Å) corresponds for all samples to a trioctahedral structure, i.e divalent ions dominate in the octahedral layer (Fanning et al., 1989).

### 3.1.2.2 Chlorite

The XPD-pattern (appendix 7.9, figure 7-27 to 7-30) of chlorite reacted at $2.6 \leq pH \leq 8.9$ indicates no major structural changes nor precipitation of crystalline secondary phases during chlorite weathering.

Although the peak-locations are identical to the unreacted chlorite the relative heights of the d(001) peaks have changed. In a perfect randomized orientation of the chlorite sample this refers to changes in heavy-metal content and distribution between the silicate and the hydroxide octahedral sites (Moore and Reynolds, 1989). No attempts to orient our sample have been made, thereby introducing uncertainty

of peak intensity variation with different degree of orientation. The variation in peak heights between different samples is too small to give conclusive information on differences in iron content and distribution.

### 3.1.3 SEM/Micro Probe Results (Biotite)

Figure 3-8 shows SEM images of biotite reacted at specified conditions in the thin-film-continuous-flow-through reactor. The biotite reacted at pH 2.8 and 7 retains the sheet structure (Figure 3-8b and c). When biotite is reacted at very low pH (pH < 2; XPD-pattern discussed above) the structure is broken and the sheets open up (figure 3-8a).

Micro probe analysis of mineral remainder from experiments at pH 2.8 and 7 shows complete depletion of potassium and inclusion of sodium (table 3-4). No significant change in silicon, iron, magnesium or aluminium content is observed. The detection of sodium is not explained by retention of sodium perchlorate since no, or negligible amounts, of chlorine are detected.

Micro probe analysis of the pH < 2-sample shows a depletion in all metals. Silicon and oxygen are the remaining main elements.

Table 3-4
Micro probe analysis [mole-%] of unreacted biotite and mineral remainder from the $CO_2$-free biotite kinetic experiments.

| Sample | K | Na |
|---|---|---|
| Unreacted | 6.8 | 0 |
| pH 2.8 | 0 | 6.8 |
| pH 7 | 0 | 14.3 |

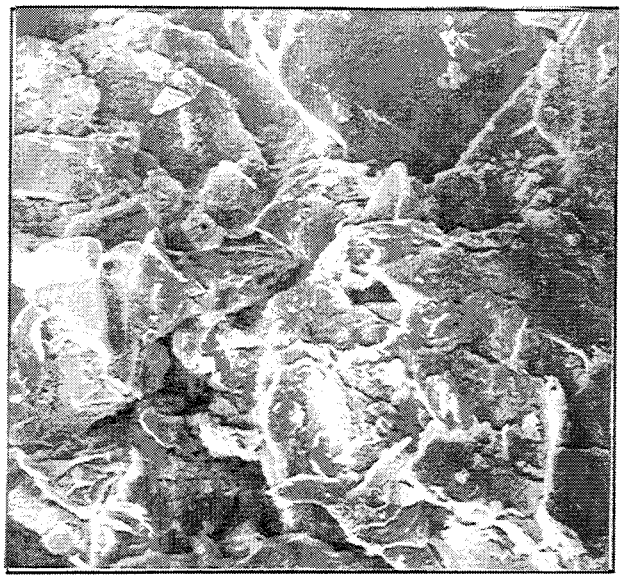

Figure 3-8a

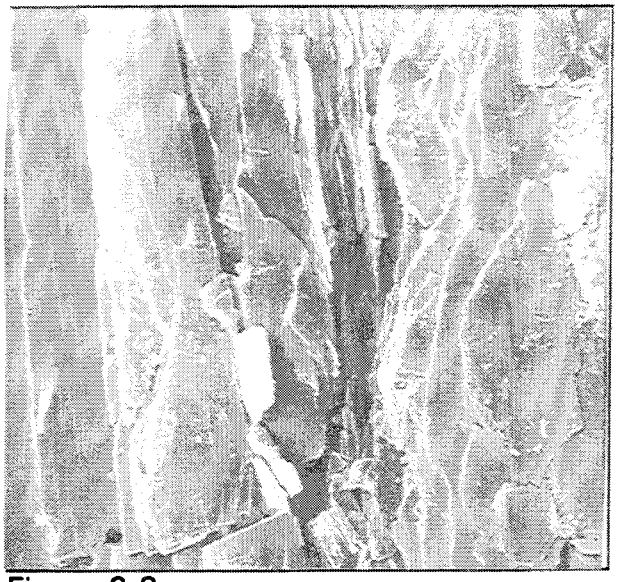

Figure 3-8c

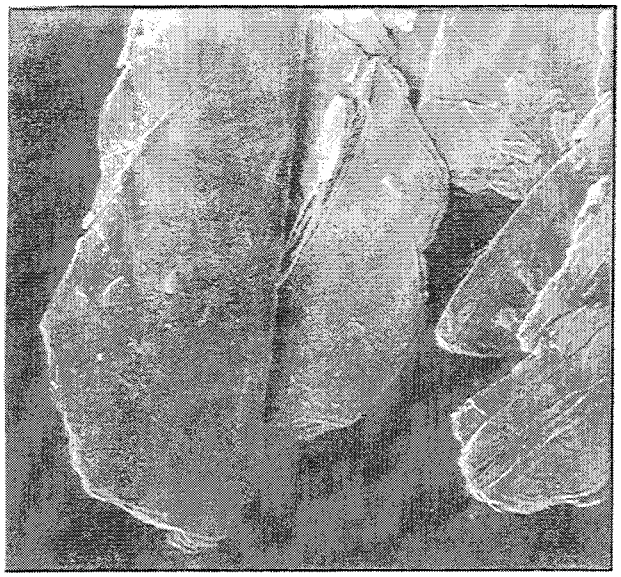

Figure 3-8b

Figure 3-8.
SEM images of mineral remainder from the kinetic experiment of biotite dissolution at different pH ($CO_2$(g)-free). a) pH <2. The structure is broken and the sheets have opened up. (Magnification 1000) b) pH = 2.8. The sheet structure is retained. (Magnification 500) c) pH = 7. The sheet structure is retained. (Magnification 500).

### 3.1.4 Mössbauer Results

Table 3-5 lists the Fe(II)/Fe(III) ratio in the fresh biotite and the mineral remainder from the thin-film-continuous flow-through reactor. Throughout the weathered samples there is a decrease in the Fe(II)/Fe(III) ratio compared to the unreacted biotite. A mass-balance calculation showed that the change can not solely be explained by preferential release of Fe(II) over Fe(III). Oxidation of structural Fe(II) is normally observed during biotite weathering (Fanning et al., 1989 and references therein).

For chlorite there is no significant difference in the Fe(II)/Fe(III) ratio between weathered and fresh mineral samples.

Table 3-5
Mössbauer analysis of fresh biotite and mineral remainder from the biotite kinetic experiments at specified conditions.

| | Fe(II) % | Fe(III)% |
|---|---|---|
| Unreacted | 76.5 | 23.5 |
| pH 2/$CO_2$-free | 9.8 | 90.2 |
| pH 3/$CO_2$-free | 53.3 | 46.7 |
| pH 5/$CO_2$-free | 46.3 | 53.7 |
| pH 7/$CO_2$-free | 47.9 | 52.1 |
| pH 8.8/1% $CO_2$ | 63.4 | 36.6 |

### 3.1.5 Discussion (Biotite)

We interpret the kinetic behaviour of potassium as fast removal of $K^+$ from the biotite interlayers, and the formation of a K-depleted region through which the $K^+$ release becomes diffusion rate-limited.

The conceptual model of Schnoor (1990) for dissolution of complex oxides predicts that an initial period of incongruent dissolution will be followed by stoichiometric dissolution, rate-limited by the slowest surface controlled elemental release rate. The progression to this pseudo-steady state passes through three stages: 1) Initial fast and incongruent release of elements rate limited by the surface reaction at each type of surface site. Build up of layers depleted in the elements released at higher rates; 2) Gradually slower and transport

controlled release of depleted elements due to diffusion through a progressively thicker depletion layer. 3) Eventually the diffusion of depleted elements becomes as slow as the surface controlled dissolution of the element forming the depletion layer. The dissolution continuous congruently, rate limited by the surface reaction, with no further build up of the depletion layer.

Although the release rate of $K^+$ decreases with time it is still faster than that of the slowest element at the end of each experiment. The release of Si, Fe ,Mg and Al is, after an initial period, linear with time throughout each experiment. This indicates that the stoichiometric stage of dissolution is not reached within the time-scale of these experiments.

The pH dependent steady-state rates of Si, Fe, Mg and Al release can be explained by:

$$R_{dissolution} = k_{acid}[H^+]^{n_{acid}} + k_{neutral} + k_{basic}[H^+]^{n_{basic}} \qquad (3\text{-}2)$$

This equation implies parallel reaction mechanisms for acid- and base catalysed dissolution reactions. Similar equations have been used by Wieland et al. (1988), Brady and Walther (1989) and Stumm and Wollast (1990) to describe chemical surface-controlled dissolution kinetics of binary oxides and silicates. Table 3-6 lists the constants fitted by the least square method to equation 3-2.

Table 3-6
Least square fitted values for the constants in the empiric rate law:

$$R_{diss} = k_{acid}[H+]^{n\text{-}acid} + k_{neutral} + k_{basic}[H+]^{n\text{-}basic}$$

for biotite dissolution ($CO_2$-free and 1 % $CO_2$ experiments)

| | Si | Fe | Mg | Al |
|---|---|---|---|---|
| Lg $k_{acid}$ | -5.75 ± 0.01 | -5.10 ± 0.17 | -5.27 ± 0.20 | -5.31 ± 0.07 |
| n-acid | -0.41 ± 0.01 | -0.51 ± 0.04 | -0.46 ± 0.04 | -0.40 ± 0.02 |
| lg $K_{neutral}$ | -7.15 ± 0.24[a] | --[c] | --[c] | --[c] |
| lg $K_{basic}$ | -10.31 ± 0.14[b] | -14.22 ± 0.23 | -9.97 ± 0.08 | -12.58 ± 0.24 |
| n-basic | -0.27 ± 0.09[b] | 0.65 ± 0.12 | 0.20 ± 0.04 | 0.54 ± 0.13 |

a) Valid in the $CO_2$-free system. b) Valid in the 1% $CO_2$ system.
c) $K_{neutral}$ was too low to be determined.

The dissolution is non-stoichiometric with preferential release of Fe, Mg and Al at low pH, and Si at higher pH. Only around pH 5 is the dissolution reaction stoichiometric. The incongruent dissolution will

cause a change of composition of the mineral. This change of composition will occur only in the outermost part of the mineral, the reacting-layer. To follow the dissolution behaviour of a complex mineral like biotite it is necessary to account for the composition as well as the depth of the reacting layer. It is reasonable to assume that the rate of release of an element (Si, Fe, Mg or Al) from the mineral at a single pH is proportional not only to surface area but also to the amount of the element in the reacting-layer:

$$R_j \propto [H^+]^n_{aq} \, N_j \, A_{BET} \qquad (3\text{-}3)$$

where

| | | | |
|---|---|---|---|
| N | amount in the reacting-layer | $A_{BET}$ | surface area |
| j | index for an element | R | dissolution rate |

We have used the release of potassium as a measure of the depth of the reacting-layer. The amount of an element in the reacting-layer is then given by equation (3-4) where $a_j$ is is calcualted from equation (2-2).

$$N_j = \frac{P_j}{P_{K^+}} a_{K^+} - a_j \qquad (3\text{-}4)$$

$P_j$ is the stoichiometric number of element (j) in the molecular formula of the mineral.

When the steady-state release rate is normalized to the amount in the reacting-layer according to:

$$R_j^* = \frac{R_j}{N_j} \qquad (3\text{-}5)$$

the trends in the pH dependence are qualitatively similar to the end-member (hydr)oxides (fig 3-9). The normalized release rate of silicon is independent of pH in the range 3 - 8.5. As for silica (Knauss and Wolery, 1988; Brady and Walther, 1990) the dissolution reaction is faster above this region but also at lower pH. The release rate of iron and aluminium is fractional order dependent on solution proton concentration showing similarities with the simple oxides $Al_2O_3$ and FeOOH studied by Furrer and Stumm (1986) and Zinder et al. (1986) respectively. The magnesium release rate is also fractional order dependent on pH in the acid region but independent of proton concentration above pH = 7.

### 3.1.5.1 Modelling of Release Rates of Non-Exchangeable Elements from Biotite

We model the observed dissolution behaviour in the $CO_2$-free system as three parallel reaction mechanism with the rates $R_{acid}$, $R_{neutral}$ and $R_{basic}$, each dominating in the acid, neutral and basic pH region respectively. The total dissolution rate is the sum:

$$R^* = R^*_{acid} + R^*_{neutral} + R^*_{basic} \qquad (3\text{-}6)$$

The activated complex for proton promoted dissolution reactions is postulated by Furrer and Stumm (1986) to be a surface site surrounded by Z protons. Wieland et al. (1988) suggests that the concentration of such a activated surface site is proportional to the mole fraction of protonated surface sites raised to Z.

$$R^*_{acid} = \kappa_{acid} X^Z_{>SOH_2^+} \qquad (3\text{-}7)$$

where X denotes a mole fraction, $>SOH_2^+$ denotes a protonated surface site and Z an integer value. We model the $R_{neutral}$ to be independent of proton concentration.

$$R^*_{neutral} = \kappa_{neutral} \qquad (3\text{-}8)$$

For the hydroxyl promoted dissolution we treat the activated state as being a site surrounded by Y deprotonated sites. The rate will then, analogous to the acid promoted reaction, be :

$$R^*_{basic} = \kappa_{basic} X^Y_{>SO^-} \qquad (3\text{-}9)$$

The acid base reactions of mineral surfaces are described by the following reactions for which the surface complexation model (Stumm and Morgan, 1981) can be used (see appendix 6.8):

$$>SOH \leftrightarrows >SO^- + H^+$$

$$>SOH + H^+ \leftrightarrows >SOH_2^+$$

In the modelling procedure we have fixed the Z=Y values for iron, magnesium, aluminium and silicon to 2, 2, 3, 4 respectively according to the postulation by Stumm and Wollast (1990) and Furrer and Stumm (1986) for Z to equal the oxidation state of the element. Then the rate and surface-acidity constants were varied to fit the data starting from acidity constants found in the literature (aluminum

oxide (8, -8.8,Caroll-Webb and Walther, 1988), iron oxide (7.3,-10,Bruno et al., 1992a) and silica (-3,-6.7,Schindler et al., 1976)). The surface speciation was calculated by the computer program C-Haltafall (Östhols, 1994) using the diffuse layer model (Dzombak and Morell, 1990) for electrostatic effects on the surface. The constants used for the model curves in figure 3-9 are listed in table 3-7. It is important to note that the model curves are adjusted to fit the data using the the combination of the surface complexation- and the activated complex- theory, indicating the usefulness of such an approach for a complex mineral like biotite.

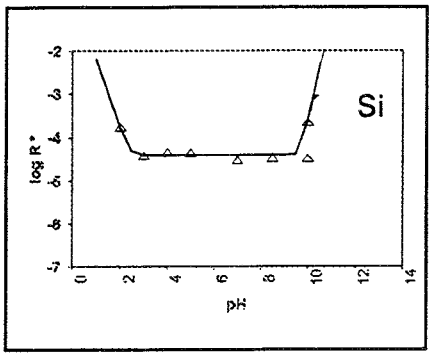


Figure 3-9a

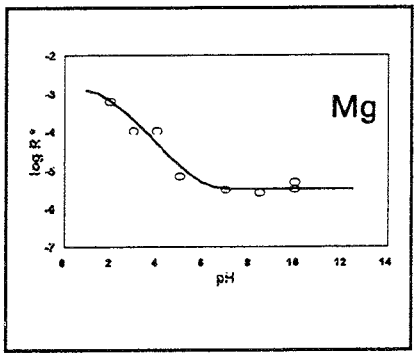


Figure 3-9c

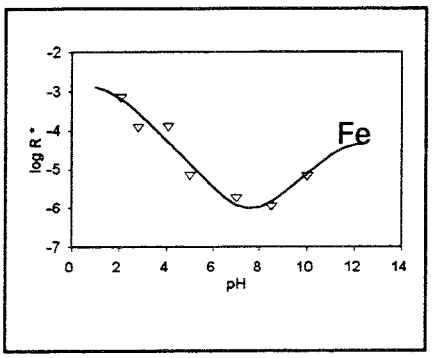


Figure 3-9b

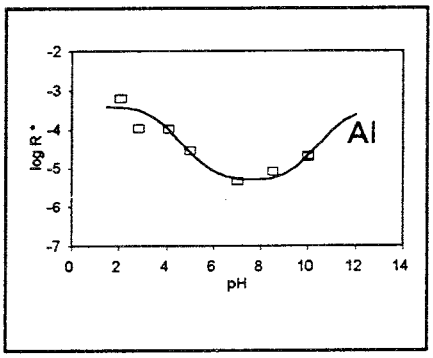


Figure 3-9d

Figure 3-9.
Log of normalized dissolution rates [moles biotite $m^{-2}$ $h^{-1}$ $moles^{-1}$] vs pH. Model curves (See text) are derived for the biotite end-member oxides from the combination of the surface complexation model for equilibrium at oxide surfaces (Stumm and Morgan, 1981) and the activated complex theory for mineral dissolution (Furrer and Stumm, 1986; Wieland et al., 1988). a) silicon b) iron c) magnesium d) aluminium.

Table 3-7
Model constants used in the surface-chemically-controlled dissolution rate modelling in figure 3-9.

| | Si | Fe | Mg | Al |
|---|---|---|---|---|
| $K_1$ (acidity constant) | 1 | 5 | 5 | 7 |
| $K_2$ (acidity constant) | -12 | -8 | -11 | -8 |
| $\kappa_{acid}$ (rate constant) | 2 | -2.8 | -2.8 | -3.4 |
| Z=Y | 4 | 2 | 2 | 3 |
| $\kappa_{neutral}$ (rate constant) | -4.4 | -6.3 | -5.5 | - |
| $\kappa_{basic}$ (rate constant) | 4.7 | -4.3 | - | -3.5 |

### 3.1.6 Conclusions

* The release of Mg, Fe and Al from biotite is highly pH dependant in the region $2<pH<10$ and qualitatively resembles the behaviour of the binary end-member oxides. The release of Si is independent of pH in the near-neutral pH region.

* Biotite dissolution is highly non-stoichiometric, on the time-scale of the experiment, with preferential release of Fe, Mg and Al in the acid region and Si in the near-neutral and alkaline region. The conceptual model of Schnoor (1990) for dissolution of complex oxides predicts that the dissolution will eventually be congruent and rate limited by the slowest surface controlled elemental release due to the formation of depletion layers.

* There is no significant effect of (bi)carbonate on Fe, Mg Al or K release from biotite. Si, on the other hand is released at a slower rate in the $CO_2$-system.

* The release of elements from chlorite is less pH dependent and less non-stoichiometric than the release from biotite. In the near neutral pH region the dissolution rates of the two minerals are similar.

* The release of potassium is diffusion controlled as indicated by a linear plot of accumulated release vs time.

We interpreted this as a formation of a potassium depleted surface-layer through which the reaction is diffusion controlled.

* The release of Si, Fe, Mg and Al is controlled by a surface reaction mechanism on the time-scale of the experiment. The pH dependence of the dissolution rate can be explained by parallel acid- and base-catalysed reactions.

## 3.2 RESULTS FROM EQUILIBRIUM EXPERIMENT

### 3.2.1 Wet-Chemistry Results

#### 3.2.1.1 Biotite

Figure 3-10 shows the equilibrium concentrations of elements in solutions contacted with biotite at specified conditions. Below pH ≈ 4 the solution concentrations are weakly pH dependent and the solution composition close to stoichiometric. At higher pH the solution concentration and composition are highly pH dependent. The results from the batch experiments and the titration experiments are in fair agreement. The silicon data show the biggest discrepancy with lower concentrations obtained from the batch experiment than from the titration experiment. This may be due to extensive alteration of the solid phase at extreme pH, prior to equilibration at higher pH during the continuous titration.

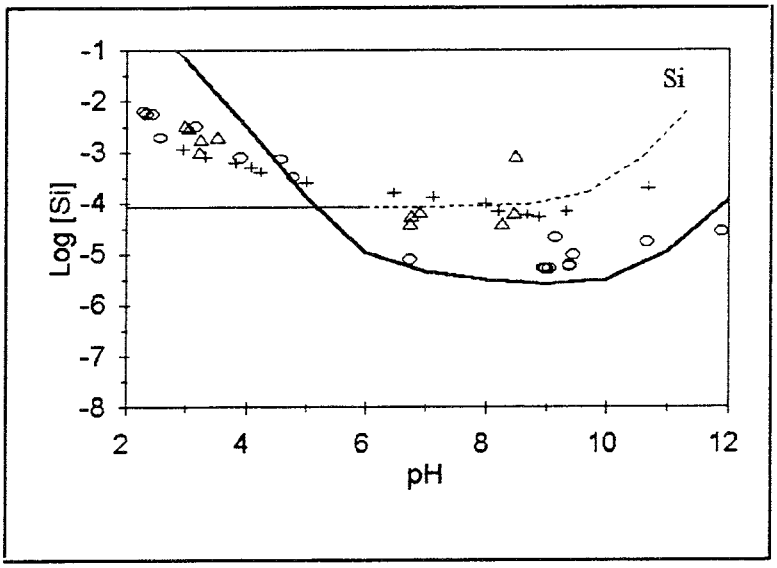


Figure 3-10a

Figure 3-10a
Solution concentrations in experiments where biotite has been reacted with ionic medium ($CO_2$-free experiment). Model curves represent solubility of secondary phases calculated by Harphreeqe. O Batch experiments; + titrations started at low pH; ▵ titrations started at high pH. a) Si. - - - Quartz- —— Clay-solubility. The modelling and model curves are discussed in section 3.2.4.

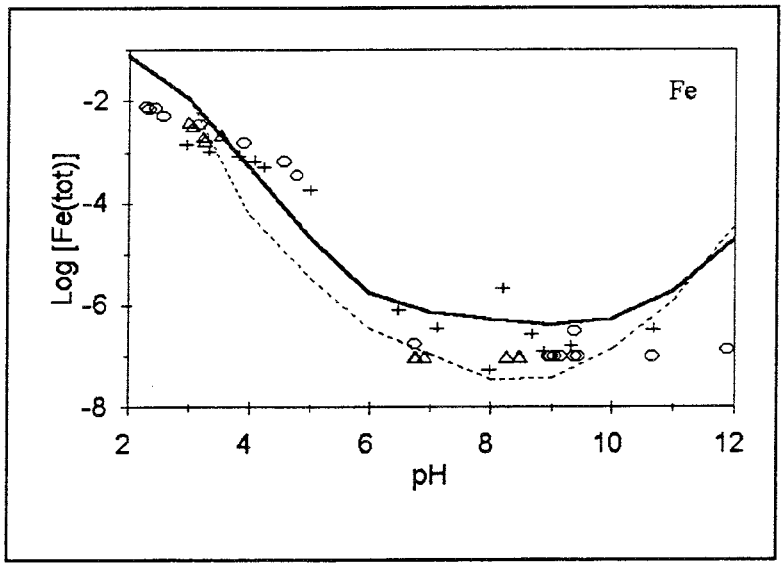


Figure 3-10b

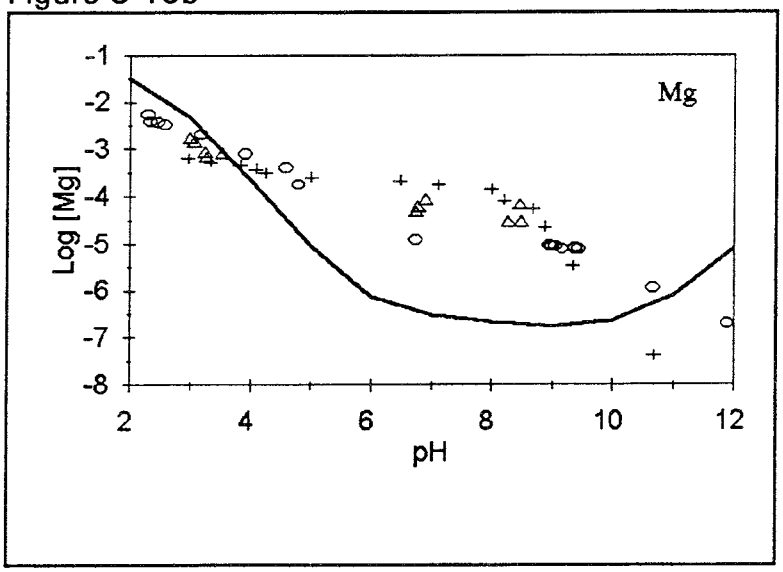


Figure 3-10c

Figure 3-10b,c.
Solution concentrations in experiments where biotite has been reacted with ionic medium ($CO_2$-free experiment). Model curves represent solubility of secondary phases calculated by Harphreeqe. O Batch experiments; + titrations started at low pH; ▵ titrations started at high pH. b) Fe. - - - amorphous Fe(III)-(hydr)oxide-, —— Fe(II)-clay-solubility; c) Mg ——Fe(II)-clay-solubility. The modelling and model curves are discussed in section 3.2.4.

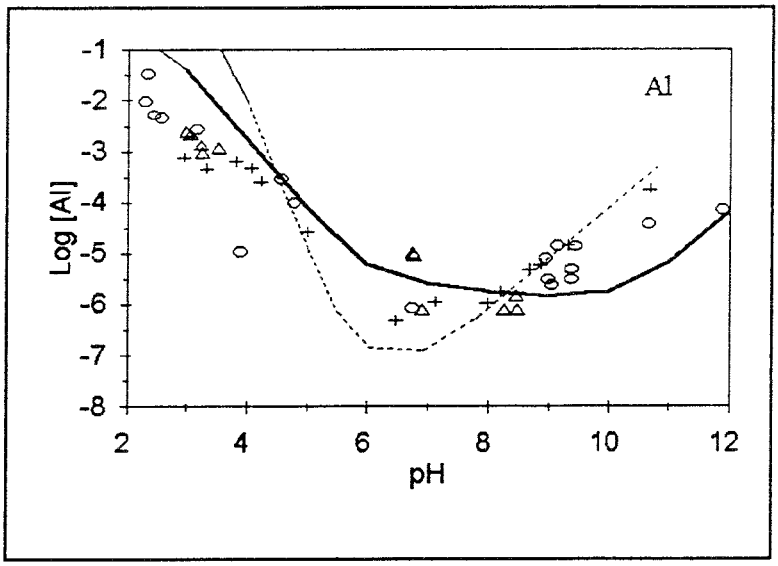


Figure 3-10d

Figure 3-10d
Solution concentrations in experiments where biotite has been reacted with ionic medium ($CO_2$-free experiment). Model curves represent solubility of secondary phases calculated by Harphreeqe. O Batch experiments; + titrations started at low pH; ▵ titrations started at high pH. d) Al - - - Gibbsite —— Fe(II)-Clay. The modelling and model curves are discussed in section 3.2.4.

Calculation of the saturation index, SI ($SI = lgQ - lgK_s$, where Q is the actual ion product corresponding to the solubility constant) for samples (pH 0.3; 1.3; 2.3; 3.2; 3.9; 4.8; 6.7; 9.0 and 10.7) from the batch experiments by the computer program Harphreeq (Brown et al., 1991) using the Hatches database (Cross and Ewart, 1989) shows that in the pH region $0.3 < pH < 3.9$ the solution is over-saturated with respect to "simple" Si-phases like quartz, cristobalite and amorphous $SiO_2$. At near neutral pH the SI indicates over-saturation to several phases, for example gibbsite, kaolinite, illite, paragonite and some smectites (eg beidellite, montmorillonite, and nontronite) and some zeolites (eg heulandite and mordenite). At pH 10.7 the solution is oversaturated to chrysotile, nontronite, saponite, phlogopite and talc.

Mass balance calculations for the pH region $0.3 < pH < 3.9$ show an relative enrichment of Si in the solid material. In the near neutral pH region corresponding calculations show relative enrichment of Fe and depletion of Mg in the solid material.

In the biotite-$H_2O$-$CO_2$(g)-system Mg, Al and Si concentrations do not significantly differ from the $CO_2$-free system. Fe shows higher solution concentrations at high pH when (bi)carbonate is present which may be due to the formation of Fe(II)- (Bruno et al., 1992b) or Fe(III)- (Bruno et al., 1992a) (bi)carbonate-complexes.

The concentration of potassium in solution is about $10^{-3}$-$10^{-2}$ M in the entire pH/$P_{CO2}$ region studied. This probably reflects an ion-exchange reaction. Table 3-8 lists the total iron concentrations and the pe-values obtained in a continuous titration. The $E_h$-values are low, and indicate the preferential release of Fe(II).

Table 3-8
Total iron concentrations and $E_h$-values from a continuous biotite titration experiment.

| pH | Log Fe(tot) | $E_h$(GC) [mV] | $E_h$(Pt) [mV] | $E_h$(Pt) [mV] | $E_h$(Au) [mV] |
|---|---|---|---|---|---|
| 3.55 | -3.01 | 214.6 | 392.5 | 412.3 | 371.0 |
| 3.17 | -2.73 | 169.3 | 383.2 | 393.0 | 383.2 |
| 3.24 | -2.76 | 314.9 | 434.3 | 440.5 | 433.0 |
| 3.53 | -2.66 | 370.3 | 446.7 | 459.9 | 449.0 |
| 3.06 | -2.47 | 385.1 | 470.2 | 470.7 | 470.0 |
| 2.98 | -2.40 | 443.9 | 484.6 | 482.5 | 484.5 |
| 3.23 | -2.69 | 337.6 | 455.1 | 455.8 | 456.4 |
| 2.91 | -2.44 | 548.2 | 552.6 | 552.6 | 552.6 |
| 3.37 | -2.51 | 545.2 | 547.7 | 547.7 | 547.7 |
| 2.12 | -2.58 | 623.4 | 627.2 | 627.2 | 627.2 |
| 2.38 | -2.61 | 614.6 | 617.8 | 617.8 | 617.8 |
| 3.31 | -2.61 | 381.5 | 473.4 | 476.4 | 473.9 |

GC - Glassy carbon electrode; Pt - Pt-sheet electrode; Au - Au-sheet electrode.

### 3.2.1.2 **Chlorite**

A small number of batch equilibrium experiments in the $H_2O/CO_2$ system has been made with chlorite to make comparisons with biotite. The output concentrations of iron, magnesium and silicon are very similar to the one obtained from biotite indicating that the same secondary phases are controlling the solubility in both systems. However, the aluminium concentrations are lower in the case of chlorite at pH above 9. Another difference is the lower tendency of chlorite to buffer the pH.

### 3.2.2 **XPD Results** (Biotite)

Figure 3-11 shows the XPD pattern of mineral phases from the biotite batch equilibrium experiments. At pH≤2.6 there is no expansion of the inter-layer (compare section 3.1.2). At higher pH (pH≥3.6) the d(001) peak shifts towards longer distances, indicating an expansion of the interlayer. The main peak is found around $2\theta$ = 8.4 deg (12 Å) indicating the formation of a sodium smectite or a hydro-biotite (compare section 3.1.2), however the additional peak at $2\theta$ = 7.1 deg (14 Å) is typical for a vermiculite (Brindley and Brown, 1980, table 5.18).

Consistent with the kinetic experiments the typical peaks for kaolinite are found in several samples (up to pH 4.6). No other crystalline secondary metal oxide or simple silicate is found. However, at pH 0.3, some broad low-intensity peaks are present, indicating the formation of a semi-amorphous phase.

In some of the patterns (figure 3-11 and appendix 7.9) the existence of a peak around $2\theta$ = 25 deg (5 Å) is present. Fanning et al. (1989) ascribe such peaks to an Al-rich octahedral sheet in the mica structure. This peak can also be due to vermiculite (Brindley and Brown, 1980, table 5.18) or gibbsite (Wilson, 1966; Brindley and Brown, 1980, table 5.18).

The location of the d(060) peak (1.51-1.56 Å) corresponds for all samples to a trioctahedral structure (Fanning et al., 1989).

### 3.2.3 **SEM/Micro Probe Analysis**

Figure 3-12 shows the SEM image of some of the samples from the batch equilibrium experiment. The images of these samples ( 0.3<pH<2.3) indicate that there is a tendency for breaking up the structure at extremely low pH. At pH 0.3 small islands of precipitates are found on the basal plane (Figure 3-12c). The examination of this plane by micro probe reveals an enrichment of silicon (table 3-9).

Micro probe analysis (table 3-9) of these solids indicates that any sodium enrichment observed is due to sodium perchlorate retention. Consistently there is no significant depletion of potassium. At pH 0.3 there is a significant loss of K, Mg, Fe and Al. When the analysis is done with the electron beam parallel to the basal plane
($\perp$ to the paper plane in figure 3-12) no K, Mg, Fe or Al is detected.

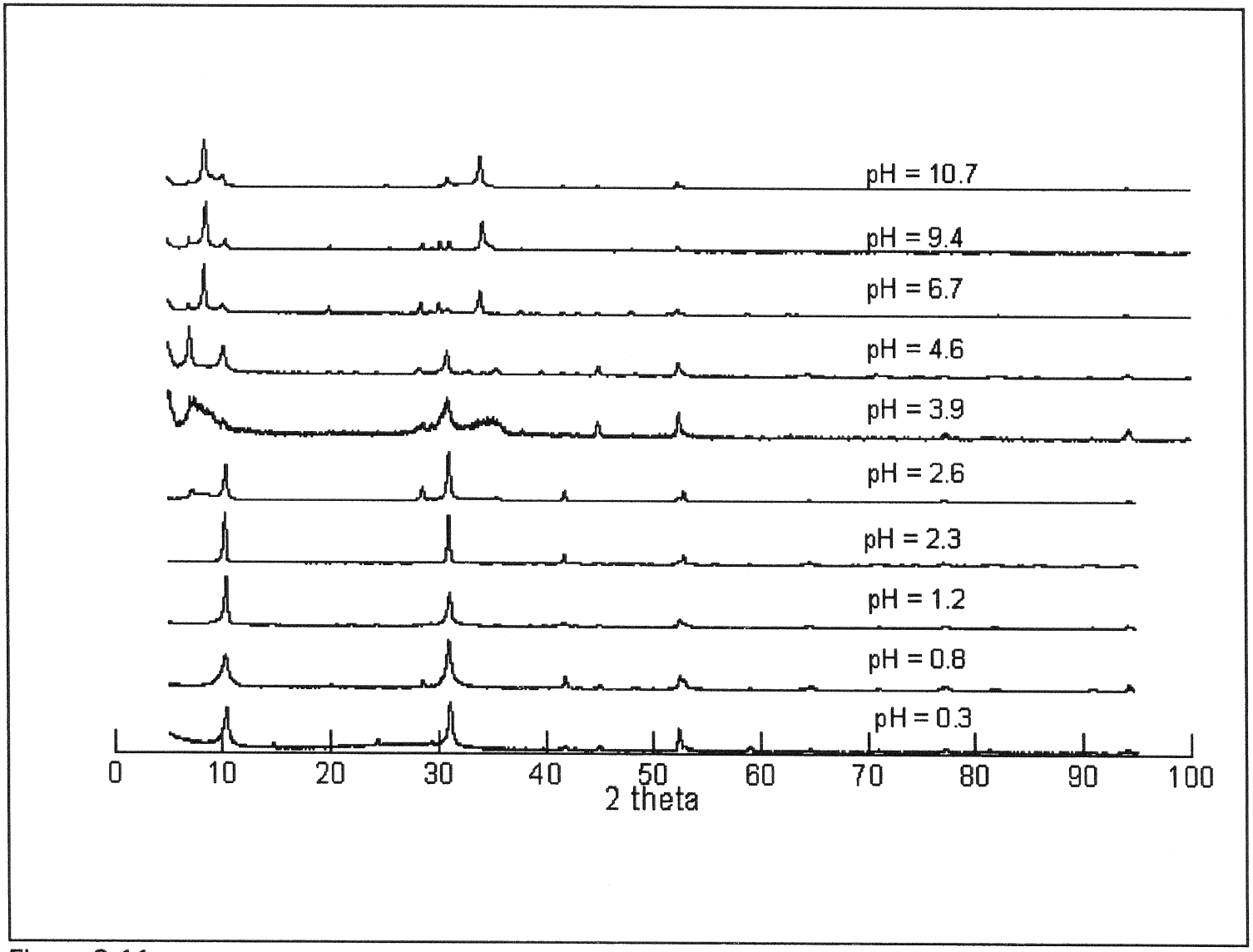


Figure 3-11
XPD reflections from mineral samples reacted in the biotite batch equilibrium experiment.

Table 3-9
Micro-probe analysis [mole %] of minerals from the biotite batch experiments.

| | K | Na | Si | Fe | Mg | Al | Cl |
|---|---|---|---|---|---|---|---|
| Fresh | 6.8 | 0 | 18 | 8 | 4 | 5.4 | - |
| pH 2.3 | 6.5 | 0.2 | 19 | 8 | 4 | 5.4 | 0.3 |
| pH 1.2 | 4.3 | 1.4 | 21 | 6 | 3.3 | 4.1 | 1.4 |
| pH 0.3 (in plane) | 0 | 0 | 38 | 0 | 0 | 0 | 0.3 |
| pH 0.3 (parallel to plane) | 0 | 0 | 22 | 4.5 | 0.7 | 1.7 | 0.8 |

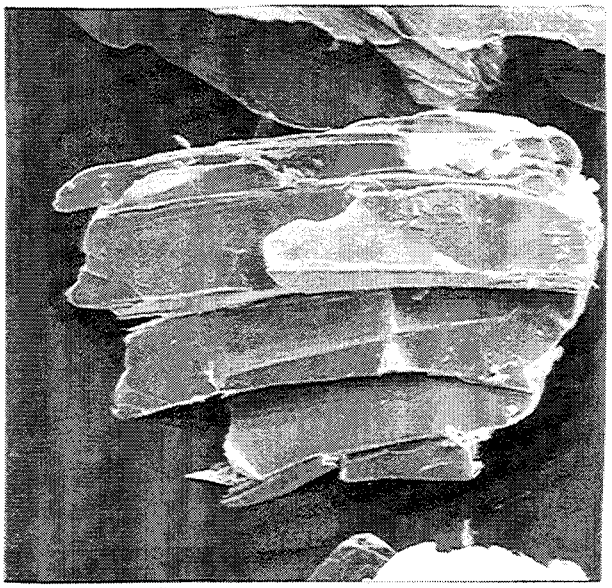

Figure 3-12a.

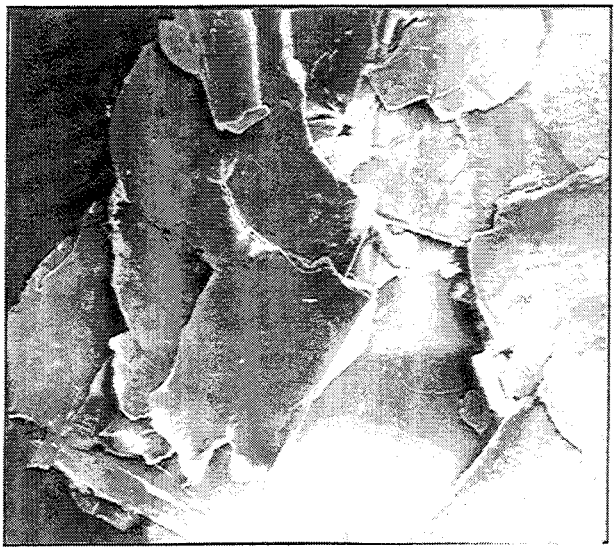

Figure 3-12b.

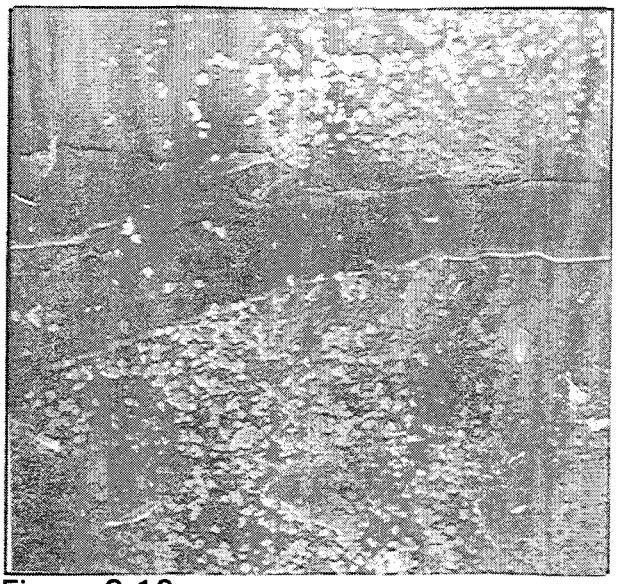

Figure 3-12c.

Figure 3-12.
SEM images of mineral remainder from the biotite batch experiments at different pH ($CO_2$(g)-free). a) pH = 2.34 (Magnification 330), b) pH = 1.18 (Magnification 200), c) pH = 0.3 (Magnification 4000). Note that even at low pH the sheets are not broken or opened up. At extreme conditions (c) small islands of precipitates are formed on the surface. The solid is highly enriched in Si according to micro probe analysis.

### 3.2.4 Discussion (biotite)

In the literature no solubility constant for biotite is reported. Helgeson (1978) points out the difficulties of determining thermodynamic properties of ferrous/ferric aluminosilicates due to the ambiguity concerning the redox state of iron. We have estimated (see appendix 6.7) the free energy of formation ($\Delta G^0_{f,298.15}$) for biotite ($K(Mg_2Fe)(Si_3Al)O_{10}(OH)_2$) using the polymer model outlined by Sposito (1986) for smectites. This model is an improvement of earlier methods ((Slaughter, 1966; Tardy and Garells, 1974; Nriagu, 1975; Chen, 1975; Mattigod and Sposito, 1978) for estimation of the $\Delta G^0_{f,298.15}$ of phyllosilicates from Gibbs free energy of formation of its end-member (hydr)oxides. The Gibb's free energy for formation of biotite was used, in combination with literature data (Sposito, 1986) on $\Delta G^0_{f,298.15}$ for aqueous species, to estimate (see appendix 6.7) the solubility constant ($lgK_s = 40 \pm 2$) corresponding to the following reaction:

$$K(Mg_2Fe)(Si_3Al)O_{10}(OH)_2(s) + 10\ H^+ \rightarrow K^+ + 2Mg^{2+} + Fe^{2+} + 3H_4SiO_4 + Al^{3+}$$

The estimated constant is reasonable compared to solubility constants of other micas given in the Hatches database (Cross and Ewart, 1989), i.e phlogopite $lgK_s = 38.22$, muscovite $lgK_s = 14.56$ and paragonite $lgK_s = 18.48$ . This solubility product indicates that biotite is highly unstable towards weathering. We have constructed a predominance diagram (fig 3-13) valid for our experimental conditions including several possible secondary weathering products. The diagram shows that biotite is stable only at high pH and low pe. It also shows that clay minerals are the thermodynamically most important weathering products at neutral pH and moderate pe.

Consistent with the low stability of biotite, the equilibrium data is not explained by stoichiometric dissolution of biotite (reaction given above), but rather by 1) exchange of the inter-layer ion (see section 3.2.4.3); 2) the formation of secondary solubility controlling solids by non-stoichiometric transformation of biotite and/or precipitation (see section 3.2.4.1).

In spite of the predicted instability of biotite, the XPD reflections of the reacted mineral phases all show the characteristic d(001) peak of micas. We interpret the presence of biotite as a core of unaltered biotite covered by secondary mineral phases. The biotite is prevented from further dissolution due to blocking of the reactive biotite surface by secondary weathering products.

The XPD reflections of the mineral phases from experiments at higher pH all indicate the characteristic expansion of the silicate

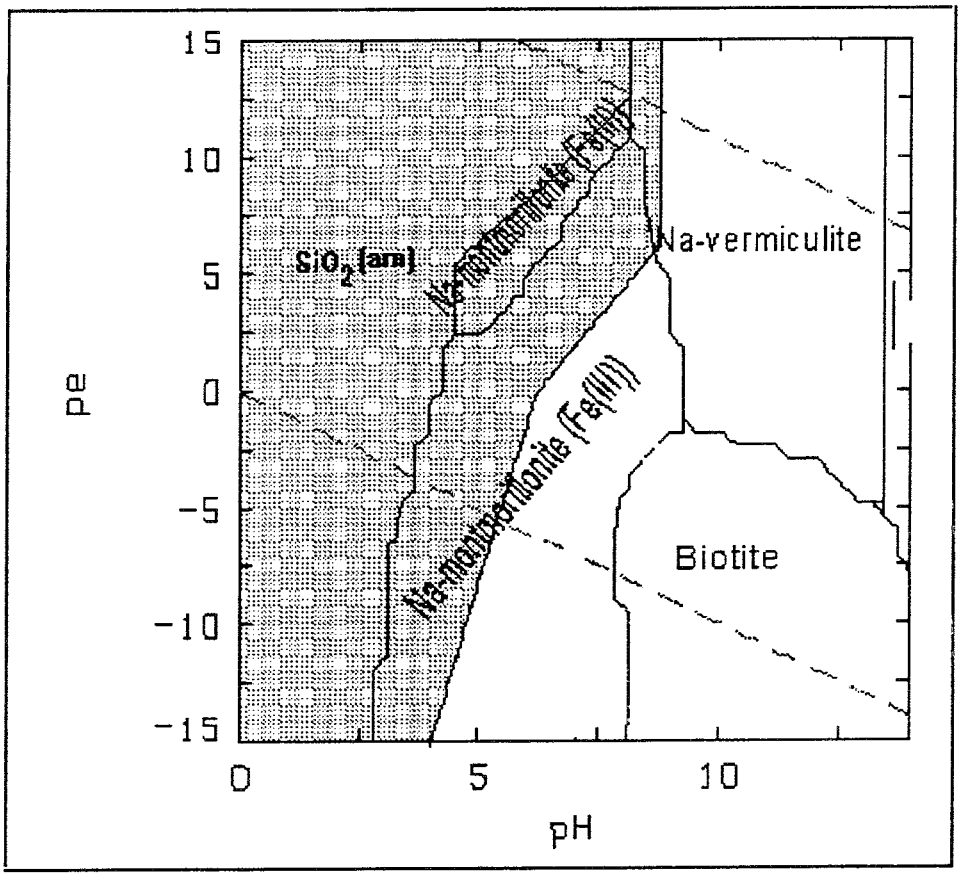


Figure 3-13.
Predominance diagram calculated, using the SED computer program (Puigdomènech and Åberg, 1987), for 1 mM biotite (ideal) in 0.5 M $NaClO_4$. Si is the main component. Grey area represents quartz stability.
The following solid phases have been considered:
Brucite [a], $Fe(OH)_3(s)$[b], Na-Montmorillonite (Fe(II) and Fe(III))[c], K-Montmorillonite (Fe(II) and Fe(III))[d], Na-Montmorillonite (Fe(II) and Fe(III))[c], Na-vermiculite[c], K-vermiculite[d], Biotite[c], Gibbsite[a], $SiO_2$(am)[a], Quartz[a,e]. Only mono-nuclear hydrolysis species[a] were considered.
a) Constant taken from the Hatches database (Cross and Ewart, 1989); b) $lgK_s = 2.5$ (see section 3.2.4.2); c) $\Delta G^0_{f,298.15}$ estimated accordingly to Sposito (1986) (See appendix 7.7); d) $lgK_s$ taken from the Na saturated mineral; e) stability field given by the shaded area.

structure. This is due to the introduction of hydrated (or hydrolysed) ions and/or water in the interlayers, i.e formation of a clay mineral. We have not been able to identify the specific type or composition of the clay from the present data set. To determine the type of clay mineral, i.e smectite, vermiculite or inter-layered clay, specific X-ray methods are required, relating d(001) spacings to the structure of oriented mineral samples following specific chemical or heat treatments (Caroll, 1970; Brindley and Brown, 1980; Moore and Reynolds, 1989). The elemental composition of the clay could not be calculated by mass balance equations for the experimental systems since 1) the amount of biotite altered is unknown; 2) the amount of "simple" secondary phases precipitated is not determined. The micro probe analysis (table 3-9; sample pH 2.3) could not be used for calculations on the clay mineral stoichiometry since the detected amounts of Fe, Mg and Al are, within experimental uncertainties, identical to the unreacted biotite. Consistently, the X-ray pattern of the mineral remainder from the batch experiments (Figure 3-11; pH 2.3; pH 2.6; pH 3.9 and pH 4.6) reveals that biotite is the dominating phase in the low pH-region. Again, we interpret this as a core of biotite covered by secondary mineral phases.

3.2.4.1 Solubility Controlling Phases

Stoichiometric dissolution of biotite according to

$$K_{0.8}(Mg_{0.84}Fe^{II}_{1.10}Fe^{III}_{0.22}Al_{0.49})(Si_{3.18}Al_{0.82})O_{10}(OH)_2 + 9.28\ H^+ + 0.72\ H_2O \dashrightarrow 0.8\ K^+ + 1.1\ Fe^{2+} + 0.22\ Fe^{3+} + 3.18\ H_4SiO_4(aq) + 1.31\ Al^{3+} + 0.84\ Mg^{2+}$$

would give a strong pH dependence for the solubility. However, the data show a weak pH dependence in the acid pH region indicating that secondary phases are formed.

Although SI-calculations show that the solutions are not saturated with respect to biotite below pH 10, the XPD patterns of the reacted minerals indicate that biotite is a main constituent of the solid material. We interpret this as a core of biotite covered by secondary, solubility controlling phases. Batch experiment ($2 < pH < 12$) run with different biotite to solution ratios (0.7 - 18 g/l) and equilibrated under different periods of time (7-60 days) show approximately the same element concentrations indicating that the solution composition is not kinetically controlled in this pH region.

The solubility data is best illustrated by separating the data points into three pH-regions, the very acid region ($pH < 2$), the acid region ($2 < pH < 4.5$) and the near-neutral to alkaline region ($pH > 4.5$).

In the very acid region (2<pH, not shown in figure 3-10, see appendix 7.4) the solution concentration and composition is most likely not controlled by solution-mineral equilibrium, but rather by kinetic effects such as slow break down of the sheet structure and diffusion through surface precipitates, causing the very low pH-dependence of solution concentration of Si, Fe, Mg and Al. This idea is supported by the SEM-images of a biotite sample reacted at pH 0.3 shown in figure 3-12c, where small islands of precipitates rich in Si (micro probe analysis; table 3-9) are seen on the cleavage plane, and figure 3-12c, where the break-up of the sheet-structure is shown. The XPD pattern of this sample has, superimposed on the pure biotite reflection peaks, some broad humps indicating the presence of substantial amounts (>5% for detection by XPD-methods according to Caroll (1970)) of "semi-amorphous" material. Mass-balance calculations on solution/mineral composition show the solid to be rich in Si. These observations are consistent with a surface coverage of amorphous silica. It is not likely that the solution is in equilibrium with this phase since 1) SI-calculations show that the solution is oversaturated; and 2) there is a pH dependence in the Si concentration. Kittrick (1969) states that super saturation with respect to amorphous $SiO_2$ and quartz is often encountered in natural and laboratory systems and attributes this to the slow precipitation/dissolution rate of these phases.

In the less acid region (2<pH<4.5, figure 3-10) the solution concentrations of elements are close to stoichiometric. The pH trend in solution concentrations of Mg, Si and Al can not be explained by equilibrium with simple secondary phases (figure 3-10). The solubility is more probably controlled by a complex alteration product of biotite, i.e a clay mineral. The X-ray pattern of the mineral remainder from the batch experiments (Figure 3-11; pH 2.3; pH 2.6; pH 3.9 and pH 4.6) reveals that biotite is the dominating phase in the low pH-region. Again, we interpret this as a core of biotite covered by secondary mineral phases. Kaolinite was identified by means of its XPD pattern in some of the samples from this pH region. A plot (not shown) of pH -1/3 pAl vs pSi yields a line with the slope $1.1 \pm 0.2$ which deviates from the theoretical slope of 1/3 for solutions in equilibrium with kaolinite. This indicates that the solution composition is not controlled by the solubility of this phase. The disequilibrium with respect to kaolinite, although present, may be due to kinetic effects like 1) slow conversion of a clay into kaolinite; or 2) slow precipitation from an oversaturated solution.

Since the solution concentrations of Fe(II) are close to stoichiometric to Si, Al and Mg in this pH-region, it is probable that the same solid phase is controlling the solubility of these components. No pure Fe(II)-clay is reported in the literature. However, since most of the clays

that have been reported are found in soils, which generally are in contact with oxic surface water, Fe(II)-clays may not necessarily be as infrequent as their absence in the literature indicates. Laaksoharju et al. (1994) report elemental stoichiometry of precipitates found, at reducing conditions (characteristic $E_h$ = -250 mV), in the redox zone at the Äspö Hard Rock Laboratory. They concluded that the Si/Al ratio in the examined precipitates is typical for clay minerals, and suggested the formation of a smectite or a mixed layer (illite/smectite) clay. The elemental composition of the precipitates corresponds to the formula:

$$Na_{0.343}K_{0.455}Ca_{0.180}(Mg_{0.230}Fe^{II}_{0.554}Al_{1.297})(Si_{3.381}Al_{0.619})O_{10}(OH)_2$$

The calcualted content of interlayer ions (Na, K and Ca), which is very high, is probably erranous and may be explained by the prescence of sodium-, potassium- or calcium salts in the analysed samples.

We have used a sodium clay with a composition corresponding to the one given above to model our biotite data. Our experiments were carried out in 0.5 M $NaClO_4$ making a Na-clay the most probable to form (see section 3.2.4.3). We estimated the solubility product of the clay as we did for biotite (appendix 7.7). The model line in figure 3-10, represents the solubility of this clay ($Na_{1.19}(Mg_{0.23}Fe^{II}_{0.55}Al_{1.29})(Si_{3.38}Al_{0.62})O_{10}(OH)_2$) in 0.5 M $NaClO_4$ calculated by the Harphreeq-program (Brown et al., 1991). Although the experimental data does not fit the model curves exactly, the clay solubility can explain the pH trend in the solution concentrations of elements and predict the right order of magnitude for actual concentrations.

Our model is simple, it only includes the solubilty of one secondary phase. A rigourous model for our laboratory system would have to include 1) dissolution of biotite; 2) precipitation of secondary phases; and 3) ion-exchange reactions. Such a model would account for the stoichiometry of the various reactions, and may, for example, better explain the observed high concentrations of magnesium. However, a simple solubilty model, like the one outlined here, may be appropriate for a natural fracture zone where dissolved ions are continously transported away.

Our redox measurements indicates that the Fe(II)/Fe(III) ratio in solution is high, $10^2$-$10^6$. The Fe(III)-concentration in solution is not stoichiometric to Fe(II) or any of the other elements. This indicates that another phenomenon than clay-solubility is controlling the Fe(III) concentration, possibly the solubility of a Fe(III)-(hydr)oxide (see section 3.2.4.2).

In the near-neutral to alkaline pH region the solution concentration of

Si (Fig 3-10a) seems to be controlled by quartz in the titration experiment. In the batch experiments a clay mineral is more likely the one controlling the solubility. The difference in results from the two experimental methods may be explained by the fact that the titrations where started at extreme pH (3 and 9 respectively) and the solution may in these cases have been quickly oversaturated with respect to both solids, quartz being the kinetically favoured to precipitate although more soluble. Aluminium concentration (fig 3-10d) seems to be controlled by gibbsite.

Equilibrium concentrations of iron from the batch and the titration experiments are similar. Since no redox speciation is available in this pH region, we can only consider the two limiting cases where the total iron concentration is dominated by one of the redox states:

1) If total iron reflects Fe(III), i.e Fe(II) released from the biotite has been oxidized by trace amounts of oxygen, the solubility is apparently controlled by amorphous Fe(III) hydroxide.

   In the batch experiments a solution concentration of molecular oxygen on the order 0.1 mg/l would be enough to quantitatively oxidize any Fe(II)-released, assuming that Fe(II) release is stoichiometric to Mg release. In spite of the precautions to exclude oxygen from the experiments, it cannot be excluded that such low trace concentrations of oxygen were present. In titrations, going from acid pH to the alkaline pH region, the $E_H$ measurements indicate Fe(II) to be the dominant redox species at low pH. A pathway for Fe-depletion in solution, when going towards more alkaline conditions, would then be 1) oxidation of Fe(II) followed by 2) precipitation of an Fe(III)-hydroxide. From the solution concentrations of iron at different pH, a consumption of oxygen necessary to oxidize relevant amounts of Fe(II) can be estimated on the order $\approx 3$ mg/l around pH 5. Although it is possible that the gas stream purging the solution carried some trace amounts of oxygen it is not plausible that it supplied such amounts. From this we can conclude that at least in the case of the titration experiments it is not plausible that Fe(tot) reflects only Fe(III).

2) If, on the other hand, total iron is dominated by Fe(II), any Fe(III) released from the biotite has precipitated as a less soluble Fe(III) (hydr)oxide. This is consistent with the solubility product found for Fe(III) hydroxide formed in the less acid pH region (see section 3.2.4.2) The total

iron concentration is too low to be controlled by a Fe(II)-(hydr)oxide or simple Fe(II)-silicate (fayalite).

The concentration of magnesium (Figure 3-10c) in solution is likewise far too low to be explained by brucite ($Mg(OH)_2$) or magnesium silicate (chrysotile, sepiolite, forsterite, enstatite) equilibrium. The solution concentration of Fe(II) and Mg may instead be controlled by equilibrium with a clay mineral. Alternatively, the concentration of these elements could be kinetically controlled. When biotite dissolves in a batch or titration experiment, the solution rapidly becomes oversaturated with respect to some secondary mineral phases. These phases may precipitate on the biotite surface, yielding a biotite core covered by precipitates and alteration products. Elements that are not in equilibrium with secondary phases may be prevented from further accumulation in solution due to dissolution inhibition by weathering products blocking the reactive biotite surface.

### 3.2.4.2 Redox Conditions

The experimental determination of redox conditions was only possible in the acid pH region. At higher pH (pH>4) the solution redox buffer capacity was to low to make $E_h$ measurements possible. The redox potential is clearly determined by the Fe(II)/Fe(III) redox couple since no other redox couple is present in the system. The redox potential is given by the expression:

$$e = e^0_{Fe^{2+}/Fe^{3+}} + g\,lg\frac{[Fe^{3+}]}{[Fe^{2+}]} \qquad (3\text{-}10)$$

Where $e^0$ is the standard potential [mV], and g the nernstian factor (59.16 mV at 25 °C).

We test the hypothesis that the $Fe^{3+}$- concentration is determined by '$Fe(OH)_3$ (s)' solubility :

$$'Fe(OH)_3\ (s)' + 3H^+ \rightleftarrows Fe^{3+} + 3\ H_2O$$

$$\log K_s = lg[Fe^{3+}] + 3 * pH \qquad (3\text{-}11)$$

Grenthe et al. (1992) demonstrate how experimental $E_H$/pH/$Fe^{2+}$ data can be used to determine a solubility product for the semi-amorphous iron-hydroxide by combining equations 3-10 and 3-11:

$$e = e^{0}_{Fe^{2+}/Fe^{3+}} + g \log K_s - g\,([Fe^{2+}] + 3pH) \qquad (3\text{-}12)$$

We do not have Fe(II) measurements in our data set. However, since the pH and $E_h$ are low, the following approximation seems reasonable:

$$[Fe(tot)] = [Fe(II)] + [Fe(III)] \approx [Fe^{2+}] \qquad (3\text{-}13)$$

Using the data in figure 3-14 we estimated $\log K_s = 2.48 \pm 0.17$ (error estimate given as one standard deviation) for $Fe(OH)_3(s)$. The slope of the fitted line in figure 3-14, which equals g, and the actual value of log $K_s$, close to what is found for amorphous iron (hydr)oxides, validates our model.

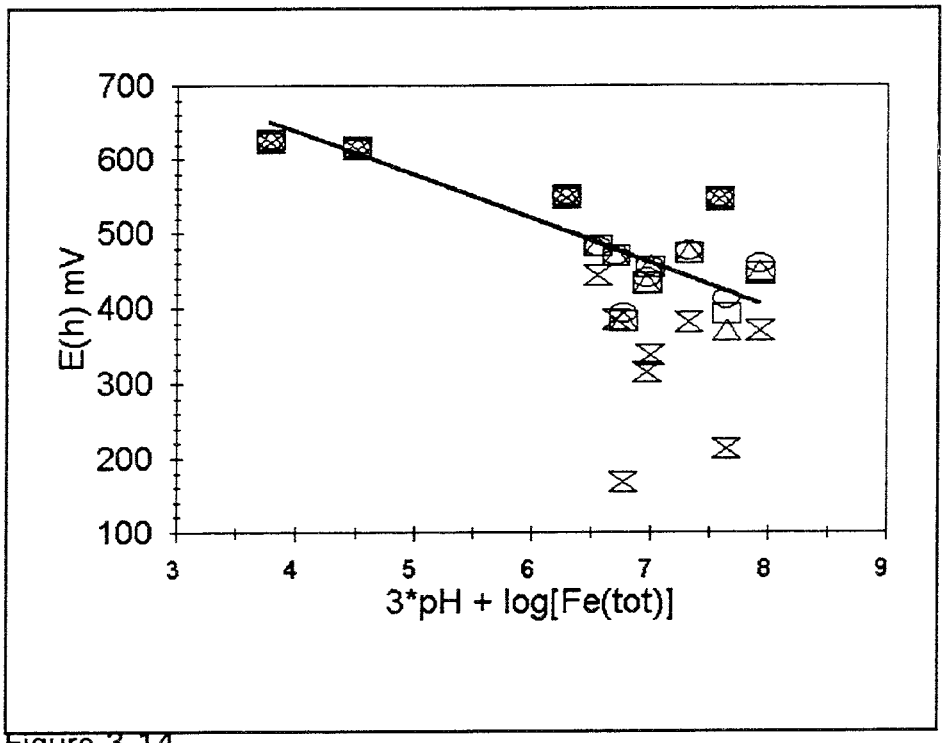


Figure 3-14.
E(h) vs log[Fe(II)] + 3pH from the titration started at the acid side. The line has the theoretical slope of g and represents the best fit to the data points. Electrodes: X Glassy carbon; □ sheet Pt; ○ sheet Pt; Δ sheet Au.

3.2.4.3 Ion-exchange reactions

The concentration of potassium in solution is about $10^{-3}$-$10^{-2}$ M in the whole pH region studied. This can be explained by an ion-exchange reaction according to:

$$\text{K-Biotite} + Na^+(\text{hydrated}) \rightarrow \text{Na(hydrated)-clay} + K^+$$

(By definition (Fanning et al., 1989; Brindley and Brown, 1980) micas are 2:1 phyllosilicates with non-hydrated interlayer ions. Smectite and vermiculite (clays) are 2:1 phyllosilicates with hydrated interlayer ions and/or contains molecular water in the interlayer. A "Na-biotite" should rather be named "Na-clay". Usually the transformation of biotite to a clay causes changes in the silicate-structure in addition to the exchange of inter-layer ions. (Fanning et al., 1989, and references therein.))

The micro probe analysis (table 3-4 and 3-9) shows depletion of potassium and enrichment of sodium in the mineral during the experiments. This is consistent with the ion-exchange reaction suggested above. In the most acid region, protons might be competing with sodium in the exchange reaction. The equilibrium expression for the reaction given above is:

$$K_{Na} = \frac{[K^+]\{Na\text{-}mineral\}}{[Na^+]\{K\text{-}mineral\}} \qquad (3\text{-}14)$$

where curved brackets refers to exchange sites [moles/l] in the mineral. The density of exchangeable sites, $S_T$ [moles/g], is given by:

$$\frac{m}{V} S_T = \{Na\text{-}mineral\} + \{K\text{-}mineral\} \qquad (3\text{-}15)$$

where m is mass [g] of mineral and V [l] is total volume in the experiment.

A mass balance on K gives the additional equation:

$$[K^+] = \{Na\text{-}mineral\} \qquad (3\text{-}16)$$

$K_{Na}$ and $S_T$ are too strongly correlated to both be fitted from the data set. Exchange constants for monovalent metal ions on clays are usually close to 1 (Fletcher and Sposito, 1989). Using this assumption, $S_T$ is estimated to be $0.0011 \pm 0.0002$ moles/g for the 75-125 $\mu$m size-fraction (error estimate is based on one standard

deviation).

### 3.2.5 Conclusions

* Biotite is only thermodynamically stable at conditions of high pH and low pe. At moderate pH and pe, clay minerals are the thermodynamically most important weathering products.

* When biotite dissolves in a closed system the solution rapidly becomes oversaturated with respect to some secondary mineral phases. These phases may precipitate on the biotite surface, yielding a biotite core covered by precipitates and alteration products. The biotite may then be prevented from further dissolution due to blocking of the reactive biotite surface by secondary weathering products.

* At very acid pH (pH $< 2$) the solution composition is not controlled by mineral - solution equilibrium. The flat pH dependence and the presence of biotite is explained by kinetic control of the dissolution.

* At less acid pH ($2 < pH < 4.5$) solution concentrations of Al, Fe(II), Mg and Si are apparently controlled by a clay mineral. Fe(III) concentrations are controlled by an amorphous Fe(III) (hydr)oxide.

* In the near-neutral to basic pH region different solubility models can be applied:

  Fe a) Fe(tot) is controlled by a Fe(II)-clay or kinetic effects. Fe(III) is controlled by a Fe(III)-hydroxide.

  or

  b) Fe(tot) is controlled by an amorphous Fe(III)-hydroxide. Fe(II) is oxidized by trace amounts of oxygen.

  Al Aluminium concentrations are controlled by gibbsite.

  Mg Mg is controlled by clay equilibrium or kinetic effects.

Si Silicon is controlled by quartz (titration experiments) or a clay mineral (batch experiment). The difference in result from the two methods can be explained by kinetic effects.

* $E_h$ measurements in the low pH region ($2<pH<4$) indicate the preference for Fe(II) in solution, and the development of aqueous reducing capacity and reducing conditions during biotite weathering.

* The solution concentration of potassium is controlled by an ion-exchange reaction where sodium exchanges for potassium. In the most acid pH region, protons might compete with sodium for the exchange sites. The total exchange capacity, $S_T$, is estimated to be $0.0011 \pm 0.0002$ moles/g for the 75-125 $\mu$m size-fraction (error estimate is based on one standard deviation)

# 4. IMPLICATIONS FOR THE PERFORMANCE OF A DEEP REPOSITORY

## 4.1 TECHNICAL BACKGROUND

During the construction of a HLNW repository a large amount of oxidants will be introduced into the repository system. The amount of oxidants introduced may eventually effect the geochemical stability of the repository system by affecting both the chemical stability of the canister and the spent fuel matrix. This could eventually result in an enhanced radionuclide release. In the post-closure period most of the oxidants will be taken up by the remaining reducing capacity of the repository. The granitic bedrock constitutes the largest pool of reducing capacity in the system. Additional reducing capacity is linked to the presence and availability of organic carbon and Fe(II), both in the groundwater and the fissure fillings. In order to assess the effect of the remaining oxidants in the post-closure period it is critical to quantify the following factors:

1) The reducing capacity of the groundwater-rock system
2) The time-scale for the potential depletion of oxidants from the system.

These factors will determine two of the characteristic intensity parameters to define the geochemical stability of a repository system: low $E_h$ and an appropriate amount of available Fe(II).

Among the various factors that define the reducing capacity of the bedrock, the weathering of Fe(II)-containing clays in the fissure fillings appears to be critical. Therefore, we have studied the kinetics and thermodynamics of the low temperature alteration of biotite and chlorite. By using the information collected in well controlled laboratory experiments we can derive estimates for the contribution of the weathering of Fe(II) clays to be compared to other potential oxidant scavenging phenomena, e.g. organic degradation and oxidant diffusion into the rock matrix. This information will be used to evaluate the contribution of Fe(II)-clay weathering to the overall reducing capacity of the repository system.

We do not imply that Fe(II)-silicate weathering will necessarily control the depletion of molecular oxygen and the development of reducing conditions. However, in order to better formulate conceptual and mathematical models for transport and reaction in deep groundwaters this process must be compared with other important processes such as hydrologic transport, diffusion in the rock matrix and microbiological activity.

## 4.2 CONSUMPTION OF MOLECULAR OXYGEN

### 4.2.1 The Capacity of Minerals for Uptake of Molecular Oxygen

Once the repository has been closed to the atmosphere, molecular oxygen will be depleted from the ground water system by reduction. In the ground water system several reductants are present (see figure 4-1), i.e 1) organic carbon; 2) sulphide minerals (mainly pyrite) 3) minerals containing reduced transition metals (i.e Mn(II) and Fe(II)), that potentially can react with dissolved oxygen. Grenthe et al. (1992) pointed out the importance of Fe(II)-oxidation processes, such as the oxidative weathering of biotite

$$K(MgFe^{II}_2)(AlSi_3O_{10})(OH)_2\,(s) + \tfrac{1}{2}\,O_2 + 8\,H_2O + 3H^+ \rightarrow$$
$$Al(OH)_3(s) + 2\,Fe(OH)_3\,(s) + K^+ + Mg^{2+} + 3\,Si(OH)_4,$$

to the redox reactions of groundwater systems. White and Yee (1985) studied the consumption of molecular oxygen by Fe(II)-silicate (hornblende, augite and biotite) containing laboratory systems at room temperature and pressure. They reported an initial period ($\sim$ 11 days) of rapid $O_2$ consumption followed by much slower steady-state uptake over a period of $\sim$ 16 weeks. We have used the reported amount of $O_2$ consumed during the initial period to estimate capacities of rapid $O_2$ uptake (table 4-1).

Pirhonen and Pitkänen (1991) studied the long-term oxidation of ferrous iron in naturally and artificially fractured crystalline rocks and minerals at $P_{02}$ = 100 bar. Naturally fractured samples generally had a greater porosity compared to the artificially fractured samples, presumable due to the greater physical alteration from higher rock strain. The weight percent of Fe(II) of the naturally and the artificially fractured samples was approximately the same before the experiments. All reacted samples showed a decrease of between 5-30% in the Fe(II)/Fe(III) ratio within a reaction zone at the sample surface. The artificially fractured samples all had a well-defined reaction layer of 10 mm depth or less. The naturally fractured samples showed between 20-30% decrease in the Fe(II)/Fe(III) ratio with a reaction that extended more than 14 mm into the sample. It was not possible to determine the full depth of the layer due to the restricted sample size. These results suggest that more porous rock provides greater access of groundwater and solutes into the rock matrix; i.e. more rapid and extensive matrix diffusion.

If diffusion is slow compared to chemical reactions that consume oxygen within the rock matrix, kinetic-enhanced mass transfer of oxygen from solution will occur (Neretnieks, 1985). If the rate of diffusion depends critically on the physical structure of the strained zone, the depth of reaction may depend only on the depth of the

strained zone (Eliasson, 1993): i.e. the reacting solution will have a negligible rate of diffusion into the unaltered rock.

Pirhonen and Pitkänen (1991) also reported that the redox capacity of whole rock samples (metadiorite, granite, metabasite, granodiorite and fracture samples) is in the range of 18-620 moles/$m^3$. They report changes in Fe(II) and Fe(tot) contents of some mineral powders (biotite, hypersthene, hornblende, olivine, magnetite and pyrite) after 12 weeks of reaction. We have used their data to estimate the long-termed redox capacity of these minerals (table 4-1).

Table 4-1.
Estimated redox capacity of mineral powder.

| Mineral | Capacity for fast $O_2$ consumption[a] [moles/$m^2$] | Capacity of long-termed $O_2$ consumption[b] [moles/$m^2$] |
|---|---|---|
| **BIOTITE** | $1.5*10^{-6}$ | $2.8*10^{-4}$ |
| **HORNBLENDE** | $1.1*10^{-6}$ | $1.9*10^{-5}$ |
| **AUGITE** | $5.2*10^{-6}$ | na |
| **HYPERSTHENE** | na | $3.2*10^{-5}$ |
| **OLIVINE** | na | $4.5*10^{-5}$ |
| **PYRITE** | na | 0[#] |
| **MAGNETITE** | na | $3.4*10^{-4}$ |

[#] No change in Fe(II)/Fe(tot) ratio reported. na: Data not available.
a) Estimated from White and Yee (1985, figure 12). b) Estimated from Pirhonen and Pitkänen (1991, table 4 and appendix 7. An specific surface area of 1 $m^2/g$ was assumed since only the interval 1-5 $m^2/g$ was reported.). The capacity of $O_2$ consumption is estimated indirectly by the changes in Fe(II) content of the mineral using a calculation method that is similar to the one Pirhonen and Pitkänen (1991) used for whole rock samples.

### 4.2.2 Time-Scale for Depletion of Molecular Oxygen

The time scale for depletion of dissolved oxygen by reaction with rock, or by reaction with dissolved iron(II) released from rock, can be estimated for the case of oxygen in a conductive fracture at the time of repository closure.

Equation 4-1 calculates the time scale ($\tau$) to deplete a closed reservoir of dissolved molecular oxygen, where $R_{O\ uptake}$ is the rate of oxygen consumption.

$$\tau_{anoxic} = \frac{[O_2]_{dissolved}}{R_{O_2 uptake}} , \qquad [h] \qquad (4\text{-}1)$$

We apply this equation to two different path-ways for depletion of dissolved oxygen:

1) First we consider the case of slow release of Fe(II) from the silicate mineral into solution followed by rapid reaction with dissolved oxygen.

   a) Fe(II)-silicate + protons → Fe(II) (aq) + base cations + secondary minerals

   b) Fe(II) + dissolved oxygen + protons → Fe(III) + water

   The oxygen reduction rate is a zero-order reaction with respect to dissolved oxygen concentration since the overall rate is determined by the slow release of Fe(II) into solution. The reaction is also zero-order with respect to Fe(II)-minerals due to the large excess of such minerals compared to the amount of dissolved oxygen.

   Equation 4-2 calculates the rate of oxygen uptake where $A_W$ [$m^2$/l] is wetted surface area; $f_m$ [moles mineral/moles total] is mole fraction of mineral m; $P_{Fe(II)}$ [moles Fe(II)/moles mineral] is mole fraction of Fe(II) in mineral m.

$$R_{O_2 uptake} = \frac{A_W f_m R_{diss.} P_{Fe(II)}}{4} , \qquad [\frac{moles}{l\ h}] \qquad (4\text{-}2)$$

   Each mole of oxygen reacts with four moles of Fe(II).

   Using the rate of Fe-release from Fe(II)-silicates obtained in this study, the turnover time of molecular oxygen is estimated to be in the range of 50-300 years (table 4-2).

   The half-life ($t_{1/2}$ ) for oxygen cannot be calculated because the overall rate of oxygen depletion is only dependent on the very slow dissolution reaction, and not on the concentration of oxygen in solution.

2) Alternatively, in the case of direct oxygen uptake at mineral surfaces, the half-life for oxygen can be calculated assuming a first order decay for oxygen concentration in solution (equation 4-3).

$$\frac{d[O_2]_{(aq)}}{dt} = -k[O_2]_{(aq)} \qquad (4\text{-}3)$$

The half-life is calculated by integrating equation 4-3 between $t=0$ and $t_{1/2}$, and setting the concentrations $C(t_{1/2}) = 0.5 * C(t=0)$. In the experiments of White and Yee (1985), the oxygen concentration was approximately 0.25 mM when they determined $R_o$ for slow oxygen uptake by mineral surfaces. Because the rate of uptake was slow $[O_2]_{(aq)}$ did not change dramatically during the rate determination. The first-order rate constant k is thus approximated by $\tau^{-1}$ (equation 4-4) listed in table 4-2, based on the measured rate of oxygen uptake at $[O_2]_{(aq)}$ = 0.25 mM. Equation 4-5 gives the half-life for dissolved oxygen in those experiments.

$$k = \frac{1}{[O_2]_{(aq)}} \frac{d[O_2]_{(aq)}}{dt} = \frac{R}{d[O_2]_{(aq)}} = \frac{1}{\tau} \qquad (4\text{-}4)$$

$$t_{1/2} = -\tau \ln(0.5) \qquad (4\text{-}5)$$

Table 4-2
Characteristic Time Scales for Uptake if Dissolved Oxygen by Fe(II) in fracture minerals or groundwater.
The initial dissolved oxygen concentration was 8 mg/l (0.25 mM) in all cases. Oxygen is rapidly reduced in solution, subsequent to slow release of Fe(II) from minerals during dissolution, or can be taken up directly by Fe(II) sites at mineral surfaces. In the first case, the overall reaction is zero-order in dissolved oxygen concentration, and a half-life based on first-order decay of oxygen cannot be calculated

| Mineral | Process | $R_{O2}$ (mole m-2 h-1) | $f_m$ | $P_{Fe}$ | $A_w$ ($m^2$ $l^{-1}$) | $\tau$ (years) | $t_{1/2}$ (years) |
|---|---|---|---|---|---|---|---|
| Chlorite | dissolution | $4*10^{-10}$ | 0.1 | 1 | 10 | 285 | - |
| Biotite | dissolution | $2*10^{-9}$ | 0.1 | 1 | 10 | 52 | - |
| Biotite | $O_2$ uptake | $5*10^{-10}$ | 0.1 | 1 | 10 | 240 | 166 |
| Hornblende | $O_2$ uptake | $1.9*10^{-9}$ | 0.1 | 1 | 10 | 59 | 41 |
| Augite | $O_2$ uptake | $1.4*10^{-9}$ | 0.1 | 1 | 10 | 84 | 58 |

The results in table 4-2 compare $\tau$ and $t_{1/2}$ for various mineral or rock types. The relative abundance of reactive mineral or rock type is based on the amount of biotite present in fresh granite samples during

the Block Scale Redox Experiment (Banwart et al. (1992) p. 36). the other minerals or rock types are calculated assuming the same relative abundance. The surface are of rock in contact with the flow path (10 $m^2\ l^{-1}$) is based on results from tracer studies carried out in a fracture at Stripa (Andersson et al., 1989). Samples of biotite and chlorite from the Block Scale Redox Experiment (Banwart et al., 1994a) show Fe(II) content of 76-84% and 56-67% respectively. For simplicity, and given the very approximate nature of these calculations we assign a value of $P_{Fe} = 1$ for all rock types and minerals.

The Fe(II) dissolution rates and oxygen uptake rates measured in this study and by White and Yee (1985), respectively, can be used as measures of $R_{O2}$. Table 4-3 tabulates time scales for oxygen depletion and half-lives for dissolved oxygen as calculated by equation 4-1 to 4-5. These time scales represent the relative rate of chemical reaction to be compared with rates of other processes such as diffusion, aerobic respiration of organic carbon, and groundwater flow.

## 4.3 ACCUMULATION OF Fe(II) IN SOLUTION

Once anoxic conditions are reached, the dissolution of Fe(II)-minerals will accumulate dissolved ferrous iron in the ground water. Analogous to equation 4-1 and 4-2, we estimated a time scale of $10^1$ months to reach a Fe(II) concentration of $10^{-5}$ moles/l (characteristic for undisturbed conditions in a fracture zone at Äspö, (Banwart et al., 1992)) in a granitic groundwater under anoxic conditions (table 4-3).

Table 4-3
Time-scale to reach a Fe(II) concentration in solution of $10^{-5}$ moles/l in an anoxic fracture zone.

| | Build up of Fe(II) in solution[a] [DAYS] |
|---|---|
| **BIOTITE** | **189** |
| **CHLORITE** | **2083** |

a) We used the data from the kinetic experiments of biotite and chlorite dissolution and $A_W = 10\ m^2/l$ determined for the wetted surface area of a fracture zone during the Stripa field investigations (Andersson et al., 1989). We used $f_m = 0.1$ according to $f_{biotite} = 0.1$ in the host rock of a fracture zone at the Äspö Hard Rock Laboratory (Banwart et al., 1992). We used a characteristic concentration of Fe(II), [Fe(II)] = $10^{-5}$ moles/l, observed in an undisturbed fracture zone at 70 m depth at the Äspö Hard Rock Laboratory (Banwart et al., 1992).

## 4.4 AN EQUILIBRIUM MODEL FOR REDOX POTENTIALS IN DEEP GROUND WATERS

Several redox couples are major species in natural groundwaters. However, Grenthe et al. (1992) have shown that the Fe(II)/Fe(III) redox couple is controlling measured redox potentials in deep granitic aquifers. Grenthe et al. (1992) and Smellie and Laaksoharju (1992) reported redox potentials in the range of -100 to -400 mV and a characteristic Fe(II) concentration of $10^{-5}$ M for such deep groundwaters. The main source of Fe(II) in these systems are Fe(II)-silicates, such as biotite and chlorite (Banwart et al. 1992). The ultimate objective of this study was to determine the solution redox conditions coupled to biotite weathering in the near-neutral pH region.

We have measured redox potentials in the range of 350-650 mV (table 3-8) developed during biotite dissolution in the pH region $2<pH<4$. We model these observed redox potentials by the following equilibrium reaction (see section 3.2.4.2):

$$Fe^{2+} + 3\,H_2O \rightarrow Fe(OH)_3(s) + 3\,H^+ + e^-$$

Probably due to the very low total concentration ($\sim 10^{-7}$ M) of dissolved Fe(III), we did not obtain reliable and stable redox potentials at $pH>4$. We have modelled the experimental equilibrium data by the solubility of secondary (see section 3.2.4.1), i.e an Fe(III)-(hydr)oxide and a Fe(II)-clay. This model is based on observed solution concentrations during laboratory weathering of biotite and the identification, using XPD, of kaolinite and a clay-mineral as secondary weathering products (section 3.2.4.1 and 3.2.2 respectively). The model predicts redox potentials (table 4-4) in the range of -200 to -400 mV at neutral pH and qualitatively agrees with the field data reported by Smellie and Laaksoharju (1992) and Grenthe et al. (1992). We conclude that 1) weathering of Fe(II) silicate is important for the redox condition of a granitic aquifer; and 2) Fe(II)-clays may be controlling dissolved Fe(II)-concentrations and thereby, together with the solubility of Fe(III)-(hydr)oxides, measured redox potentials in deep groundwaters.

Table 4-4
Estimated and measured $E_H$ values developed during biotite weathering.

| pH | $E_H$ measured in biotite equilibrium experiments. [mV] | $E_H$ estimated from $Fe(OH)_3(s)$ solubility[a] and observed Fe(tot) concentrations in biotite equilibrium experiments.[b] [mV] | $E_H$ estimated from $Fe(OH)_3(s)$- and Fe(II)clay[c] solubility[a]. [mV] |
|---|---|---|---|
| 2.1 | 626 | 650 | 330 |
| 3.2 | 459 | 455 | 217 |
| 4.6 | na | 225 | 396 |
| 6.7 | na | 77 | -195 |
| 7.1 | na | -12 | -261 |
| 8.0 | na | na | -383 |
| 9.4 | na | -408 | -473 |
| 11.9 | na | -828 | -666 |

na - data not available.
a) Calculated using the Harphrq program (Brown et al., 1991).
b) We assumed [Fe(II)] = [Fe(tot)] and Fe(III)-control by the Fe(III)-hydroxide discussed in section 3.2.4.2.
c) We assumed Fe(II)-concentration control by the solubility of the Fe(II)-clay discussed in section 3.2.4.1 and Fe(III) solubility control by the hydroxide discussed in section 3.2.4.2. We used the Harphrq computer program (Brown et al., 1991) to calculate the solubility and speciation.

## 4.5 APPLICATION TO THE REDOX BUFFER CAPACITY OF A DEEP REPOSITORY

### 4.5.1 Redox Scales

Figure 4-1 shows a series of redox scales of relevance to groundwater chemistry and repository performance assessment. The scales are Eh-pH diagrams defined at a single pH. Here we show the electrochemical potentials of major and trace element redox couples that exist in the repository environment. On each scale, oxidized species (or phases) for each element are shown on the left side, and reduced species are shown on the right side. Reactants on the right

side of the scale are reducing relative to those above it on the left side of the scale. We represent reduced sulfur by the dominant solution species $HS^-$, although sulfide minerals can also represent a significant reservoir of reduced sulfur.

The dashed line extending across Figure 4.1 at about -400 mV is the potential calculated in section 4.4 of this report for oxidation of iron(II)-bearing clay to iron(III) hydroxide. The hydrothermal (chlorite) and low-temperature (clays) weathering products of biotite in granitic groundwaters thus provide significant reducing capacity to groundwater flow paths, with respect to molecular oxygen. The redox potential for the oxidative weathering of these minerals is significantly lower than the corrosion potential of copper by oxygen. If there is more mineral iron(II) than molecular oxygen, and if there is sufficient time for the redox reactions to go to completion, then the presence of these minerals will ultimately maintain redox conditions in the repository at conditions favourable to the chemical stability of the copper canisters. Under these reducing conditions, the radionuclides listed in Figure 4.1 remain confined as sparingly soluble mineral phases.

### 4.5.2 Redox Capacities

The relative concentrations of oxidizing and reducing major element reactants will dominate the capacity of the aquifer to oxidize other elements that are introduced (copper, spent fuel). This capacity follows a strict chemical definition (Scott and Morgan, 1990).

The redox capacity of a system is the net concentration of oxidants and reductants with respect to a chosen reference redox potential. Selecting the reference potential depends on the performance assessment issue. Reactions related to the redox stability of the copper canisters and to the confinement of radionuclides are summarized in Figure 4.1. The amount of reductant or oxidant present as a solid phase is expressed as moles of reactant, based on the total mass of mineral present, divided by the porosity of the flow path contacting the mineral. Iron(III) hydroxide can be expressed as

$$[Fe(OH)_3(s)] = \frac{mf}{\theta} \qquad (4\text{-}6)$$

where m has units of kg of mineral, f is the moles of Fe(III) per kg of iron(III) mineral, and $\theta$ is the flow porosity.

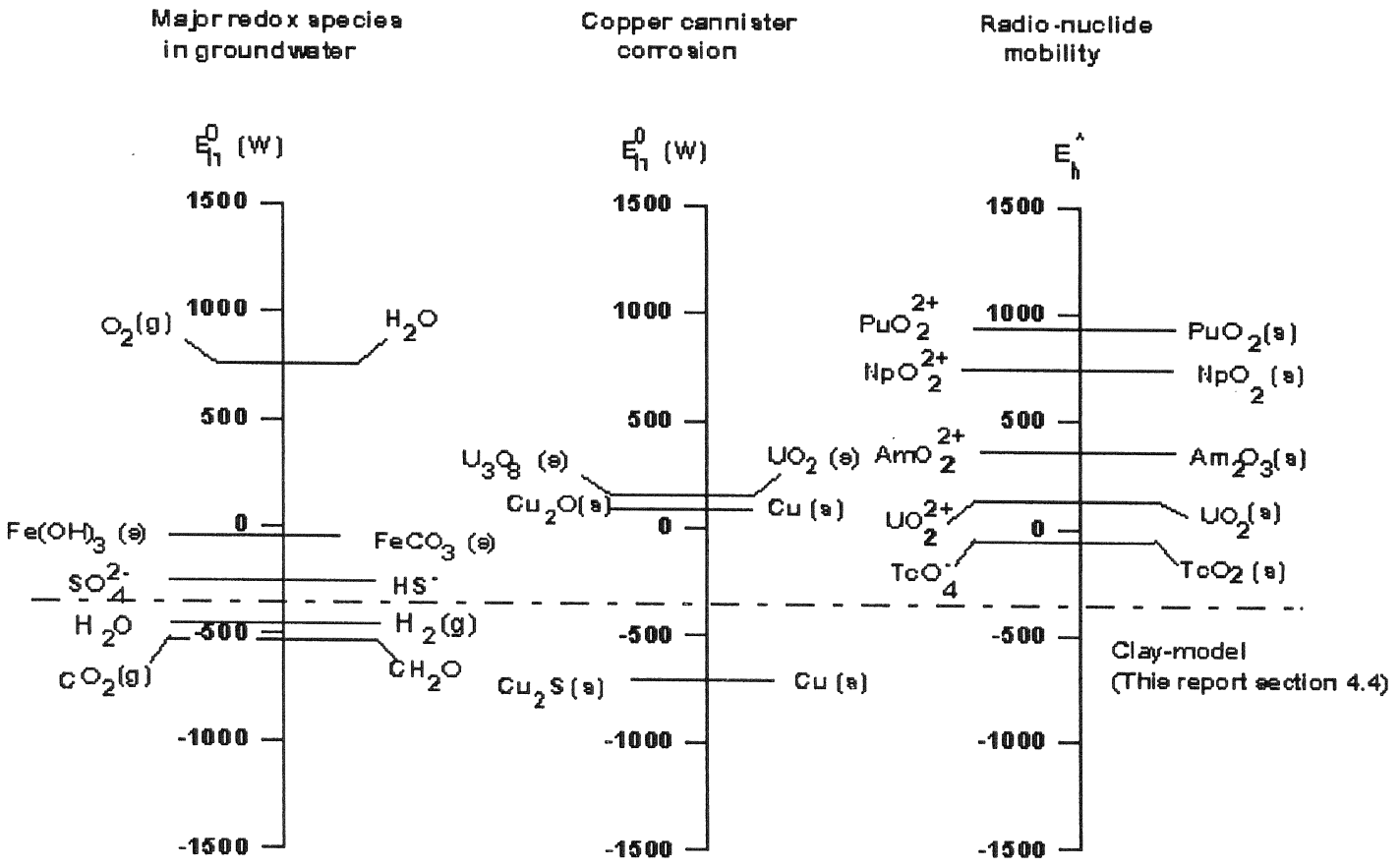


Figure 4-1.
$e^0$ (W) (mV) /$pe^0$ (W) for major redox couples in the groundwater, the copper canister, and some radionuclides (pH 7, 25 °C). The dashed line indicates predicted redox potential for an Fe(II)-clay in equilibrium with a Fe(III)-(hydr)oxide (see section 4.4). Thermodynamic data: Radio nuclides - Hatches database (Cross and Ewart, 1989); Lagerman (1990); Major aqueous redox couples (Bard et al., 1985; Stumm and Morgan, 1981); Cu-system (KBS-90 appendix B (approximate constants)). (W) denotes pH 7 and 1M concnentration of other reactants. * Denotes pH 7 and $10^{-10}$ M concentration of radionuclides.

The oxidizing capacity (OXC) of the repository with respect to copper corrosion by molecular oxygen is the sum of electron equivalents of oxidants ($O_2$(g)) in the repository minus the sum of electron equivalents of all reductants below this potential. Equation 4-7 defines the OXC provided by the major elements in the repository. The corresponding reducing capacity (RDC) is defined as RDC = - OXC.

$$OXC = 4\,[O_2] - [FeCO_3(s)] - 8\,[HS^-] - [Fe(II)\,clay] - 4\,[CH_2O] \qquad (4\text{-}7)$$

A net abundance of reductants buffers the repository environment against molecular oxygen, thereby preventing copper corrosion. More specifically, the oxidizing or reducing capacity of the repository defines the amount of reductants or oxidants which must be added to reach a specific $E_h$. The biotite hosted in the fresh granite is not explicitly considered. The main alteration products of biotite are clay minerals at low temperatures, as demonstrated in this study, and chlorite at high temperatures (Barnhisel and Bertsch, 1989). These minerals are usually present in a thick (1 - 10 cm) altered layer overlying the host granite that confines conductive fractures (Banwart et al.,1994a). Biotite is thus physically separated from the flow path by this altered layer.

Figure 4-1 shows that sulfate is oxidizing with respect to corrosion of copper metal to copper sulfide. These reactions are kinetically inhibited and do not progress at temperatures and pressures anticipated in a deep repository (KBS-3, Volume III).

In the presence of $HS^-$, copper metal is unstable with respect to carbon dioxide or water reduction with hydrogen production. The thermodynamic driving force for this reaction is the formation of highly insoluble copper sulfide (CuS (s)). The production of dissolved sulfide species by microbial sulfate reduction can therefore lead to canister instability. In this case, the reference redox potential for canister stability is that for sulfate reduction rather than copper corrosion to CuS (s). Sulfate reduction represents a redox potential threshold below which CuS (s) can form due to sulfide production, and thus drive the redox potential for copper corrosion to extremely low values where oxidation by water or other oxidants is possible. With respect to the potential for sulfate reduction given in figure 4-1, the reducing capacity is defined by equation 4-8.

$$RDC = +4\,[CH_2O] + [Fe(II)\text{-}Clay] - 4\,[O_2] - [Fe(OH)_3(s)] \qquad (4\text{-}8)$$

This formal treatment of the reducing capacity for the deep environment requires site specific data for quantitative estimate of redox capacities in the repository:

1 the relative mass abundance of organic carbon, molecular oxygen and sulfate at the time of repository closure,

2. the relative mass abundance of redox-active minerals, and their composition, in contact with groundwater flow paths.

3. the flow porosity

If canister failure occurs, radionuclides will be released into the geosphere. Redox sensitive radionuclides (Pu, Np, Am, U, Tc) are highly soluble when oxidized but form sparingly soluble solid phases when reduced. These reactions are represented by the redox-scale on the right side in figure 4-1. Under oxic conditions the soluble species predominate and the radionuclides are thus mobile with the groundwater flow. The redox potential calculated by the solubility equilibrium model for $Fe(OH)_3$ (s) /Fe(II)-clay lies well below the redox potentials for the radionuclides. Fracture filling clay minerals can therefore act as reductants to 1) consume oxygen, thereby helping maintain reducing conditions, or 2) react directly with radionuclides to reduce them to insoluble, and thus immobile, solid phases. These fracture fillings can also act as adsorption barriers against migration of non-redox-sensitive radionuclides (Cs) as well (KBS-3, Section 12.6-12.7).

### 4.5.3 Conceptual Model for Evolution of Redox Capacity in the Repository

Because of slow reaction kinetics, major element redox couples are generally not in equilibrium with each other in natural waters. Although calculated redox potentials indicate the relative tendency for the couples to react, the distribution between species contributing to the net OXC or RDC will not be governed by chemical equilibrium. The time evolution of net OXC or RDC must be considered. Figure 4.2 represents the evolution of OXC with time during the construction, operation and post-closure phases of the repository.

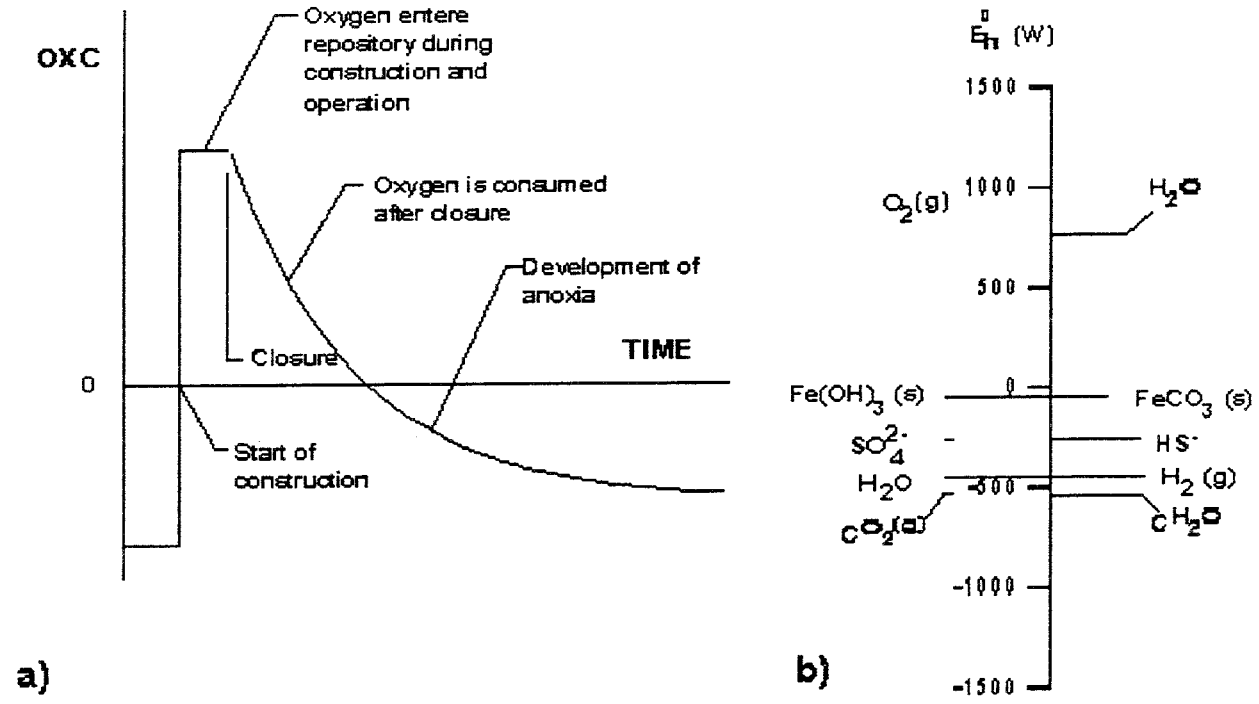


Figure 4-2
a) A conceptual representation of the evolution of oxidizing capacity with time during construction, operation and after closure of the repository. Oxygen will be introduced during the construction and operation. After closure, reaction with sulfide, iron(II) minerals and organic carbon will reduce oxygen to water, allowing the repository to again reach reducing conditions. Net oxidizing capacity (OXC > 0) means a remaining source of oxidants that can corrode copper metal.
b) A redox scale for major species in groundwater. This scale shows the redox intesity factor $E_h$ [mV] that can be reached by adding or removing oxidants from the repository.

Calculating the evolution of oxidizing capacity with time requires a coupled mathematical description of the dominant transport processes and chemical reactions that influence the time evolution of the major oxidizing and reducing species and phases that contribute to net OXC:

1. oxygen reduction by iron(II) minerals, sulfides and organic carbon,

2. iron(III) mineral reduction by sulfides and organic carbon,

3. sulfate reduction by organic carbon.

Oxygen and iron(III) reduction by sulfide minerals was summarized recently by Strömberg and Banwart (1994) and Wersin et al. (1994). Iron reduction by organic carbon has been studied within the Äspö Redox Experiment in Block Scale (Banwart et al., 1994b). Sulfate reduction by organic carbon was also recently studied within the Äspö project (Laaksoharju et al., 1994b). The Äspö Redox Experiments in Detailed Scale (REX) (Banwart and Wikberg, 1994) aims to study the reduction of oxygen by iron(II) minerals in the deep environment of the Äspö Hard Rock Laboratory.

### 4.5.4 A Methodology for Calculating the Half-Life of Dissolved Oxygen in the Closed Repository

We apply the conceptual model of Wersin et al. (1994) for coupled diffusion and reaction of oxygen trapped in the repository. They applied dimensional analysis of the 1-D diffusion reaction equation for oxygen trapped in the bentonite backfill around the canister at the time of closure. Trace amounts of sulfide minerals present in the clay matrix provide reducing capacity with respect to dissolved oxygen. The Damköhler number (Da), a dimensionless variable, compares the rate of chemical reaction with the rate of diffusion (equation 4-9). k is the first-order decay constant for reduction of oxygen by sulfide minerals trapped in the bentonite, l is the diffusion path length, and $D_e$ is the effective diffusion coefficient for oxygen within the clay backfill.

$$Da = \frac{kl^2}{D_e} \qquad (4\text{-}9)$$

They demonstrated that for oxygen trapped in the bentonite backfill. Da = 1500, showing diffusion fluxes to be negligible compared to the rate of reaction. In this case, the time scale for depletion of oxygen is only dependent on the first-order chemical reaction given in equation (4-10).

$$\frac{d[O_2]_{(aq)}}{dt} = -k[O_2]_{(aq)} \qquad (4\text{-}10)$$

The half-life depends only on the values of k (equation 4-11) .

$$t_{1/2} = -\frac{\ln(0.5)}{k} \qquad (4\text{-}11)$$

The value of k depends on the activation energy of the reaction, which is dependent on pressure (P) and temperature (T). The reaction

rate will also depend on the relative abundance of sulfide mineral, and the ratio of wetted mineral surface area to pore water volume. k is therefore an effective (or "pseudo") first-order decay constant that lumps effects of other parameters such as the amount of sulfide mineral and the effect of aqueous species ($H^+$, $OH^-$, etc) that may catalyse or inhibit the reaction The values of k and $t_{1/2}$ therefore depend on site- and design-specific parameters; T,P, mineral composition of backfill, pH and ionic composition of the groundwater.

Equation 4-11 can be extended to consider reaction of oxygen with all reductants present in the backfill, fractures and rock at the time of backfill; Fe(II)-minerals, sulfides, organic carbon (See figure 4-1). We define a rate expression for first-order decay of oxygen by all reactions occurring in parallel (equation 4-12).

$$\frac{d[O_2]_{(aq)}}{dt} = -k_{Fe(II)}[O_2]_{(aq)} - k_{sulfide}[O_2]_{(aq)} - k_{org.\,carbon}[O_2]_{(aq)} \qquad (4\text{-}12)$$

Equation (4-13) is the corresponding equation for the half-life of oxygen where Σk refers to the sum of all effective first-order constants defined in equation (4-11).

$$t_{1/2} = -\frac{\ln(0.5)}{\sum k} \qquad (4\text{-}13)$$

The relative values of k will depend on the reaction and site-specific parameters mentioned above. Results from previous (see section 4.2) and ongoing (see section 4.5.3) investigations of these reaction processes will form the scientific basis for evaluating the fate of molecular oxygen in the repository at the time of closure. As in the study of Wersin et al. (1994) it is also necessary to consider these chemical aspects together with transport phenomena. The calculation of oxygen depletion by coupled transport- and reaction-mechanisms therefore requiers design- and site-specific information on parameters for oxygen transport in the groundwater; effective diffusivities, transmittivities, dispersion coefficients, etc.

## 5. ACKNOWLEDGEMENTS

We are grateful to Jan Blomquist and Per Kjäll at the department of Physics, University of Stockholm, for making Mössbauer analysis and to Nils Lange at the department of Material Science and Engineering, Royal Institute of Technology, Stockholm, for making SEM analysis. We are obliged to Bengt Lindquist and Torbjörn Skiöld at the section for Mineralogi, Naturhistoriska Riksmuseet, Stockholm for providing the mineral samples.

## 6. REFERENCES


Acker J, Bricker P (1992) The influence of pH on biotite dissolution and alteration kinetics at low temperature. Geochim Cosmochim Acta 56:3073-3092

Allen B.L, Hajek B.F (1989) Mineral occurrence in soil environments.in Minerals in Soil Environments. Dixon J, Weed S,(Editors) Soil Sci Soc Am, Wisconsin pp.161-198

Andersson P, Gustafsson E, Olsson O (1989) Investigations of flow distribution in a fracture zone at the Stripa mine, using the radar method, results and interpretation. Technical Report 89-33 The Swedish Nuclear Fuel and Waste Management Company (SKB), Stockholm

Bailey S.W (1972) Determination of chlorite compositions by x-ray spacings and intensities. Clays and Clay Minerals 22:381-388

Bain D.C (1977) The weathering of ferruginous chlorite in a podzol from argyllshire, scotland. Geoderma 17:193-208

Banfield J.F, Eggleton R.A (1988) Transmission electron microscope study of biotite weathering. Clays clay min 36(1):47-60

Banwart S, Laaksoharju M, Nilsson A-C, Tullborg E-L, Wallin B (1992) The large scale redox experiment - Initial characterization of the fracture zone. Progress report 25-92-04 for The Swedish Nuclear Fuel and Waste Management Company (SKB), Stockholm.

Banwart S, Gustafsson E, Laaksoharju M, Nilsson A-C, Tullborg E-L, Wallin B (1994a) Large-scale intrusion of shallow water into a vertical fracture zone in crystalline bedrock. Water Resources Research 30(6):1747-1763

Banwart S, Gustafson E, Laaksoharjy M, Tullborg E.L, Wallin B, Pedersen K, Wikberg P (1994b) . Technical Report for The Swedish Nuclear Fuel and Waste Management Company (SKB), Stockholm, in review

Banwart S, Wikberg P (1994) Redox experiment in detailed scale (REX) Test plan for The Swedish Nuclear Fuel and Waste Management Company (SKB), Stockholm, in preparition (versoin 1.1)

Bard A.J, Parson R, Jordan J (1985) Standard potentials in aqueous solution. IUPAC. Marcel Dekker Inc. New York

Barnhisel R, Bertsch P.M (1989) Chlorites and Hydroxy-interlayered vermiculite and smectite. In: Dixon J., Weed S. (Editors) Minerals in soil environments. Soil Science Society of America, Wisconsin,pp. 729-787

Basett W.A, (1959) The origin of the vermiculite deposit at Libby, Montana. Amer Min 44:282-299

Berg A, Banwart S (1994a) Anorthite surface speciation and weathering reactivity in bicarbonate solutions at 25° C. In: Paul J, Praider C-M (editors) Carbon dioxide chemistry: Environmental issues. The Royal Soc Chem, Cambridge, pp 305-316

Berg A, Banwart S (1994b) A surface reaction model for carbonate ligand-accelerated dissolution of Ca-feldspar under elevated $pCO_2$ at natural water conditions of pH, temperature and Pressure. Submitted

Blum A, Lasaga A (1988) Role of surface speciation in the low-temperature dissolution of minerals. Nature 331:431-433

Bock R, Marr L (1979) A Handbook of decomposition methods in analytical Chemistry, Blackie Group

Brady P.V, Walther J.V.(1990) Kinetics of quartz dissolution at low temperatures. Chem Geol ,82:253-264

Brady P.V, Walther J.V.(1989)Controls on silicate dissolution rate in neutral and basic pH solutions at 25 °C. Geochim Cosmochim Acta 53:2823-2830

Brindley G.W, Brown G (1980) Crystal structures of clay minerals and their X-ray identification. Mineralogical Society, London

Brown P.O, Howards A. Sharland S.N, Tweed C.J (1991) Harphreeq.. Geochemical speciation program based on phreeqe user guide. Theoretical Studies Department, Radwaste disposal division B424.2 Hornwall Laboratory, Didcot Oxon OX110RA

Bruno J, Casas I, Puigdomènech I (1991) The kinetics of dissolution of $UO_2$ under reducing conditions ant the influence of an oxidized surface layer ($UO_{2+x}$):Application of a continuous flow through reactor. Geochim Cosmochim Acta 55:647-658

Bruno J, Stumm W, Wersin P, Brandberg F (1992) On the influence in mineral dissolution:I.The thermodynamics and kinetics of hematite dissolution in bicarbonate solution at T = 25 °C Geochim Cosmochim Acta 56:1139-1147

Bruno J, Wersin P, Stumm W (1992b) On the influence of carbonate in mineral dissolution: II The solubility of $FeCO_3$ (s) at 25 °C and 1 atm total pressure. Geochim Cosmochim Acta 56:1149-1155

Caroll D (1970) Clay minerals: A guide to their X-ray identification. The Geological Society of America,Special paper 126, Colorado 1970

Caroll-Webb S, Walther J (1988) A surface complex reaction model for the pH dependence of corundum and kaolinite dissolution rates. Geochim Cosmochim Acta 52:2609-2623

Chen C-H (1975) A method of estimation of standard free energies of formation of silicate minerals at 298.15 °K. Amer J Sci 275:801-817

Cho H.D, Mermut A.R (1992) Evidence for halloysite formation from weathering of ferruginous chlorite. Clays Clay Min 40(5):608-619

Clemency C.V, Lin F-C (1981) Dissolution kinetics of phlogopite II Open system using an ion-exchange resin. Clays Clay Min 29(2):107-112

Coleman N.T, Leroux F.H, Cady J.G (1963) Biotite - hydrobiotite - vermiculite in soils. Nature 198:409-410

Cross J.E, Ewart F.T (1989) HATCHES - A thermodynamic database management system. Proceedings of the Conference on Chemistry and Migration Behaviour of Actinides and Fission Products in the Geosphere 1989.

Deer W.A, Howie R.A, Zussman J (1963) Rock forming minerals. III Sheet silicates. Longman, London.

Dzombak D.A , Morel F.M.M, (1990) Surface Complexation Modeling- Hydrous Ferric Oxide.Wiley & Sons . USA

Eliasson (1993) Mineralogy, geochemistry, and petrophysics of red coloured granite adjecent to fractures Technical Report 93-06 for The Swedish Nuclear Fuel and Waste Management Company (SKB), Stockholm

Fanning D, Keramidas V, El-Desoky M (1989) Micas.in Minerals in Soil Environments. Dixon J, Weed S,(Editors) Soil Sci Soc Am, Wisconsin pp.551-634

Farmer V.C, Wilson M.J (1970) Experimental conversion of biotite to hydrobiotite. Nature 226:841-842

Fletcher P, Sposito G (1989) The chemical modelling of clay/electrolyte interactions for montmorillonite. Clay Miner. 24(2):375-391

Fordham A.W (1990) Weathering of biotite into dioctahedral clay minerals. Clay Min 25:51-63

Furrer G, Stumm W (1986) The coordination chemistry of weathering:I Dissolution kinetics of $\gamma$-$Al_2O_3$ and BeO. Geochim Cosmochim Acta 50:1847-1860

Gran G (1981) Calculation of equivalence volumes in potentiometric titrations. Ph.D thesis The Royal Institute of Technology (Dept of Analytical Chemistry), Stockholm

Gilkes R,J, Little I.P (1972) Weathering of chlorite and some associations of trace elements in permian phyllites in southeast Queensland. Geoderma 7:233-247

Grant W.H (1964) Chemical weathering of biotite-plagioclase gneiss. Clays Clay Min 12:455-463

Grenthe I, Stumm W, Laaksoharju M, Nilsson A.-C, Wikberg P (1992) Redox potentials and redox reactions in deep groundwater systems. Chem Geol 98:131-150

Helgeson H.C (1978) Summary and critique of the thermodynamic properties of rock-forming minerals. American journal of science 278A

Herbillon A.J, Makumbi M.N (1975) Weathering of chlorite in a soil derived from a chloriticoschist under humid tropical conditions. Geoderma 13:89-104

Holdren G.R, Berner R.A (1979) Mechanism of feldspar weathering I. Experimental studies. Geochim Cosmochim Acta 43:1161-1171

Johnson L.J (1964) Occurrence of regularly interstratified chlorite-vermiculite as a weathering product of chlorite in a soil. Amer Min 49:556-572

Karlsson F, Pedersen K (1994) Investigations of Subterranean Bacteria. Their importance to performance assessment. Technical Report The Swedish Nuclear Fuel and Waste Management Company (SKB), Stockholm. In prep.

KBS-90 (1978) Koppar som kapslingsmaterial för icke upparbetat kärnbränsleavfall. Bedömning ur korrosionssynpunkt. Report for The Swedish Nuclear Fuel and Waste Management Company (SKB), Stockholm.

KBS-3 Kärnbränsle cykelns slutsteg. Använt kärnbränsle-KBS-3. III Barriärer. Report for The Swedish Nuclear Fuel and Waste Management Company (SKB), Stockholm.

Kittrick, J.A (1969) Soil minerals in the $Al_2O_3$-$SiO_2$-$H_2O$ system and a theory of their formation. Clays Clay Min 17:157-166

Knauss K.G, Wolery T.J (1988) The dissolution kinetics of quartz as a function of pH and time at 70 C. Geochim Cosmochim Acta 52:45-53

Knauss K.G, Wolery T.J (1989) Muscovite dissolution kinetics as a function of pH and time at 70 C Geochim Cosmochim Acta 53:1493-1501

Laaksoharju M, Degueldre C, Tullborg E.L, Skårman C (1994a) Progressl report for The Swedish Nuclear Fuel and Waste Management Company (SKB), Stockholm, in prep.

Laaksoharju M, Pedersen K, Wallin B, Gustafson G, Rhen F, Tullborg E-L, Wikberg P (1994b) Microbial Sulphate Reduction in the Äspö HRL Tunnel, Technical Report The Swedish Nuclear Fuel and Waste Management Company (SKB), Stockholm, in preparation

Lagerman B (1990) Complex formation in the actinoid-$H_2O$-$CO_2$(g) system. Thesis. Royal Institute of Technology, dept of inorganic chemistry.

Lin F-C, Clemency C.V (1981a) The dissolution kinetics of brucite, antigorite, talc and phlogopite at room temperature and pressure. Amer Min 66:801-806

Lin F-C, Clemency C.V (1981b) Dissolution kinetics of phlogopite I Closed system. Clays Clay Min 29(2):101-106

Lin F-C, Clemency C.V (1981c) Dissolution kinetics of phlogopite II Open system using an ion-exchange resin. Clays Clay Min 29(2):107-112

Mattigod S, Sposito G (1978) Improved method for estimating the standard free energy of formation (delta G) of smectites. Geochim Cosmochim Acta 42:1753-1762

Moore D.M, Reynolds R.C jr (1989) X-ray diffraction and the identification and analysis of clay minerals. Oxford University press. New York

Neretnieks I. (1985) Some uses on natural analogues in assessing the function of a HLW repository. Chemi Geol, 55

Newman A.C.D, Brown G (1987) The Chemical Constitution of Clays. In Chemistry of Clays and Clay Minerals. A.C.D Newman (Editor). Longman Scientific & Technical, London.

Norrish K (1973) Factors in the weathering of mica to vermiculite. Proc Int Clay Conf Madrid 1972 .pp 83-101

Nriagu J.O (1975) Thermochemical approximations for clay minerals. The American Mineralogist 60:834-839

Pirhonen V, Pitkänen P (1991) Redox capacity of crystalline rocks: laboratory studies under 100 bar oxygen pressure. Technical report 91-55. The Swedish Nuclear Fuel and Waste Management Company (SKB), Stockholm

Post J.L, Janke N.C (1972) Properties of 'swelling' chlorite in some mesozoic formations of California. Clays and Clay Minerals 22:67-77

Puigdomènech I, Åberg M (1987) Input, Sed och Predom: Datorprogram för beräkning och uppritning av logaritmiska diagram. Report TRITA-OOK-3010 Deptartment of Inorganic Chemistry. Royal Inst. of Tech. Stockholm ,Sweden

Rabenhorst M.C, Fanning D.S, Foss J.E (1982) Regularly interstratified chlorite/vermiculite in soils over meta-igneous mafic rocks in Maryland Clays Clay Min 30(2):156-158

Rausell-Colom J.A, Sweatman T.R, Wells C.B, Norrish K (1965) Studies in the artificial weathering of mica. In Experimental Pedology. Hallsworth-Crawford (Editor) Butterworths, London.

Ross G.J, Kodama H (1974) Experimental transformation of chlorite into a vermiculite. Clays Clay Min 22:205-211

Ross G.J, Wang C, Ozkan A.I, Rees H.W (1982) Weathering of chlorite and mica in a New Brunswick podzol developed on till derived from chlorite.mica schist: Geoderma 27:255-267

Ross G.J (1969) Acid dissolution of chlorites: Release of magnesium, iron and aluminium and mode of acid attack. Clays and Clay Minerals 17:347-354

Ross G.J (1975) Experimental alteration of chlorites by chemical oxidation. Nature 255:133-134

Schindler P.W, Wälti E, Fürst B, (1976) The role of surface hydroxyl groups in the surface chemistry of metal oxides. Chimia 30(2):107-109

Schnitzer M, Kodama H (1976) The dissolution of micas by fulvic acid. Geoderma 15:381-391

Schnoor J.L (1990) Kinetics of chemical weathering: A comparison of laboratory and field weathering rates. In: Stumm W (editor) Aquatic chemical kinetics, Wiley, New York, pp 475-504

Schott J, Berner R, Sjöberg L (1981) Mechanism of pyroxene and amphibole weathering -I. Experimental studies of iron-free minerals. Geochim Cosmochim Acta 45:2123-2135

Schott J, Berner A (1985) Dissolution mechanism of pyroxenes and olivines during weathering. In The chemistry of Weathering. Drever J.I (editor) Reidel Publ. Comp, pp 35-53

Scott A.D, Amonette J (1988 ) Role of iron in mica weathering. In Iron in soils and Clay minerals. Stucki J.W, Schwertenmann U ( Editors) Reidel publishing company.pp 537-625

Scott A.D and Morgan J.J (1990) Energetics and conservative properties of redox systems. In: Melchoir D.C , Basset R.L (editors) ACS Symp Ser 419: Chemical Modeling in aqueous systems II.

Slaughter M (1966) Chemical binding in silicate minerals. Part III. Application of energy calculations to the prediction of silicate mineral stability. Geochim Cosmochim Acta 30:323-339

Smelli J, Laaksoharju M (1992) The Äspö Hard Rock Laboratory: Final evaluation of the hydrogeochemical pre-investigations in relation to existing geologic and hydraulic conditions. Technical Report 92-31 The Swedish Nuclear Fuel and Waste Management Company (SKB), Stockholm

Sposito G (1983) On the surface complexation model of oxide - aqueous solution interface. J Coll. Int. Sci 91(2):329-340

Sposito G (1986) The polymer model of thermochemical clay mineral stability. Clays Clay Min 34(2):198-203

Stoch L, Sikora W (1976) Transformation of micas in the process of kaolinization of granites and gneisses. Clays Clay Min 24:1156.162

Strömberg B, Banwart S (1994) Kinetic modelling of geochemical processes at the Aitik mini´ng waste rocksite in northern Sweden Applied Geochemistry 9:583-595

Stumm W, Morgan J.J (1981) Aquatic chemistry. Wiley. New York.

Stumm W, Wieland E (1990) Dissolution of oxide and silicate minerals:Rates depend on surface speciation. In: Stumm W (editor) Aquatic chemical kinetics, Wiley, New York, pp 367-400

Stumm W, Wollast R (1990) Coordination chemistry of weathering:Kinetics of the surface controlled dissolution of oxide minerals. Rev Geophys 28(1):53-69

Tardy Y, Garrels R.M (1974) A method for estimating the Gibb's energies of formation of layer silicates. Geochim Cosmochim Acta 38:1101-1116

Trotignon L, Turpault M.-P. (1992) The dissolution kinetics of biotite in dilute $HNO_3$ at 24 °C. Proc 7th int symp on Water Rock Interactions, Utah

Trotignon M-P, Turpault L (1994) The dissolution of biotite single crystals in dilute HNO3 at 24 C: evidence of an anisotropic corrosion process of micas in acidic solutions. Geochim Cosmochim Acta. In press

Walker G.F (1949) The decomposition of biotite in the soil. Miner Mag 28:693-703

Wersin P, Spahiu K, Bruno J (1994) Time evolution of dissolved oxygen and redox conditions in a HLW repository. Technical Report 94-02 for The Swedish Nuclear Fuel and Waste Management Company (SKB), Stockholm

White A.F, Yee A (1985) Aqueous oxidation-reduction kinetics associated with coupled electron-cation transfer from iron-containing silicates at 25° C. Geochim Cosmochim Acta 49:1263-1275

Wherli B (1989) Monte Carlo simulations of surface morphologies during mineral dissolution. J Coll. Int. Sci 132(1):230-242

Wieland E, Wherli B, Stumm W (1988) The coordination chemistry of weathering :III.A generalization on the dissolution rates of minerals Geochim. Cosmochim. Acta 52:1969 - 1981

Wieland E, Stumm W (1992) Dissolution kinetics of kaolinite in acidic aqueous solutions at 25 C: Geochim Cosmochim Acta 56:3339-3357

Wilson M.J (1966) The weathering of biotite in some Aberdeenshire soils. Miner. Mag. 35:1080-1093

Wilson M.J (1970) A study of weathering in a soil derived from a biotite - hornblende rock. I. Weathering of biotite. Clay Minerals 8:291-303

Wilson M.J (1975) Chemical weathering of some primary rock - forming minerals. Soil Sci 119(5):349-355

Wogelius R, Walther J, (1991) Olivine dissolution at 25 °C: Effects of pH, $CO_2$ and organic acids. Geochim Cosmochim Acta 55:943-954

Yassoglou N.J, Nobeli C, Kostikas A.J Simopoulos (1972) Weathering of mica flakes in two soils in northern Greece evaluated by mössbauer and conversional techniques. Soil Sci Amer Proc 36:520-527

Zinder B, Furrer G, Stumm W (1986) The coordination chemistry of weathering. II. Dissolution of Fe(III) oxides. Geochim Cosmochim Acta 50:1861-1869

Östhols E, Malmström M (1994) Dissolution kinetics of $ThO_2$ in acid and bicarbonate media. Submitted.

Östhols E (1994) The C-Haltafall program system for equilibrium speciation calculations Version 1.7, Report TRITA-OOK-2062 Dept. Inorganic Chem., Royal Inst. Tech., Stockholm

# 7. APPENDIX

## 7.1 APPENDIX: Kinetic data from the biotite-$H_2O$-system

Table 7-1. Data from kinetic experiment **M2**: 0.2773 gram biotite, pH 4.06, $CO_2$-free system.

| Day | pH | F | Si [PPB] | Fe [PPB] | Mg [PPB] | Al [PPB] | K [PPB] |
|---|---|---|---|---|---|---|---|
| 0 | 4.96 | 13.32 | - | 7 | - | 478 | 58570 |
| 0 | 4.98 | 12.85 | 231 | 0 | 313 | 304 | 29386 |
| 2 | 5.98 | 2.25 | 294 | 633 | - | 659 | 18715 |
| 3 | 5.17 | 12.86 | 188 | 420 | 126 | 244 | 18616 |
| 4 | 4.58 | 13.04 | 190 | 464 | 121 | 228 | 5085 |
| 5 | 4.30 | 12.79 | 170 | 397 | - | 133 | 3611 |
| 6 | 4.20 | 13.31 | 145 | 351 | 79 | 145 | 1780 |
| 7 | 4.17 | 13.99 | 186 | 390 | - | 160 | - |
| 8 | 4.12 | 14.25 | - | 306 | 70 | 135 | - |
| 9 | 4.10 | | 108 | 307 | 63 | 133 | - |
| 10 | 4.09 | 10.02 | 106 | 315 | 63 | 147 | - |
| 11 | 4.07 | 6.14 | 104 | 226 | 57 | 124 | 0 |
| 14 | 4.00 | 17.44 | 91 | 292 | - | 107 | - |
| 15 | 4.98 | 18.8 | 92 | 252 | 49 | 93 | - |
| 16 | 3.24 | 16.23 | 113 | 202 | 42 | 89 | - |
| 17 | 4.98 | 11.73 | 272 | 895 | 221 | 350 | - |
| 18 | 3.58 | | - | 424.4 | 133.3 | 151.6 | 12 |
| 20 | 3.91 | 9.04 | 176 | 419 | 116 | 167 | - |
| 24 | 4.13 | | 349 | 455 | 223 | 120 | |
| 25 | 4.09 | 9.44 | 155 | 265 | 78 | 94 | 82 |
| 26 | 4.98 | 9.41 | 128 | 221 | 68 | 73 | - |
| 27 | 4.096 | 9.72 | - | 250.3 | 97 | 130.1 | - |
| 28 | 4.10 | 9.87 | 151 | 199 | 67 | 78 | - |
| 31 | 4.09 | 9.93 | - | - | - | - | - |
| 32 | 4.08 | 9.54 | - | 255.7 | 93.33 | 176 | - |
| 33 | 4.05 | 9.84 | 174 | 235 | 84 | 96 | 54 |

Table 7-2. Data from kinetic experiment **M3**: 0.5102 gram biotite, pH 2.80, $CO_2$-free system.

| Day | pH | F [g/h] | Si [PPB] | Fe [PPB] | Mg [PPB] | Al [PPB] | K [PPB] |
|---|---|---|---|---|---|---|---|
| 0 | - | - | 1108 | 677.5 | 3363 | 650 | 192163 |
| 0 | - | 13.6 | 3873 | 3439 | - | - | 81512 |
| 2 | 3.30 | 12.95 | 815.2 | 3061 | 717.2 | 1313 | 25254 |
| 3 | 3.06 | 13.27 | 1035 | 3886 | 903.7 | 1577 | 20864 |
| 4 | 3.01 | 13.43 | 1007 | 3426 | 825 | 1437 | 103320 |
| 5 | 2.97 | 13.54 | 1143 | 3439 | - | 5263 | - |
| 6 | 2.97 | 13.85 | 1026 | 3179 | 770 | 1333 | - |
| 7 | 2.39 | 14.18 | 909 | 2715 | - | 1103 | - |
| 8 | 2.91 | 13.79 | 604 | 2457 | 1072 | 2465 | 2424 |
| 9 | 2.91 | 18.9 | 891 | 2617 | - | 1062 | 1891 |
| 10 | 2.88 | - | 898 | 2471 | 617 | 1030 | - |
|  | - | 5.66 | 887 | 2355 | 598 | 1001 | - |
| 14 | 2.83 | 16.94 | 914 | 2516 | 628 | 1032 | - |
| 15 | - | 18.53 | 880 | 2327 | 748 | 1001 | - |
| 16 | - | 14.19 | 898 | 2423 | 630 | 1110 | - |
| 17 | 2.70 | 15.05 | 1355 | 3737 | - | 1661 | - |
| 18 | 2.69 | - | 1308 | 3767 | 955 | 1590 | 416 |
| 20 | 2.84 | 8.26 | 1288 | 2885 | 707 | 1388 | 109 |
| 24 | 2.82 | - | 1300 | 2579 | - | 1334 | - |
| 25 | 2.83 | 8.54 | 1194 | 2710 | 764 | 1245 | 914 |
| 26 | - | 8.54 | 1185 | 2725 | 759.3 | 1227 | - |
| 27 | 2.80 | 8.76 | 226 | 2038 | 536 | 1060 | - |
| 28 | 2.81 | 9.07 | 1470 | 2165 | 542 | 1055 | - |
| 31 | 2.80 | 9.08 | 1495 | 2631 | 656 | 1005 | - |
| 32 | 2.76 | 8.41 | 1395 | 2496 | 615 | 983 | - |
| 33 | 2.78 | 4.18 | 1538 | 2423 | 663 | 1058 | 734 |
| 33 | 2.78 |  | 1473 | 2595 | 645 | 1117 | - |

Table 7-3. Data from kinetic experiment **M4**: 0.4287 gram biotite, pH 5, $CO_2$-free system.

| Day | pH | F[g/h] | Si [PPB] | Fe [PPB] | Mg [PPB] | Al [PPB] | K [PPB] |
|---|---|---|---|---|---|---|---|
| 0 | - | 13.35 | 717.7 | 33.1 | 407.8 | 761.7 | 32839 |
| 1 | - | 17.13 | 261.9 | 142.9 | 114.6 | 352.2 | 14290 |
| 2 | - | 0 | 289.4 | 54.5 | 71.8 | 151.4 | 9880 |
| 3 | - | 14.71 | 113 | 21.9 | 46.3 | 106.4 | 6026 |
| 4 | - | 17.31 | 113 | 38.7 | 29.6 | 109.4 | 4065 |
| 5 | - | 17.34 | 160.4 | 18.8 | 20.6 | 32.5 | - |
| 6 | - | 10.34 | 294.8 | 10.5 | 28 | 17.1 | - |
| 8 | - | 15.12 | 392.2 | - | - | - | - |
| 9 | - | 15.11 | 375.6 | 19.8 | 28.9 | 39.3 | 1002 |
| 10 | - | 15.76 | 301.3 | 26.2 | 27.7 | 38.1 | - |
| 11 | - | 16.07 | 262.9 | 314.3 | 24.3 | 83.1 | 31 |
| 12 | - | 15.97 | 333.6 | 39.2 | 20.7 | 41.1 | - |
| 15 | - | 15.71 | - | 83 | 22 | 230 | - |
| 16 | - | 15.7 | 1152 | 81.2 | 27.9 | 84.7 | - |
| 17 | - | 15.24 | 1227.1 | 54 | 14 | 64.6 | 1033 |
| 22 | - | 15.77 | 1135 | - | - | - | - |
| 23 | - | 15.93 | 1053 | 10.6 | 12.3 | 100.9 | - |
| 24 | - | 15.61 | 1204 | 18.8 | 11 | 9.9 | - |
| 25 | - | 15.84 | 1038 | 22 | 13.4 | 68 | - |
| 26 | - | 15.93 | 1148 | 18.7 | 13.1 | 23.2 | - |
| 27 | - | 15.7 | - | 37.5 | 7.6 | 36.8 | - |
| 29 | - | 16.11 | 706.4 | 17.5 | 8.1 | 203 | 2710 |
| 30 | - | 7.67 | - | 105 | 7.1 | 21.1 | - |
| 37 | - | 7.91 | 512.3 | 20.2 | 3.9 | 22.5 | - |
| 38 | - |  | 609.3 | 25.6 | 6.1 | 29.4 | 1026 |

Table 7-4. Data from kinetic experiment **M5**: 0.4930 gram biotite, pH 8.5, $CO_2$-free system.

| Day | pH | F | Si [PPB] | Fe [PPB] | Mg [PPB] | Al [PPB] | K [PPB} |
|---|---|---|---|---|---|---|---|
| 1 | - | 14.3 | 715.8 | 51 | - | - | - |
| 2 | - | - | 620 | 5.2 | 121 | 252 | 17619 |
| 3 | - | 10.64 | 332.3 | 17 | 73.3 | 185 | 15963 |
| 4 | - | 18.6 | 584 | 33 | 60.2 | 159 | 9108 |
| 5 | - | 18.49 | 294.7 | 37.3 | 38.9 | 113 | 4876 |
| 6 | - | 12.56 | 508.5 | 16.7 | 29.1 | 138 | - |
| 7 | - | 15.99 | 643 | 4.9 | 35.4 | 57.4 | - |
| 8 | - | 16.15 | 616 | 29.1 | 35.2 | 103 | 2124 |
| 9 | - | 16.11 | 587 | 9.4 | 28.8 | 62.6 | - |
| 10 | - | 16.24 | 578 | 37.6 | 31 | 81.8 | 1234 |
| 13 | - | 15.97 | 577 | 31.9 | 20.1 | 155 | - |
| 14 | - | 16.09 | 615 | 55.3 | 21.6 | 150 | - |
| 20 | - | 16.21 | 664 | 17.1 | 11.2 | 40.7 | 982 |
| 21 | - | 16.4 | 504 | 7.2 | 7.8 | 39.3 | - |
| 22 | - | 16.3 | 508 | 10.4 | 9.1 | 267 | - |
| 23 | - | 16.1 | 623 | 106 | 11.3 | 24.7 | - |
| 24 | - | 15.83 | 555 | 21.7 | 10.7 | 66.2 | - |
| 25 | - | 16.26 | 507 | 14.8 | 8.6 | 77.1 | - |
| 28 | - | 16.82 | 723 | 9.3 | 5 | 64.1 | - |
| 35 | - | 7.91 | - | 36.6 | 8.4 | 33.4 | - |
| 36 | - | 8.1 | 798 | 28.6 | 7.6 | 22.4 | - |

Table 7-5. Data from kinetic experiment **M6**: 0.2599 gram biotite, pH 10, $CO_2$-free system.

| Day | pH | F | Si [PPB] | Fe [PPB] | Mg [PPB] | Al [PPB] | K [PPB] |
|---|---|---|---|---|---|---|---|
| 0 | - | 15.00 | 306 | 280 | 347 | 602 | 31066 |
| 2 | - | 15.00 | - | - | - | - | 34385 |
| 3 | - | 13.96 | 517 | 66.3 | 72.6 | 322 | 12925 |
| 4 | | 14.25 | 534 | 46.9 | 49.6 | 391 | 8865 |
| 5 | - | 13.87 | 502 | 100 | 41.6 | 175 | 4818 |
| 6 | - | 16.13 | 740 | 161 | 18.9 | 81.9 | - |
| 7 | - | 12.84 | 1042 | 234 | 31 | 78.3 | - |
| 8 | - | 13.14 | 1005 | 122 | 32.1 | 70.4 | 1138 |
| 9 | - | 13.52 | 1022 | 130 | 24.1 | 85.7 | - |
| 10 | - | 13.25 | 931 | 63 | 26.2 | 71.8 | 494 |
| 13 | - | 13.4 | 367 | 68.2 | 204 | - | - |
| 14 | - | 8.83 | 1059 | 334 | 50.5 | 287 | - |
| 21 | - | 15.01 | 262 | 108 | 14.4 | 147 | 799 |
| 22 | - | 15.25 | 799 | 114 | 14.8 | 54.2 | |
| 23 | - | 14.22 | - | 285 | 13.7 | 145 | - |
| 24 | - | 14.43 | 392 | 183 | 12.5 | 58.3 | - |
| 27 | - | 15.91 | 1084 | 228 | 16 | 97.2 | - |
| 28 | - | 16.27 | - | 272 | 18.4 | 133 | 1095 |
| 35 | - | 7.01 | - | 187 | 16.6 | 40.2 | - |
| 36 | - | 7.57 | 666 | 83.5 | 15.6 | 21.5 | - |
| 37 | - | 7.47 | 757 | 36.1 | 16 | 1.7 | 897 |

Table 7-6. Data from kinetic experiment **M8**: 0.5249 gram biotite, pH 7, $CO_2$-free system.

| Day | pH | F | Si [PPB] | Fe [PPB] | Mg [PPB] | Al [PPB] | K [PPB] |
|---|---|---|---|---|---|---|---|
| 1 | - | 13.85 | - | 90.1 | 2531 | 1359 | 89259 |
| 2 | - | 13.4 | 789.3 | 33.9 | 218.4 | 34 | 19484 |
| 3 | - | 13.7 | 637 | 32.3 | 112.6 | 238 | 13586 |
| 4 | - | 14.17 | 465.3 | 19.5 | 69.6 | 143.3 | 10302 |
| 5 | - | 15.2 | 476.8 | 59.2 | 61.2 | 122 | 8187 |
| 6 | - | 11.22 | 481.6 | 48.5 | 45.7 | 87.7 | 6537 |
| 7 | - | 13.04 | 375.3 | 17.1 | 46.9 | 81.6 | 6331 |
| 8 | - | 10.49 | 351.1 | 13.6 | 36 | 56 | 5208 |
| 9 | - | 10.49 | 395.3 | 12.1 | 30.1 | 51.4 | 4560 |
| 10 | - | 10.25 | - | 16.4 | 29.6 | 72.3 | 4478 |
| 11 | - | 10.55 | 359.9 | 23.2 | 24.4 | 69.8 | 3067 |
| 12 | | 10.37 | 336.3 | 15 | 25 | 78.7 | 4486 |
| 13 | - | - | - | - | - | - | 3500 |
| 14 | - | - | 1158 | 23 | 55.3 | 139.8 | 2675 |
| 15 | - | - | 700.9 | - | - | - | 2000 |
| 17 | - | 11.02 | 332 | 16.9 | 13 | 151.1 | 1540 |
| 19 | - | 11.22 | 758 | 14.8 | 13.9 | 20.5 | 1488 |
| 20 | - | 11.37 | 813 | 67.2 | 14 | 19.7 | 1248 |
| 21 | - | 11.47 | 828 | 15.3 | 15.8 | 22 | 1752 |
| 22 | - | 11.47 | 786 | 11.5 | 10.4 | 17.1 | 1632 |
| 24 | - | 11.76 | 902 | 16 | 8 | 21.6 | 1144 |
| 25 | - | 5.25 | 723 | 20.3 | 15.1 | 85.3 | 372 |
| 26 | - | 5.45 | 769 | 50.8 | 17.7 | 155.3 | 909 |
| 27 | - | 5.43 | - | - | - | - | 700 |
| 28 | - | 5.49 | 884 | 31.8 | 28.3 | 31.3 | 513 |

Table 7-7. Data from kinetic experiment **M10**: 0.3851gram biotite, pH 2, $CO_2$-free system.

| Day | pH | F | Si [PPB] | Fe [PPB] | Mg [PPB] | Al [PPB] | K [PPB] |
|---|---|---|---|---|---|---|---|
| 0.08 | - | 6.18 | 5300 | 12200 | 4544 | 3735 | 64142 |
| 0.17 | - | 11.53 | 3452 | 9048 | 2744 | 3026 | 32380 |
| 0.25 | - | 11.69 | 3731 | 9135 | 3636 | 1974 | 27052 |
| 1 | - | 12.01 | 6678 | 14961 | 3750 | 5713 | 15837 |
| 1.2 | - | 11.31 | 6592 | 14035 | 3330 | 5579 | 13296 |
| 2 | - | 11.95 | 6895 | 11970 | 2865 | 5182 | 14971 |
| 3 | - | 11.9 | 6390 | 9730 | 2711 | 3992 | 8814 |
| 4 | - | 12.16 | 6088 | 9037 | 2295 | 3703 | 7219 |
| 7 | - | 3.6 | - | 8483 | 2010 | 3681 | 9074 |
| 7.2 | - | 15.84 | 5742 | - | - | - | 7198 |
| 9 | - | 16.68 | - | 9863 | 2151 | 2920 | 4163 |
| 10 | - | 17.27 | 4682 | 6232 | 1778 | 2633 | 2811 |
| 11 | - | 16.46 | 4629 | 5511 | 1760 | 2363 | 2424 |
| 14 | - | 14.94 | 3023 | 5494 | 2574 | 1417 | 2117 |
| 15 | - | 17.04 | 3820 | 4850 | 1258 | 2133 | 1028 |
| 16 | - | 16.26 | 3479 | 4485 | 1106 | 1678 | 1608 |
| 17 | - | 16.67 | 2680 | 2838 | 2815 | 1343 | 1812 |
| 18 | | 16 | 2775 | 2945 | 838 | 1306 | 2088 |
| 20 | - | 15.59 | - | 3840 | 1027 | 1545 | 939 |
| 21 | - | 16.83 | 3026 | 3401 | 851 | 1367 | 2260 |
| 21.2 | - | 17.22 | 2977 | 3168 | 813 | 1436 | 3207 |
| 22 | - | 9.53 | 3780 | 4098 | 1049 | 1611 | 696 |
| 23 | - | 9.6 | - | 3978 | 1021 | 1599 | 888 |
| 24 | - | 9.32 | 3599 | 3998 | 1010 | 1594 | 413 |
| 25 | - | 3.96 | 6681 | 7653 | 1747 | 3093 | 1024 |
| 27 | - | 2.95 | 6611 | 6830 | 1780 | 3057 | 921 |

Table 7-8. Data from kinetic experiment **M11**: 0.2461gram biotite, pH 10, $CO_2$-free system.

| Day | pH | F [g/h] | Si [PPB] | Fe [PPB] | Mg [PPB] | Al [PPB] | K [PPB] |
|---|---|---|---|---|---|---|---|
| 0.08 | - | 5.85 | 2807 | 72 | 1564 | 697 | 101452 |
| 0.17 | - | 10.18 | 1863 | 44.2 | 542 | 471 | 48205 |
| 0.25 | - | 10.49 | 1680 | 88 | 449 | 363 | 35183 |
| 1 | - | 11.02 | 1299 | 183 | 271 | 195 | 23938 |
| 1.2 | - | 10.49 | 1439 | 405 | 228 | 189 | 19237 |
| 2 | - | 10.65 | 1075 | 443 | 183 | 201 | 10256 |
| 3 | - | 9.76 | 1715 | 147 | 60 | 7 | 6856 |
| 4 | - | 9.54 | 803 | 16 | 34 | 30 | 6095 |
| 7 | - | 6 | 796 | 228 | 44 | 110 | 2996 |
| 7.2 | - | 14.7 | 731 | 333 | 66 | 53 | 2751 |
| 9 | - | 15.06 | 1444 | 158 | 19 | 57 | 3068 |
| 10 | - | 16.09 | 1361 | 9 | 16 | 52 | 2310 |
| 11 | - | 15.19 | 1386 | 30 | 12 | 54 | 3124 |
| 14 | - | 10.25 | - | 682 | 21 | 58 | 908 |
| 15 | - | 15.68 | 1359 | 38 | 10 | 25 | 1552 |
| 17 | - | 15.43 | 1337 | 36 | 8 | 60 | 1331 |
| 18 | - | 15 | 1282 | 26 | 6 | 85 | 1082 |
| 19 | - | 14.65 | 2006 | 333 | 12 | 98 | 2743 |
| 20 | - | 14.7 | 2155 | 627 | 32 | 137 | 903 |
| 21 | - | 16.31 | 1976 | 66 | 8 | 45 | 809 |
| 22 | - | 9 | 2005 | 162 | 13 | 66 | 746 |
| 23 | - | 9.01 | 1945 | 88 | 5 | 25 | 1954 |
| 24 | - | 8.78 | 2121 | 96 | 8 | 30 | 1677 |
| 25 | - | 3.56 | 2111 | 19 | 6 | 18 | 1793 |
| 27 | - | 2.68 | 2054 | 7 | 9 | 0 | 2706 |

## 7.2 APPENDIX: Kinetic data from the biotite-$H_2O$-$CO_2$(g)-system

Table 7-9. Data from kinetic experiment **M12**: 0.1960 gram biotite, pH 6.77, 1% $CO_2$(g) i $N_2$(g).

| Day | pH | F [g/h] | Si [PPB] | Fe [PPB] | Mg [PPB] | Al [PPB] | K [PPB] |
|---|---|---|---|---|---|---|---|
| 1 .0 | - | 10.54 | 188.5 | 17.7 | 99 | 40.9 | - |
| 1.08 | - | 10.75 | 105.5 | 22.4 | 77.6 | 33 | 4544 |
| 1.16 | - | 11.26 | 111.9 | 3.2 | 59.7 | 14.1 | 3336 |
| 2.08 | 8.21 | 10.64 | 371.6 | 5.9 | 144.3 | 202.9 | 29293 |
| 4 | 8.01 | 10.31 | 178.3 | 6.4 | 52.5 | 34.2 | 5513 |
| 5 | 7.13 | 11.90 | 83.8 | 1.9 | 32.5 | 15.3 | 2605 |
| 5.08 | 6.78 | 10.90 | 191.1 | 10.1 | 38 | 57.3 | 7853 |
| 6 | 6.75 | 10.82 | 109 | 7.2 | 28.8 | u.d | 3803 |
| 7 | 6.72 | 10.74 | 92.6 | 5.7 | 20.3 | 11.1 | 1056.5 |
| 8 | 6.63 | 10.84 | 62.3 | 7.2 | 15.1 | u.d | 570.2 |
| 9 | 6.86 | 10.84 | 23.5 | 7.3 | 13.5 | u.d | 521.5 |
| 11 | 6.71 | 10.12 | 60.8 | 9.6 | 11.5 | 13.6 | 357.1 |
| 12 | 6.70 | 10.23 | 251.5 | 3.9 | 5.7 | 15.1 | 424.6 |
| 13 | 6.60 | 10.29 | 110.2 | 3.5 | 9.3 | 12.9 | 181.8 |
| 14 | 6.88 | 10.25 | 83.2 | 19.3 | 3.1 | u.d | 18.8 |
| 15 | 6.72 | 11.06 | 128.6 | 2.5 | 5.4 | 2.3 | 7.8 |
| 16 | 6.86 | 10.71 | 13 | 2.3 | 2.4 | u.d | u.d |
| 18 | 6.89 | 9.85 | 70.4 | 7.8 | 7.6 | 16.5 | - |
| 19 | 6.86 | 10.43 | 14.9 | 3.6 | 2.6 | 55.4 | u.d |
| 20 | 6.91 | 10.66 | 56.4 | 8.1 | 4.6 | 29.8 | 17.2 |
| 21 | 6.88 | 10.70 | 34.1 | 9.6 | 3.8 | u.d | u.d |
| 22 | 6.88 | 10.80 | 47.9 | 2.2 | 1.8 | u.d | u.d |
| 23 | 6.87 | 10.52 | 43.6 | 8.7 | 2.5 | 11 | 47.3 |
| 25 | 6.56 | 10.25 | 12.7 | 12.2 | 1 | 6.2 | 79.2 |
| 26 | 6.60 | 10.59 | u.d | 0.9 | 0.1 | u.d | 37.7 |
| 27 | 6.67 | 10.81 | 7.7 | 2 | 5 | 3.8 | 27 |
| 28 | 6.75 | 10.57 | 15.1 | 11.8 | 0.04 | 14.5 | 8.7 |
| 28.08 | 6.79 | 10.65 | 23.8 | 3.4 | 0.1 | 4 | 169.4 |
| 29 | 6.72 | 10.69 | u.d | 4.6 | 0.3 | u.d | u.d |
| 30 | 6.54 | 10.67 | 5.2 | 1.7 | 6.3 | 22.4 | u.d |

u.d - solution concentration under the detection limit of the ICP.

Table 7-10. Data from kinetic experiment **M13**: 0.2479 gram biotite, pH 8.11, 1% $CO_2$(g) i $N_2$(g).

| Day | pH | F [g/h] | Si [PPB] | Fe [PPB] | Mg [PPB] | Al [PPB] | K [PPB] |
|---|---|---|---|---|---|---|---|
| 1 | - | 12.47 | 192.8 | 46 | 410.5 | 89.9 | 35532 |
| 1.08 | - | 12.91 | 286.8 | 136.5 | 309.7 | 123.6 | 19803 |
| 1.16 | - | 12.30 | 266.4 | 121.1 | 198.9 | 105 | 21903 |
| 2 | 8.13 | 12.56 | 89.4 | 12.5 | 62.8 | 24.7 | 12975.9 |
| 2.08 | 8.12 | 11.99 | 93.6 | 23.3 | 50.3 | 28.2 | 7463.4 |
| 4 | 8.11 | 11.60 | 313.8 | 43.1 | 82 | 148.3 | 18039 |
| 5 | 8.10 | 12.61 | 198.6 | 8.3 | 55.5 | 112.5 | 12894 |
| 5.08 | 8.10 | 12.13 | 117.5 | 60.6 | 38.2 | 53.9 | 11319 |
| 6 | 8.11 | 12.08 | 176.9 | 37.5 | 44.1 | 95 | 5132 |
| 7 | 8.07 | 11.95 | 264.4 | 15.7 | 27.9 | 63.4 | 4023 |
| 8 | 8.09 | 11.73 | 248.9 | 12 | 18.6 | 34.9 | 1437.9 |
| 9 | 8.06 | 12.18 | 175.8 | 25.1 | 17.9 | 29.2 | 984.5 |
| 11 | 8.06 | 11.51 | 132.2 | 9.8 | 13.7 | 40.5 | 616.2 |
| 12 | 8.13 | 11.23 | 163.5 | 8.6 | 14.9 | 34.3 | 470.9 |
| 12.08 | 8.11 | 11.74 | 142.2 | 13.6 | 18.1 | 25.1 | 500.6 |
| 13 | 8.12 | 12.38 | 200.3 | 20.4 | 11.8 | 25.8 | 480.5 |
| 14 | 8.10 | 11.64 | 122.7 | 11.4 | 12 | 30 | 431.2 |
| 15 | 8.13 | 11.73 | 86.5 | 9.5 | 12 | 30 | 187 |
| 16 | 8.11 | 12.07 | 64.6 | 21.3 | 12.4 | 45.2 | 220.5 |
| 18 | 8.11 | 11.48 | 232.2 | 17 | 16.1 | 15 | 200 |
| 19 | 8.17 | 11.93 | 74.4 | 19.3 | 8.3 | 19.1 | 147.9 |
| 20 | 8.12 | 11.99 | 91 | 2.6 | 5.2 | 17.7 | 199.8 |
| 21 | 8.15 | 12 | 88.6 | 22.3 | 9.9 | 50 | 364.7 |
| 22 | 8.19 | 12.37 | 51.9 | 10.1 | 8.2 | 44.2 | 69.7 |
| 23 | 8.13 | 12.08 | 49.9 | 11.6 | 6.7 | 21.5 | 237.6 |
| 25 | 8.23 | 11.63 | 73.3 | 11 | 5.7 | 20.5 | 138.7 |
| 26 | 8.16 | 12.21 | 21 | 2.9 | 2.6 | 10 | 124.3 |
| 27 | 8.04 | 12.42 | 33.3 | 2.8 | 6.6 | 6.3 | 301.4 |
| 28 | 8.05 | 12.08 | 37.9 | 7.2 | 4.9 | u.d | 248.8 |
| 28.08 | 8.05 | 12.25 | 28.7 | 3.5 | 2.9 | u.d | 268.5 |
| 29 | 8.04 | 12.41 | 48.7 | 1.9 | 3.3 | 10.5 | 243.6 |
| 30 | 8.05 | 12.08 | 17.9 | 4.8 | 2.9 | 5.1 | 289 |

u.d - solution concentration under the detection limit of the ICP.

Table 7-11. Data from kinetic experiment **M14**: 0.4487 gram biotite, pH 8.41, 1% $CO_2$(g) i $N_2$(g).

| Day | pH | F [g/h] | Si [PPB] | Fe [PPB] | Mg [PPB] | Al [PPB] | K [PPB] |
|---|---|---|---|---|---|---|---|
| 1 | - | 10.12 | 5050 | 223.1 | 4273 | 89 | 153563. |
| 1.1 | - | 7.35 | 787 | 144.9 | 1502 | 253 | 53108 |
| 1.2 | - | 8.62 | 568 | 101.2 | 552 | 182 | 40437 |
| 2 | - | 8.26 | 453 | 78.9 | 256 | 158 | 25657 |
| 2.1 | - | 8.28 | 514 | 79.8 | 206 | 241 | 27751 |
| 2.2 | - | 9.71 | 361 | 66.9 | 160 | 143 | 17254 |
| 3 | 8.28 | 9.81 | 347 | 45.5 | 92 | 131 | 9316 |
| 4 | 8.34 | 9.47 | 279 | 43.6 | 96 | 132 | 5330 |
| 5 | 8.36 | 9.7 | 121 | 19.8 | 35 | 59.4 | 1820 |
| 6 | 8.32 | 9.90 | 36 | 14.5 | 22.3 | 52 | 860 |
| 7 | 8.35 | 9.93 | 38 | 13.7 | 22.6 | 65.7 | 819 |
| 8 | 8.38 | 8.74 | 91 | 34 | 14.4 | 57.1 | 638 |
| 9 | 8.27 | 7.96 | 250 | 12.8 | 15.6 | 50.5 | 794 |
| 12 | 8.38 | 8.71 | 733 | 10.6 | 16.6 | 54.9 | 1167 |
| 12.1 | 8.30 | 9.53 | 653 | 29.1 | 23 | 64.6 | 1254 |
| 12.2 | 8.20 | 9.38 | 43 | 19.6 | 18.9 | 90.8 | 1705 |
| 13 | 8.26 | 10.22 | 189 | 15 | 10.6 | 50.8 | 1606 |
| 14 | 8.36 | 10.1 | 103 | 11.4 | 10.1 | 53.3 | 1163 |
| 15 | 8.39 | 9.52 | 49 | 10.3 | 16.7 | 54.2 | 1183 |
| 16 | 8.54 | 8.60 | 50 | 15.2 | 4.4 | 47.2 | 848 |
| 18 | 8.38 | 9.18 | 43 | 21 | 0.3 | 22 | - |
| 19 | 8.39 | 9.52 | 27 | 17.8 | 16.3 | 61.6 | 741 |
| 20 | 8.38 | 9.02 | 6 | 12.1 | 12.8 | 43.8 | 800 |
| 21 | 8.31 | 9.23 | 0 | 14.1 | 16.7 | 54.2 | 699 |
| 21.2 | 8.33 | 4.42 | 43 | 22.4 | 22.5 | 57.6 | - |
| 22 | 8.37 | 4.38 | 188 | 13.7 | 24.3 | 61.3 | 1249 |
| 23 | 8.39 | 3.93 | 92 | 14 | 23.8 | 54.4 | 958 |
| 24 | 8.4 | 2.92 | 197 | 16.8 | 16.9 | 53.4 | - |
| 25 | 8.41 | 3.15 | 123 | 12.7 | 23.9 | 60.6 | 947 |
| 26 | 8.41 | 3.95 | 107 | 13 | 26.2 | 64.2 | 1012 |
| 27 | 8.41 | 3.61 | 113 | 11.8 | 25.6 | 61.8 | 946 |
| 28 | 8.41 | - | 116 | 28.7 | 26.1 | 67 | 1101 |

Table 7-12. Data from kinetic experiment **M15**: 0.3627 gram biotite, pH 8.75, 1% $CO_2$(g) i $N_2$(g).

| Day | pH | F [g/h] | Si [PPB] | Fe [PPB] | Mg [PPB] | Al [PPB] | K [PPB] |
|---|---|---|---|---|---|---|---|
| 1 | - | 17.23 | 1067 | 1210 | 2506.328 | 308.3 | 62748 |
| 1.1 | - | 10.87 | 2255 | 2288 | 851.8571 | 910.7 | 20496 |
| 1.2 | - | 11.69 | 157 | 196.8 | 200.2 | 65.3 | 9408 |
| 2 | - | 11.67 | 100 | 128.2 | 104 | 52 | 6625.5 |
| 2.1 | - | 11.66 | 211 | 148.8 | 96.2 | 88.9 | 4508 |
| 2.2 | - | 12.45 | 75 | 94.3 | 62.2 | 43.5 | 3602 |
| 3 | 7.58 | 11.44 | 198 | 109 | 33.5 | 49.1 | 3143 |
| 4 | 8.63 | 11.46 | 101 | 41.6 | 10 | 47.3 | 1318 |
| 5 | 8.39 | 6.651 | 49 | 30.4 | 20 | 32.2 | 1142 |
| 6 | 8.63 | 12.80 | 102 | 35.8 | 9.7 | 58.6 | 1376 |
| 7 | 8.74 | 12.93 | 397 | 36.8 | 18.1 | 73.9 | 1291 |
| 8 | 8.43 | 12.16 | 465 | 35.5 | 0.1 | 80 | 1188 |
| 9 | 8.68 | 11.63 | 98 | 37 | 12.2 | 58.5 | 1181 |
| 12 | 8.61 | - | 38 | 26.1 | 14.6 | 43.4 | 1072 |
| 12.1 | 8.66 | - | 55 | 32.2 | 2.3 | 42.4 | 974 |
| 12.2 | 8.70 | 11.42 | 330 | 50.2 | 19.7 | 81 | 1567 |
| 13 | 8.85 | 12.39 | 212 | 34.4 | 12.1 | 69.1 | 1071 |
| 14 | 8.89 | 12.65 | 453 | 81.8 | 29.2 | 115.1 | 1085 |
| 15 | 8.30 | 12.35 | - | 25 | 2.1 | 38 | 1121 |
| 16 | 8.43 | 12.86 | 109 | 27.2 | 1.1 | 51.2 | 1195 |
| 18 | 8.63 | 12.00 | 113 | 22.6 | u.d | 34.8 | - |
| 19 | 8.68 | 12.58 | 279 | 170.2 | 39.1 | 113.1 | 2308 |
| 20 | 8.75 | 12.13 | 128 | 38.7 | 11.8 | 57.9 | 1318 |
| 21 | 8.85 | 12.50 | 140 | 66.8 | 13.8 | 61.2 | 1118 |
| 21.2 | 8.49 | 5.82 | 117 | 51 | 20.8 | 56.8 | 1574 |
| 22 | 8.55 | 5.85 | 110 | 36 | 18.2 | 45.7 | 1598 |
| 23 | 8.59 | 5.66 | 123 | 33.5 | 19.5 | 52.1 | 1323 |
| 24 | 8.64 | 5.05 | 121 | 42 | 2.3 | 57 | 1398 |
| 25 | 8.69 | 4.90 | 125 | 38.2 | 11.5 | 73 | 1358 |
| 26 | 8.72 | 6.07 | 130 | 34.6 | 25.2 | 85.4 | 1515 |
| 27 | 8.76 | 5.75 | 138 | 30.3 | 11.7 | 51.5 | 1187 |
| 28 | 8.81 | - | 46.8 | 24.5 | - | 47.2 | 478.5 |

u.d - solution concentration under the detection limit of the ICP.

## 7.3 APPENDIX: Kinetic data from the chlorite-$H_2O$-$CO_2$(g)-system

Table 7-13. Data from kinetic experiment **Ka**: 0.2519 gram chlorite (125-300 $\mu$m), pH 8.18, 1% $CO_2$(g) i $N_2$(g).

| Day | pH | F [g/h] | Si [PPB] | Fe [PPB] | Mg [PPB] | Al [PPB] |
|---|---|---|---|---|---|---|
| 0 | - | 6.30 | 780 | 25 | 7025 | 163 |
| 0.12 | - | 2.67 | 117 | 6 | 566 | 103 |
| 0.79 | - | 3.83 | 227 | 5 | 323 | 92 |
| 1.08 | - | 4.28 | 62 | 25 | 220 | 55 |
| 1.79 | - | 4.62 | 62 | 33 | 183. | 59 |
| 3.91 | 8.16 | 4.36 | 227 | 81 | 134 | 61 |
| 4.91 | 8.17 | 5.01 | 360 | 57 | 88 | 23 |
| 5.79 | 8.17 | 4.82 | 119 | 56 | 84 | 32 |
| 6 | 8.16 | 4.88 | 14 | 52 | 66 | 30 |
| 7 | 8.17 | 4.99 | 75 | 50 | 61 | 14 |
| 8 | 8.18 | 4.92 | 50 | 1 | 49 | 10 |
| 9 | 8.19 | 4.12 | 106 | 4 | 44 | 25 |
| 10 | 8.16 | 3.97 | 154 | 61 | 212 | 77 |
| 11 | 8.18 | 4.67 | 198 | 29 | 107 | 62 |
| 12 | 8.17 | 4.67 | 169 | 35 | 156 | 71 |
| 13 | 8.17 | 4.79 | 165 | 30 | 115 | 58 |
| 14 | 8.18 | 4.31 | 280 | 17 | 104 | 29 |
| 16 | 8.19 | 4.20 | 198 | 17 | 105 | 19 |
| 17 | 8.18 | 4.31 | 165 | u.d | 60 | u.d |
| 18 | 8.20 | 4.71 | 278 | u.d | 53 | u.d |
| 19 | 8.19 | 5.03 | 153 | u.d | 53 | u.d |
| 20 | 8.19 | 5.13 | 143 | u.d | 39 | u.d |
| 21 | 8.18 | 4.96 | 165 | u.d | 34 | u.d |
| 22 | 8.17 | 5.13 | 151 | u.d | 31 | u.d |
| 25 | 8.12 | 9.46 | 110 | u.d | 19 | u.d |
| 26 | 8.14 | 9.80 | 107 | u.d | 20 | u.d |
| 27 | 8.18 | 9.47 | 115 | u.d | 20 | u.d |
| 28 | 8.13 | 10.59 | 80.887 | u.d | 20 | u.d |

u.d - solution concentration under the detection limit of the ICP.

Table 7-14. Data from kinetic experiment **Kb**: 0.3196 gram chlorite (125-300 $\mu$m), pH 2.60, $CO_2$-free system.

| Day | pH | F [g/h] | Si [PPB] | Fe [PPB] | Mg [PPB] | Al [PPB] |
|---|---|---|---|---|---|---|
| 0 | - | 6.22 | 808 | 205 | 8430 | 727 |
| 0.12 | - | 2.52 | 796 | 324 | 5275 | 1117 |
| 0.79 | - | 3.69 | 494 | 181 | 2205 | 855 |
| 1.08 | - | 4.19 | 465 | 241 | 1723 | 833 |
| 1.79 | - | 4.46 | 418 | 211 | 1007 | 435 |
| 3.91 | - | 4.00 | 420 | 145 | 615 | 257 |
| 4.91 | 2.65 | 4.85 | 365 | 102 | 433 | 180 |
| 5.79 | 2.65 | 4.62 | 404 | 115 | 423 | 144 |
| 6 | 2.65 | 4.65 | 247 | 83 | 377 | 105 |
| 7 | 2.65 | 4.75 | 164 | 15 | 243 | 52 |
| 8 | 2.65 | 6.15 | 293 | 55 | 392 | 144 |
| 9 | 2.66 | 3.90 | 654 | 56 | 301 | 100 |
| 10 | 2.56 | 4.21 | 148 | 1 | 58 | 31 |
| 11 | 2.55 | 4.45 | 565 | 81 | 472 | 155 |
| 12 | 2.55 | 4.44 | 440 | 51 | 413 | 153 |
| 13 | 2.55 | 4.57 | 636 | 59 | 312 | 112 |
| 14 | - | 3.33 | 613 | 52 | 65 | 162 |
| 16 | 2.56 | 4.05 | 321 | 46 | 325 | 114 |
| 17 | 2.62 | 4.20 | 317 | 97 | 418 | 136 |
| 18 | - | 4.85 | 292 | 19 | 217 | 50 |
| 19 | - | 4.90 | 266 | 24 | 23 | 74 |
| 20 | 2.60 | 4.92 | 254 | 26 | 226 | 71 |
| 21 | 2.60 | 4.77 | 299 | 98 | 289 | 102 |
| 22 | 2.59 | 4.96 | 281 | 60 | 303 | 98 |
| 25 | 2.59 | 9.25 | 147 | 9 | 102 | 33 |
| 26 | 2.59 | 9.65 | 165 | 6 | 141 | 45 |
| 27 | 2.58 | 9.277 | 206 | 35 | 152 | 74 |
| 28 | 2.53 | 10.37 | 114 | 19 | 129 | 42 |

Table 7-15. Data from kinetic experiment **Kc**: 0.3248 gram chlorite (125-300 $\mu$m), pH 3.80, 100% $CO_2$(g).

| Day | pH | F [g/h] | Si [PPB] | Fe [PPB] | Mg [PPB] | Al [PPB] |
|---|---|---|---|---|---|---|
| 0 | - | 16.15 | 1137 | 45 | 5183 | 113 |
| 0.074 | - | 7.71 | 2734 | 13 | 2397 | 19.5 |
| 0.220 | - | 5.14 | 932 | 21 | 1241 | 14 |
| 0.409 | - | 5.85 | 629 | 12 | 803 | 24 |
| 0.87 | - | 6.72 | 455 | 22 | 468 | 64 |
| 1.20 | - | 5.72 | 481 | 50 | 362 | 91 |
| 2 | - | 6.23 | 329 | 11.5 | 279 | 83 |
| 2.91 | 4.74 | 5.16 | 318 | 8.7 | 200 | 39 |
| 5.08 | 4.57 | 6.15 | 227 | 10 | 123 | 43 |
| 5.87 | 4.87 | 6.11 | 230 | 1.7 | 92 | 38 |
| 7.08 | 4.66 | 6.80 | 236 | u.d | 80 | 37 |
| 8 | 4.68 | 6.50 | 245 | 2.1 | 83 | 22 |
| 9.12 | 4.50 | 6.83 | 150 | 3 | 70 | 42 |
| 11 | 4.57 | 5.63 | 144 | 3.5 | 86 | 25 |
| 12.12 | 3.79 | 7.20 | 196 | 21 | 165 | 121 |
| 13.08 | 3.78 | 7.49 | 190 | 19 | 158 | 140 |
| 13.91 | 3.86 | 5.37 | 185 | 18 | 158 | 109 |
| 14.91 | 3.86 | 5.64 | 210 | 17 | 163 | 79 |
| 16.08 | 3.79 | 6.18 | 186 | 25 | 157 | 100 |
| 17.95 | 3.83 | 3.11 | 246 | 20 | 206 | 99 |
| 19.20 | 3.78 | 4.13 | 216 | 14 | 188 | 95 |
| 20 | 3.80 | 5.76 | 184 | 13 | 151 | 82 |
| 21.25 | 3.79 | 3.25 | 267 | 11 | 208 | 88 |
| 23.08 | 3.76 | 5.20 | 219 | 18 | 136 | 70 |
| 25.45 | 3.82 | 4.51 | 203 | 6 | 156 | 58 |
| 26.08 | 3.80 | 5.97 | 218 | 87 | 124 | 61 |
| 27.04 | 3.80 | 5.56 | 224 | 82 | 132 | 78 |
| 28 | 3.77 | 5.87 | 185 | 9 | 111 | 58 |
| 29.08 | 3.76 | 6.37 | 130 | 10 | 129 | 49 |
| 29.25 | 3.76 | 4.48 | 182 | 63 | 140 | 51 |
| 29.95 | 3.789 | 5.57 | 289 | 0.5 | 129 | 52 |
| 32.16 | - | 3.37 | 349 | 18 | 182 | 70 |
| 32.91 | 3.81 | 4.47 | 239. | 2 | 142 | 62 |
| 33.25 | 3.79 | 3.42 | 239 | 136 | 141 | 56 |
| 33.91 | 3.81 | 6.05 | 167 | 308 | 115 | 35 |
| 35 | 3.76 | 5.79 | 157 | u.d | 112 | 34 |

u.d - solution concentration under the detection limit of the ICP.

Table 7-16. Data from kinetic experiment **Kd**: 0.2239 gram chlorite (75-125 $\mu$m), pH 7.12, 100% $CO_2$(g).

| Day | pH | F [g/h] | Si [PPB] | Fe [PPB] | Mg [PPB] | Al [PPB] |
|---|---|---|---|---|---|---|
| 0 | - | 14.74 | 1141 | 97 | 6225 | 220 |
| 0.07 | - | 5.37 | 901 | 26 | 1606 | 55 |
| 0.22 | - | 5.50 | 635 | 9 | 1045 | 41 |
| 0.40 | - | 5.75 | 455 | 5 | 425 | 24 |
| 0.87 | - | 6.66 | 647 | 15 | 243 | 25 |
| 1.20 | - | 5.68 | 339 | 19 | 270 | 44 |
| 2 | - | 6.23 | 258 | 4 | 158 | 17 |
| 2.91 | 6.98 | 4.50 | 512 | 18 | 237 | 38 |
| 5.08 | - | 7.04 | 216 | 5 | 68 | 16 |
| 5.87 | - | 6.01 | 183 | 5 | 85 | 11 |
| 7.08 | 7.16 | 7.03 | 185 | 6 | 49 | 27 |
| 8 | 5.81 | 7.00 | 199 | u.d | 52 | u.d |
| 9.12 | - | 6.41 | 175 | 7 | 43 | u.d |
| 11 | - | 5.61 | 135 | u.d | 45 | u.d |
| 12.12 | 6.69 | 7.05 | 162 | u.d | 36 | u.d |
| 13.08 | 6.79 | 7.44 | 139 | u.d | 30 | u.d |
| 13.91 | 7.17 | 5.28 | 123 | u.d | 26 | 16 |
| 14.91 | 7.17 | 5.43 | 132 | 3 | 36 | u.d |
| 16.08 | 7.11 | 6.54 | 129 | 4 | 44 | u.d |
| 17.95 | 7.51 | 3.02 | 153 | u.d | 20 | 17 |
| 19.20 | 6.96 | 4.05 | 122 | u.d | 28 | 11 |
| 20 | 7.14 | 5.66 | 102 | u.d | 42 | 1 |
| 21.25 | 7.36 | 3.27 | 141 | u.d | 19 | 8 |
| 23.08 | 7.11 | 5.18 | 101 | u.d | 29 | 14 |
| 25.45 | 7.24 | 4.51 | 120 | u.d | 34 | 12 |
| 26.08 | 6.98 | 5.87 | 163 | 141 | 54 | 32 |
| 27.04 | 7.10 | 5.42 | 187 | 123 | 32 | 27 |
| 28 | 6.94 | 6.15 | 129 | u.d | 40 | 1.7 |
| 29.08 | - | 6.37 | 79.5 | u.d | 43 | u.d |
| 29.25 | - | 4.75 | 113 | 77 | 22 | 3 |
| 29.95 | 7.17 | 4.71 | 147 | u.d | 23 | u.d |
| 32.16 | 7.48 | 3.44 | 267 | u.d | 17 | 5.5 |
| 32.91 | - | 4.42 | 127 | 1 | 18 | u.d |
| 33.25 | 7.31 | 3.39 | 178 | 198 | 27 | u.d |

u.d - solution concentration under the detection limit of the ICP.

Table 7-17. Data from kinetic experiment **Ke**: 0.2500 gram chlorite (75-125 $\mu$m), pH 8.92, 100% $CO_2$(g).

| Day | pH | F [g/h] | Si [PPB] | Fe [PPB] | Mg [PPB] | Al [PPB] |
|---|---|---|---|---|---|---|
| 0 | - | 13.67 | 766 | 167.6 | 4908 | 150.7 |
| 0.07 | - | 6.26 | 522.5 | 150.8 | 1928 | 142.3 |
| 0.22 | - | 5.28 | 351 | 125 | 1194 | 162.6 |
| 0.40 | - | 5.90 | 179 | 67.35 | 687 | 148.9 |
| 0.87 | - | 7.09 | 560 | 71.2 | 400 | 133.5 |
| 1.20 | - | 5.83 | 120 | 80.7 | 376 | 126.2 |
| 2 | - | 6.25 | - | 34.4 | 267 | 88.7 |
| 2.91 | 8.99 | 5.37 | 106 | 36.1 | 214 | 86.7 |
| 5.08 | 9.13 | 6.20 | 22.5 | 18.7 | 57 | 49.4 |
| 5.87 | 8.89 | 6.03 | 4.5 | 15.9 | 107 | u.d |
| 7.08 | 8.93 | 6.74 | 61 | 11.8 | 96 | 43.8 |
| 8 | 9.00 | 6.71 | 61 | 15.5 | 71 | 29.7 |
| 9.12 | 8.95 | 6.73 | 39 | 11.1 | 11 | u.d |
| 11 | 8.96 | 5.83 | 22 | u.d | 51 | u.d |
| 12.12 | 8.75 | 7.46 | 35 | u.d | 70 | u.d |
| 13.08 - | 8.83 | 7.52 | 9 | u.d | 61.3 | u.d |
| 13.91 | 8.84 | 5.50 | 21.6 | 10.2 | 49.6 | u.d |
| 14.91 | 8.90 | 5.82 | 2.5 | 9.9 | 47.1 | u.d |
| 16.08 | 8.93 | 6.23 | 14 | 8 | 59 | u.d |
| 17.95 | 8.84 | 3.18 | 22 | 5.5 | 76.2 | u.d |
| 19.20 | 8.86 | 4.22 | u.d | u.d | 69.4 | u.d |
| 20 | 8.89 | 5.85 | u.d | 9.5 | 72.8 | u.d |
| 21.25 | 8.92 | 3.38 | 17 | u.d | 81.7 | u.d |
| 23.08 | 9.02 | 5.35 | 5 | 5.6 | 58.9 | u.d |
| 25.45 | 9.08 | 5.71 | 76 | u.d | 105.5 | u.d |
| 26.08 | 9.07 | 6.08 | 24.5 | 200.5 | 23.3 | u.d |
| 27.04 | 9.10 | 5.61 | 60 | 188 | 30.7 | u.d |
| 28 | 8.86 | 6.01 | 38 | u.d | 75.6 | u.d |
| 29.08 | 8.90 | 6.70 | u.d | 11.9 | 85.9 | 31.9 |
| 29.25 | 8.91 | 11.13 | 20 | u.d | 49.7 | u.d |
| 29.95 | 8.93 | 5.52 | 99 | 12.3 | 70.75 | u.d |
| 32.16 | 3.75 | 3.84 | 137 | 16.7 | 63.5 | u.d |
| 32.91 | 8.95 | 4.50 | 138 | u.d | 77.1 | u.d |
| 33.25 | 8.92 | 3.54 | 64 | u.d | u.d | u.d |
| 33.91 | 8.92 | 6.19 | 18 | 3.7 | 78.9 | u.d |
| 35 | 8.93 | 1.60 | 113 | u.d | 86.6 | u.d |
| 35.41 | 8.88 | 6.57 | 8.5 | u.d | 47.25 | u.d |
| 36.20 | 8.89 | 2.41 | 97.5 | u.d | 93.1 | u.d |

u.d - solution concentration under the detection limit of the ICP.

## 7.4 APPENDIX: Equilibrium data from the biotite-$H_2O$-system

Table 7-18. Data from batch experiments, biotite, $CO_2$(g)-free.

| Sample | pH | log [Si ] | log [Fe (tot)] | log [Mg ] | log [Al ] | K |
|---|---|---|---|---|---|---|
| 6 | 9.43 | -5.01 | u.d | -5.11 | -4.86 | -3.14 |
| 1 | 9.37 | -5.21 | -6.50 | -5.08 | -5.50 | -3.11 |
| 2 | 9.37 | -5.23 | u.d | -5.10 | -5.31 | -3.05 |
| 4 | 8.94 | -5.27 | u.d | -5.04 | -5.10 | -3.09 |
| 3 | 8.99 | -5.28 | u.d | -5.04 | -5.50 | -2.70 |
| 5 | 9.04 | -5.28 | u.d | -5.04 | -5.63 | -3.03 |
| 8 | 3.90 | -3.110 | -2.81 | -3.10 | -4.97 | -2.60 |
| 13 | 11.88 | -4.55 | -6.87 | - | -4.14 | -3.18 |
| 12 | 10.67 | -4.75 | u.d | -5.93 | -4.41 | -3.13 |
| 11 | 9.15 | -4.67 | u.d | -5.10 | -4.84 | -3.02 |
| 7 | 2.57 | -2.71 | -2.28 | -2.48 | -2.34 | -2.44 |
| 10 | 6.73 | -5.10 | -6.76 | -4.91 | -6.08 | -2.94 |
| 14 | 0.3 | -2.20 | -1.75 | -1.86 | -1.65 | -1.83 |
| 15 | 0.8 | -2.20 | -1.90 | -2.05 | -1.87 | -1.99 |
| 16 | 1.88 | -2.38 | -2.28 | -2.52 | -2.33 | -2.44 |
| 17 | 3.17 | -2.50 | -2.44 | -2.68 | -2.55 | -2.44 |
| 18 | 4.58 | -3.13 | -3.16 | -3.39 | -3.53 | -2.46 |
| 19 | 4.78 | -3.48 | -3.43 | -3.73 | -4.02 | -3.60 |
| 21 | 0.3 | -1.75 | -1.49 | -1.72 | -1.54 | -1.73 |
| 22 | 2.45 | -2.24 | -2.13 | -2.42 | -2.28 | -2.18 |
| 23 | 1.25 | -2.03 | -1.91 | -2.17 | -1.98 | -2.09 |
| 24 | 0.82 | -1.96 | -1.83 | -2.08 | -1.89 | -2.02 |
| 25 | 0.6 | -1.97 | -1.76 | -2.00 | -1.81 | -1.99 |
| 26 | 2.34 | -2.25 | -2.16 | -2.40 | -1.47 | -2.25 |
| 28 | 1.74 | -2.62 | -2.67 | -2.87 | -2.70 | -0.34 |
| 29 | 1.83 | -2.15 | -1.93 | -2.17 | -1.98 | -2.09 |
| 30 | 2.31 | -2.21 | -2.11 | -2.26 | -2.01 | -2.27 |
| 31 | 1.83 | -2.21 | -2.11 | -2.30 | -1.33 | -0.38 |
| 32 | 1.88 | -2.49 | -2.51 | -2.65 | -2.44 | -0.65 |
| 33 | 0.64 | -1.77 | -1.45 | -1.67 | -1.50 | -1.63 |
| 34 | 1.35 | -2.06 | -1.76 | -2.01 | -1.81 | -1.96 |
| 35 | 0.45 | -1.57 | -1.28 | -1.50 | -1.24 | -1.50 |
| 36 | 1.18 | -2.21 | -2.24 | -2.45 | -2.25 | -2.20 |

u.d - solution concentration under the detection limit of the ICP.

Table 7-19. Data from titration experiments, biotite, $CO_2$(g)-free.

| Sample | pH | $E_h$[mV] | log [Si ] | log [Fe] | log (Mg ] | log [Al ] | log [K ] |
|---|---|---|---|---|---|---|---|
| b1 | 3.819 | - | -3.21 | -3.07 | -3.33 | -3.19 | -2.91 |
| b2 | 4.086 | - | -3.29 | -3.15 | -3.41 | -3.32 | -3.00 |
| b3 | 4.243 | - | -3.39 | -3.28 | -3.50 | -3.59 | -3.00 |
| b4 | 5.004 | - | -3.59 | -3.73 | -3.58 | -4.56 | -3.13 |
| b5 | 6.479 | - | -3.8 | -6.09 | -3.66 | -6.31 | -3.16 |
| b6 | 7.119 | - | -3.88 | -6.44 | -3.74 | -5.95 | -3.23 |
| b7 | 7.989 | - | -4.01 | -7.27 | -3.85 | -5.98 | -3.31 |
| b8 | 8.208 | - | -4.17 | -5.66 | -4.08 | -5.76 | -3.52 |
| b9 | 8.67 | - | -4.22 | -6.57 | -4.26 | -5.31 | -3.20 |
| b10 | 8.875 | - | -4.27 | -6.90 | -4.65 | -5.21 | -3.54 |
| b11 | 9.337 | - | -4.17 | -6.79 | -5.47 | -4.85 | -3.37 |
| b12 | 10.68 | - | -3.7 | -6.46 | -7.38 | -3.74 | -3.34 |
| t1 | 6.74 | - | -4.4 | u.d | -4.31 | -4.98 | -2.77 |
| t2 | 6.76 | - | -4.24 | u.d | -4.19 | -5.03 | -2.76 |
| t3 | 6.89 | - | -4.18 | u.d | -4.06 | u.d | -2.75 |
| t4 | 8.45 | - | -4.2 | u.d | -4.16 | -5.83 | -2.73 |
| j1 | 8.26 | - | -4.39 | u.d | -4.51 | u.d | -2.94 |
| j2 | 3.34 | - | -3.09 | -2.98 | -3.28 | -3.34 | -2.51 |
| j3 | 2.95 | - | -2.95 | -2.85 | -3.19 | -3.12 | -2.49 |
| p1 | 1.91 | - | -2.35 | -2.32 | -2.56 | -2.39 | -2.52 |
| J1:920924 | 8.47 | - | -3.07 | u.d | -4.51 | u.d | -1.3472 |
| J1:921012 | 3.55 | - | - | -3.01 | - | - | - |
| -J1:921022 | 3.17 | 386.4. | - | -2.73 | - | - | - |
| J1:921210 | 3.24 | 435.9 | -2.74 | -2.76 | -3.15 | -3.02 | -2.75 |
| J1:930127 | 3.53 | 451.9 | -2.69 | -2.65 | -3.06 | -2.92 | -2.63 |
| J1:930209 | 3.06 | 470.3 | -2.52 | -2.46 | -2.81 | -2.65 | -2.82 |
| J1:930223 | 2.98 | 483.8 | -2.46 | -2.39 | -2.74 | -2.60 | -2.73 |
| J1:930319 | 3.23 | 455.8 | -2.9 | -2.68 | -3.03 | -2.86 | -2.98 |
| J1:930624 | 2.91 | 551.5 | - | -2.44 | - | - | -2.98 |
| J1:930915 | 3.37 | 547.1 | - | -2.51 | - | - | - |
| J1:931014 | 2.12 | 626.2 | - | -2.58 | - | - | - |
| J1:931107 | 2.38 | 617.0 | - | -2.61 | - | - | - |
| J1:931128 | 3.31 | 474.6 | - | -2.61 | - | - | |

u.d - solution concentration under the detection limit of the ICP.

## 7.5 APPENDIX: Equilibrium data from the biotite-$H_2O$-$CO_2$-system

Table 7-20. Data from batch expriments, biotite, $CO_2$(g)-system.

| Sample | pH | tot alk [M] | Si | Fe | Mg | Al |
|---|---|---|---|---|---|---|
| A | 9.26 | 0 | 477.7 | 46.9 | 339.4 | 1056.5 |
| B | 8.4 | 83 | 595.6 | 63.3 | 554 | 154.2 |
| C | 8.45 | 250 | 866.8 | 162.1 | 763.9 | u.d |
| D | 8.44 | 333 | 1844.2 | 1007.5 | 11124 | 361.7 |
| E | 8.43 | 500 | 1096.2 | 754.2 | 2279.8 | 128.2 |
| F | 9.16 | 667 | 1261.4 | 1574.2 | 2254 | 702.5 |
| G | 9.42 | 750 | 1157.55 | 1435.8 | 1594.2 | 1486.6 |
| H | 10.12 | 917 | 1155.15 | 1105 | 1029.5 | 2388.4 |
| I | 11.35 | 1000 | 4435.6 | 687.6 | 101.8 | 9714.7 |

Potassium not analysed. u.d - solution concentration under the detection limit of the ICP.

Table 7-21. Data from titration experiments, biotite, $CO_2$(g)-system.

| Sample | pH | Gas [%$CO_2$] | Si [PPB] | Fe [PPB] | Mg [PPB] | Al [PPB] |
|---|---|---|---|---|---|---|
| C6-931107 | 3.70 | 1 | 29695 | 54509 | 10364 | 12239 |
| C6-931004 | 6.47 | 1 | 1676 | 382 | 525 | 38 |
| C6-931013 | 3.93 | 1 | 11114 | 24521 | 4485 | 5225 |
| C6-930915 | 8.33 | 1 | 1121 | 13.6 | 429 | 143 |
| c6-930830 | 8.56 | 1 | 1359 | 74 | 479 | 218 |
| C3-930809 | 7.54 | 10 | 1311 | u.d | 1131 | 73 |
| C3-930819 | 7.73 | 10 | 3976 | u.d | 1472 | 45 |
| C4-930819 | 8.64 | 10 | 3680 | 731 | 808 | 353 |
| C5-931107 | 7.95 | 10 | 2938 | 44 | 672 | 41 |
| C5-931013 | 7.51 | 10 | 2652 | u.d | 701 | 44 |
| C5-931004 | 6.10 | 10 | 3068 | u.d | 784 | 19 |
| C5-930915 | 4.49 | 10 | 3112 | 3628 | 876 | 817 |
| C5-930830 | 5.48 | 10 | 2518 | 370 | 531 | 24 |
| C2:1 | 4.68 | 10 | 1460 | u.d | 295 | 51 |
| C1:1 | 5.50 | 10 | 2178 | 10 | 366 | 18 |
| C1:2 | 8.08 | 10 | 1776 | u.d | 317 | 87 |

Potassium not analysed. u.d - solution concentration under the detection limit of the ICP.

## 7.6 APPENDIX: Equilibrium data from the chlorite-$H_2O$-$CO_2$(g)-system

Table 7-22. Data from batch expriments, chlorite, $CO_2$(g)-system.

| Sample | pH | tot alk. [M] | Si [PPB] | Fe [PPB] | Mg [PPB] | Al [PPB] |
|---|---|---|---|---|---|---|
| J | 8.47 | 250 | 277.75 | 142 | 1742.2 | 130.5 |
| K | 8.89 | 0 | 535.2 | 39.9 | 2260 | - |
| L | 8.34 | 83 | 623.8 | 44 | 5459.8 | 77.6 |
| M | 8.4 | 333 | 266.2 | 409 | 3919.6 | - |
| N | 8.53 | 500 | 783.2 | 832.4 | 13668.7 | 242.7 |
| O | 9.13 | 667 | 1943.5 | 592.9 | 2350.5 | 245.3 |
| P | 9.35 | 750 | 2424.7 | 470.6 | 1840.3 | 313.9 |
| Q | 10.13 | 917 | 3969.6 | 542.2 | 972.8 | 385 |
| R | 11.27 | 1000 | 4524.8 | 524.7 | 95.8 | 268.2 |

## 7.7 APPENDIX: Estimation of solubility-product of phyllosilicates

Due to the lack of experimental data, and the need of information on the stability of clay minerals, and phyllosilicates in general, several methods for estimating the Gibb's free energy of formation ($\Delta G^0_{f,298.15}$) of these minerals have been reported in the literature, i.e. (Slaughter, 1966; Tardy and Garells, 1974; Nriagu, 1975; Chen, 1975; Mattigod and Sposito, 1978; Sposito, 1986).

These methods all calculates the $\Delta G^0_{f,298.15}$ of the sheet mineral by summation of $\Delta G^0_{f,298.15}$ for simple (hydr)oxides. The calculated value is then modified, by theoretical or empirical methods, to compensate for the "polymerization-energy".

We have used the method outlined by Sposito (1986) to estimate the $\Delta G^0_{f,298.15}$ for ideal biotite ($K(Mg_2Fe(II))(AlSi_3)O_{10}(OH)_2$):

Biotite can be regarded as a combination of it´s end-member (hydr)oxides:

$$1\,KOH + 2\,Mg(OH)_2 + Fe(OH)_2 + Al(OH)_3 + 3\,SiO_2{\cdot}2H_2O = K(Mg_2Fe(II))(AlSi_3)O_{10}(OH)_2 + 10H_2O$$

The $\Delta G^0_{f,298.15}$ is then calculated as:

$$\Delta G^o_{f,biotite} = \Delta G^o_{f,KOH} + 2\Delta G^o_{f,Mg(OH)_2} + \Delta G^o_{f,Fe(OH)_2} + \\ + \Delta G^o_{f,Al(OH)_3} + 3\Delta G^o_{f,SiO_2{\cdot}2H_2O} - 10\Delta G^o_{f,H_2O} - |\Delta G^o_{corr.}| \qquad (7\text{-}1)$$

where

$$|\Delta G^0_{corr.}| = 41.34 + 921.66\,(\frac{xR}{Z}) \qquad (7\text{-}2)$$

where x ($x_{biotite} = 1$) is the number of -, R is the Shannon-Prewitt radii ($R_K = 0.138$ nm (Sposito (1986, table 3)) of -, and Z ($Z_K = 1$) the charge of the exchangeable ion.

Using the $\Delta G^0_{f,298.15}$ for the (hydr)oxides given by Mattigod and Sposito (1978, table 1) the $\Delta G^0_{f,\,biotite}$ is calculated to be $-5453 \pm 11$ kJ/mole. The standard deviation is taken from the mean absolute difference between $\Delta G^0_{f,exp}$ and $\Delta G^0_{f,est}$ given by Sposito (1986) for 14 smectites.

The $\Delta G^{0}_{react.}$ for the reaction

$$K(Mg_2Fe(II))(AlSi_3)O_{10}(OH)_2(s) + 10\ H^+ \rightarrow K^+ + 2Mg^{2+} + Fe^{2+} + Al^{3+} + 3\ H_4SiO_4(aq)$$

is estimated to $-231 \pm 11$ KJ/mole using Hess' law and the $\Delta G^{0}_{f,298.15}$ given by Mattigod and Sposito (1978, table 1).

Using the relation

$$\Delta G^{0}_{react.} = -RT\ln K \qquad (7\text{-}3)$$

the $\lg K_s$ is calculated to be $40 \pm 2$.

## 7.8 APPENDIX: Acid-base equilibrium at mineral surfaces.

When a metal oxide or a silcate mineral comes in contact with water the surfae is hydrated, i.e surface OH-groups are formed. The acid and base reactions of mineral surfaces is (de)protonation reactions of these OH-groups i.e:

$$>SOH + H^+ \rightleftharpoons >SOH_2^+$$

$$>SOH \rightleftharpoons >SO^- + H^+$$

where >S refers to a surface site.

The surface complexation model (Stumm and Morgan, 1981) describes the surface equilibrium by the following equations:

$$K_1 = \frac{\{>SOH_2^+\}}{\{>SOH\}[H^+]} e^{-\frac{F\Psi}{RT}} \qquad (7\text{-}4)$$

$$K_2 = \frac{\{>SO^-\}[H^+]}{\{>SOH\}} e^{-\frac{F\Psi}{RT}} \qquad (7\text{-}5)$$

where curly brackets refers to surface concentrations (moles $m^{-2}$) and the exponential term is a correction for surface charge effects where $\Psi$ denotes a surface potential, F Faraday´s constant, R the gas constant and T the absolute temperature. Several different models developed for describing the electric behaviour of the surface have been used in the literature (See for example review by Sposito (1983)). We use the diffuse-layer-model (also called double-layer model) (Dzombak and Morel, 1990) which describes the mineral/solution interface as comprised by two layer of charge: 1) A surface layer 2) A diffuse layer of counter ions in the solution.

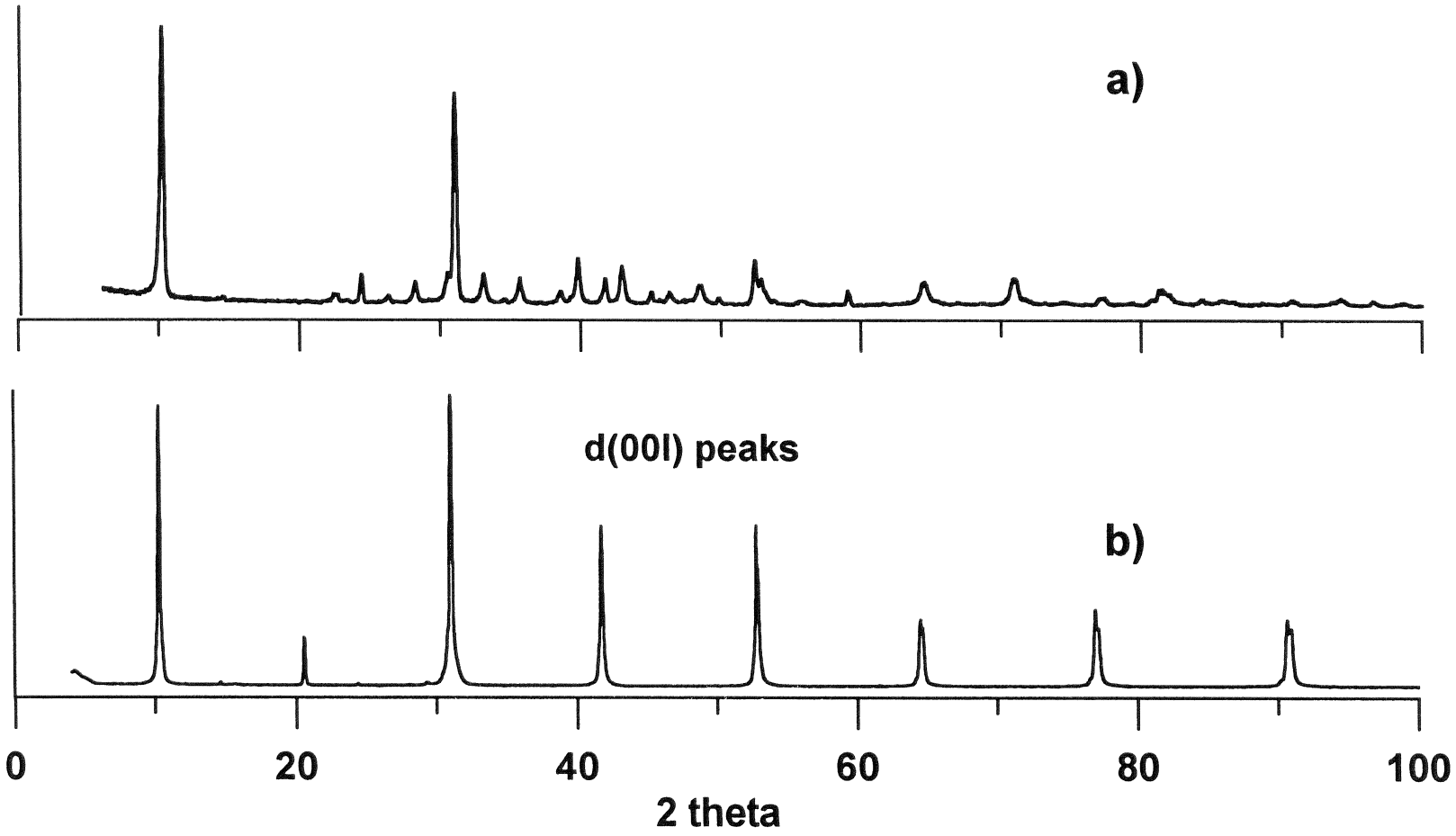


Figure 7-1.
XPD pattern of biotite. a) mineral powder (no orientation)
b) mineral flake (inter-layer plane perpendicular to the Xray beam).

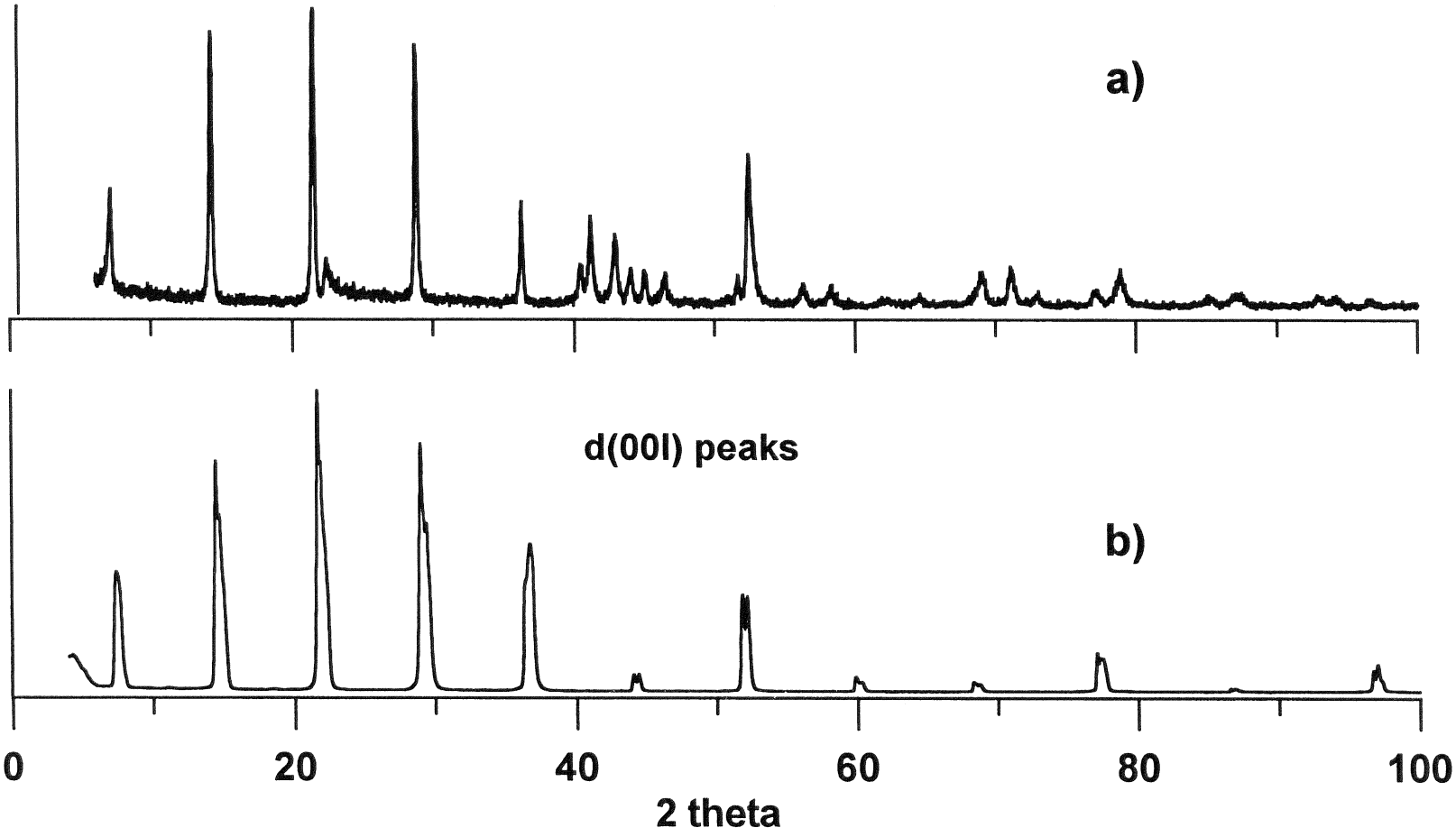


Figure 7-2.
XPD pattern of chlorite. a) mineral powder (no orientation)
b) mineral flake (inter-layer plane perpendicular to the Xray beam).

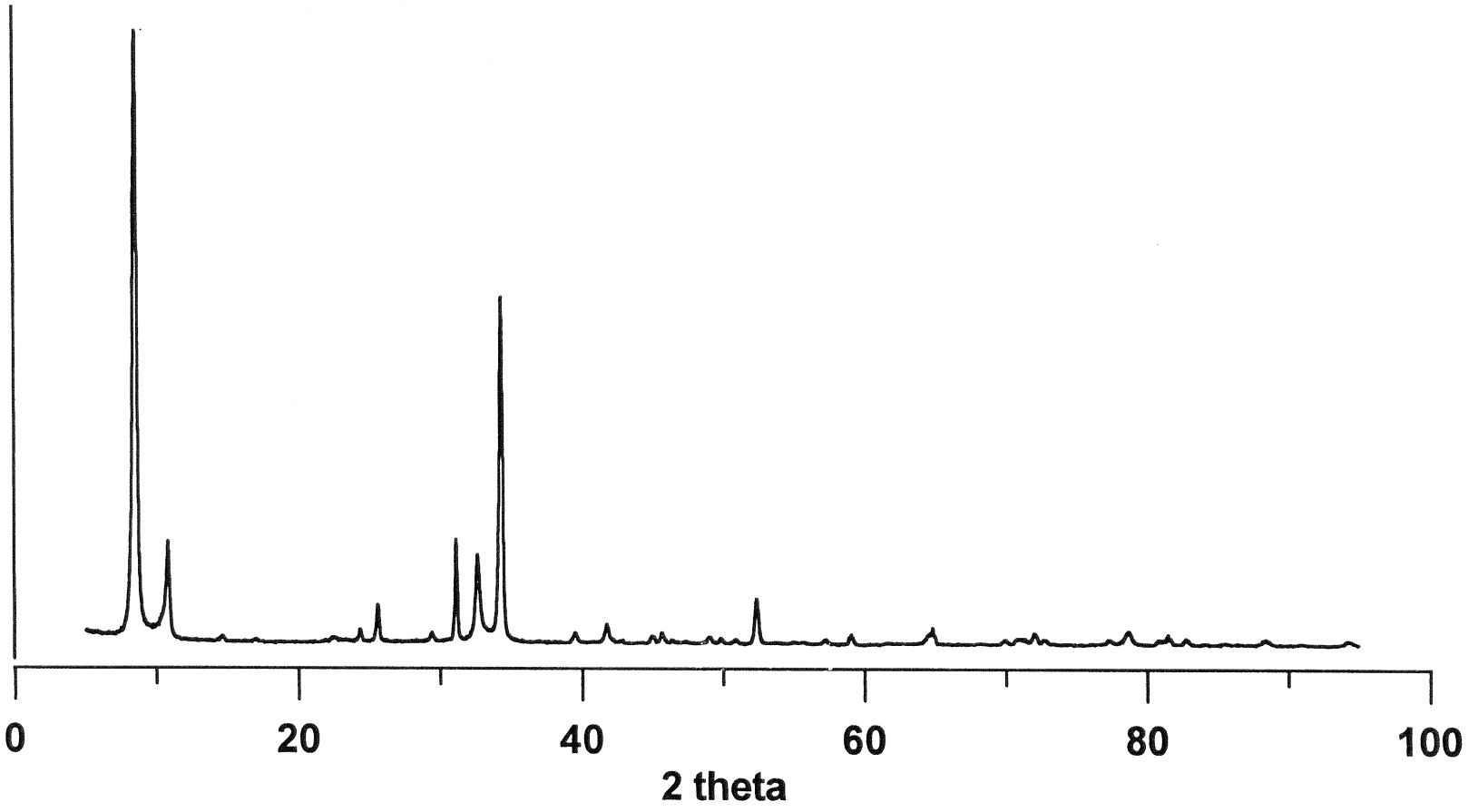


Figure 7-3.
XPD pattern of mineral from the kinetic experiment of biotite dissolution at pH 4.06 (M2).

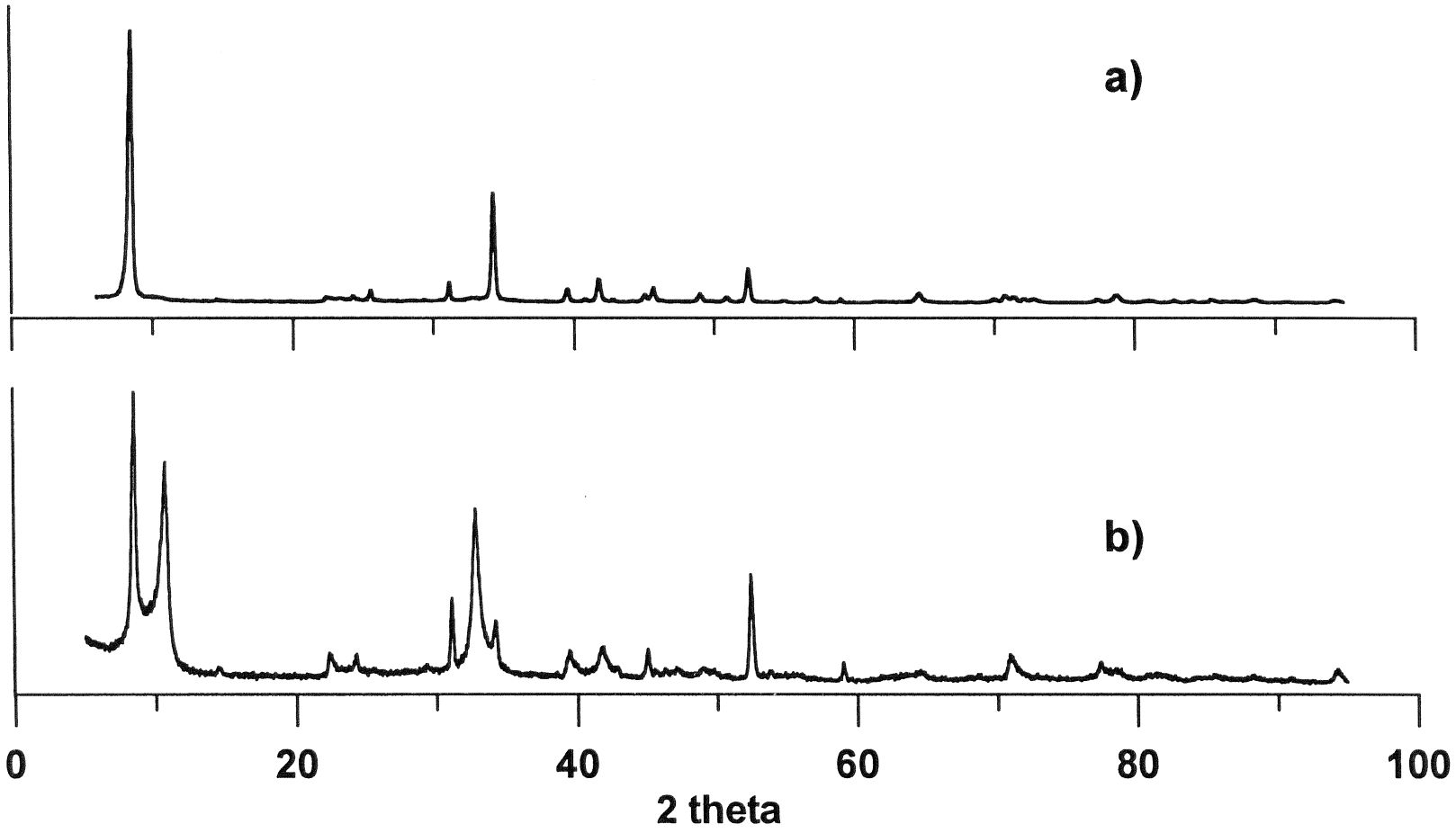


Figure 7-4.
XPD pattern of mineral from the kinetic experiment of biotite dissolution at pH 2.80 (M3). a) darker phase b) lighter phase.

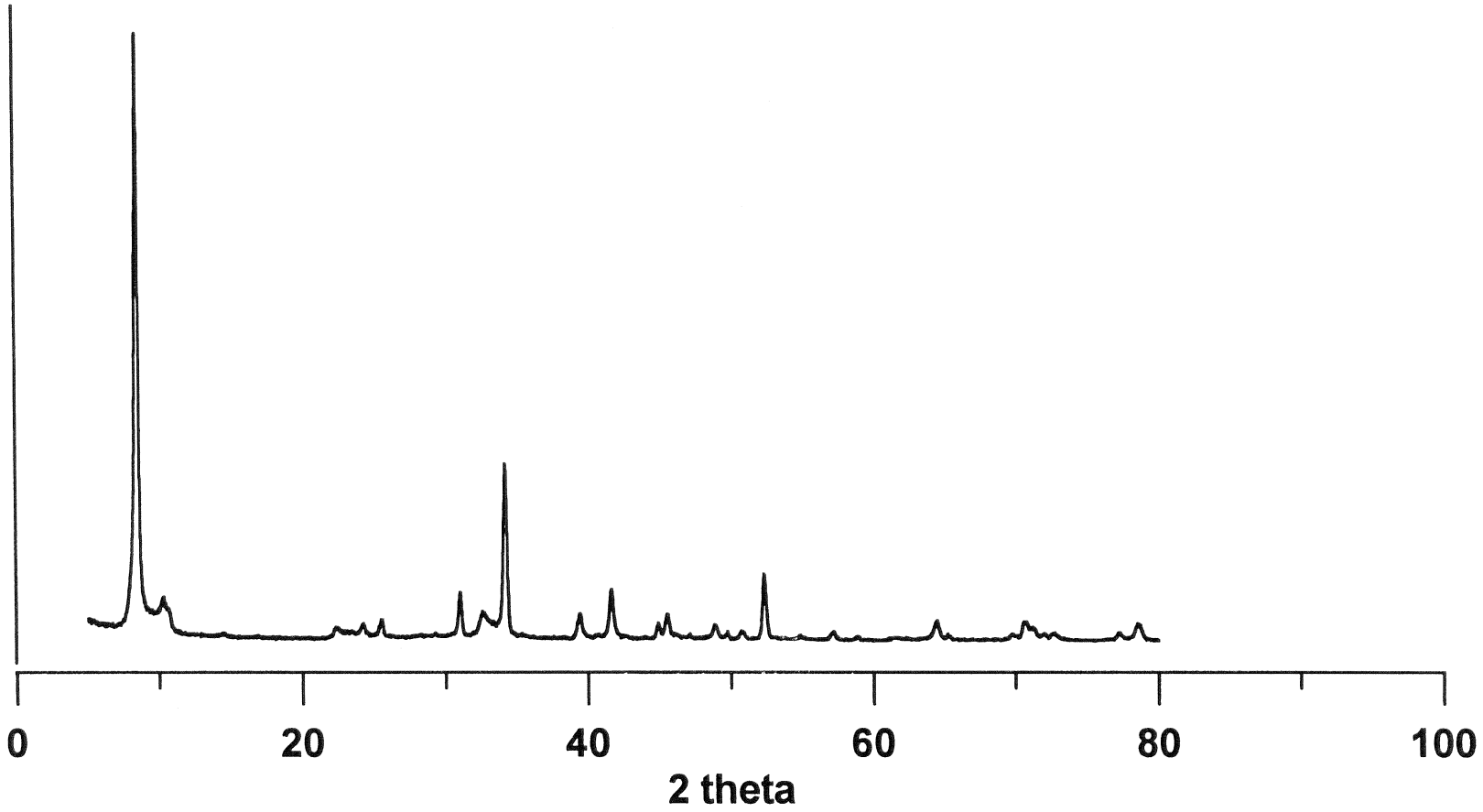


Figure 7-5.
XPD pattern of mineral from the kinetic experiment of biotite dissolution at pH 5 (M4).

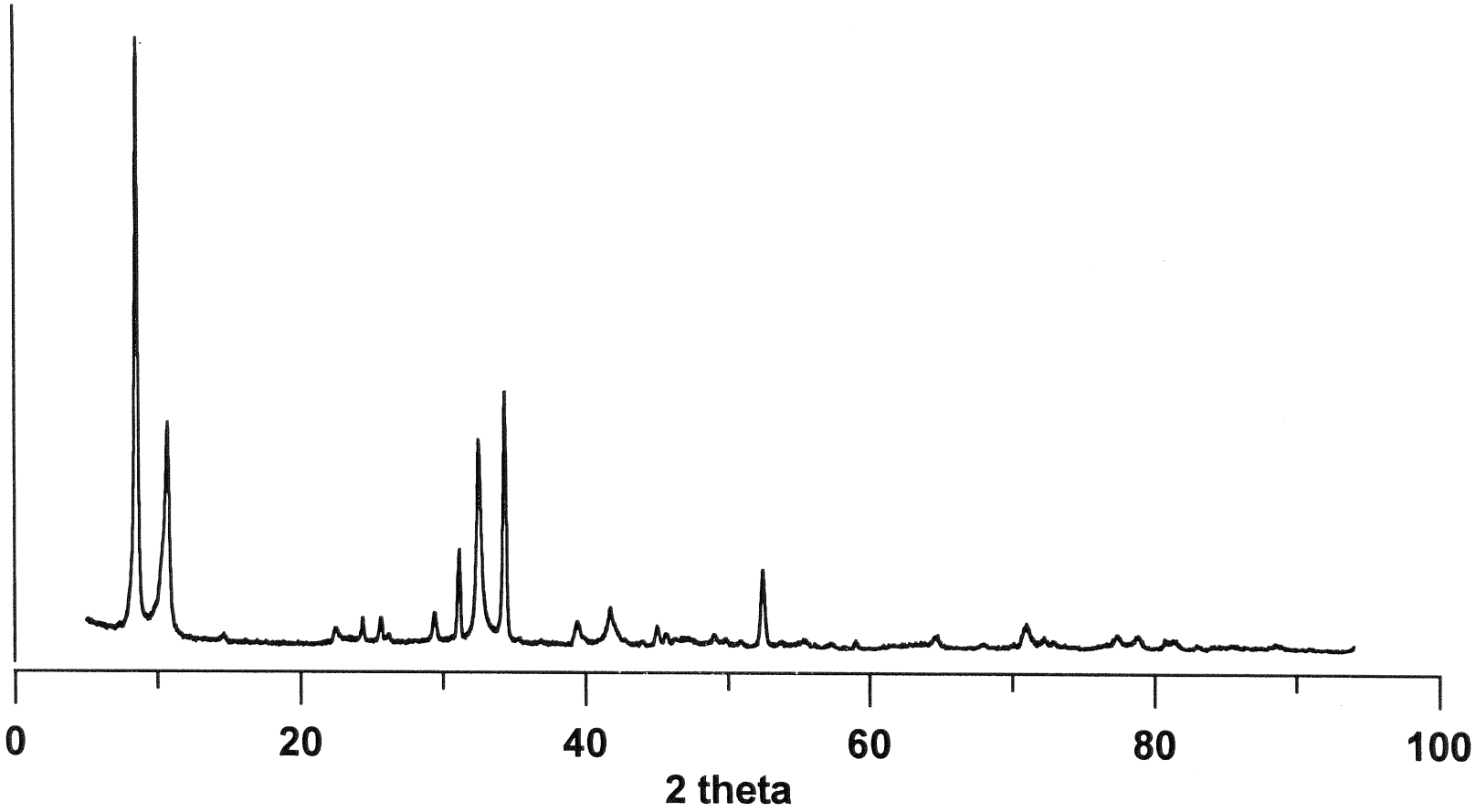


Figure 7-6.
XPD pattern of mineral from the kinetic experiment of biotite dissolution at pH 8.5 (M5).

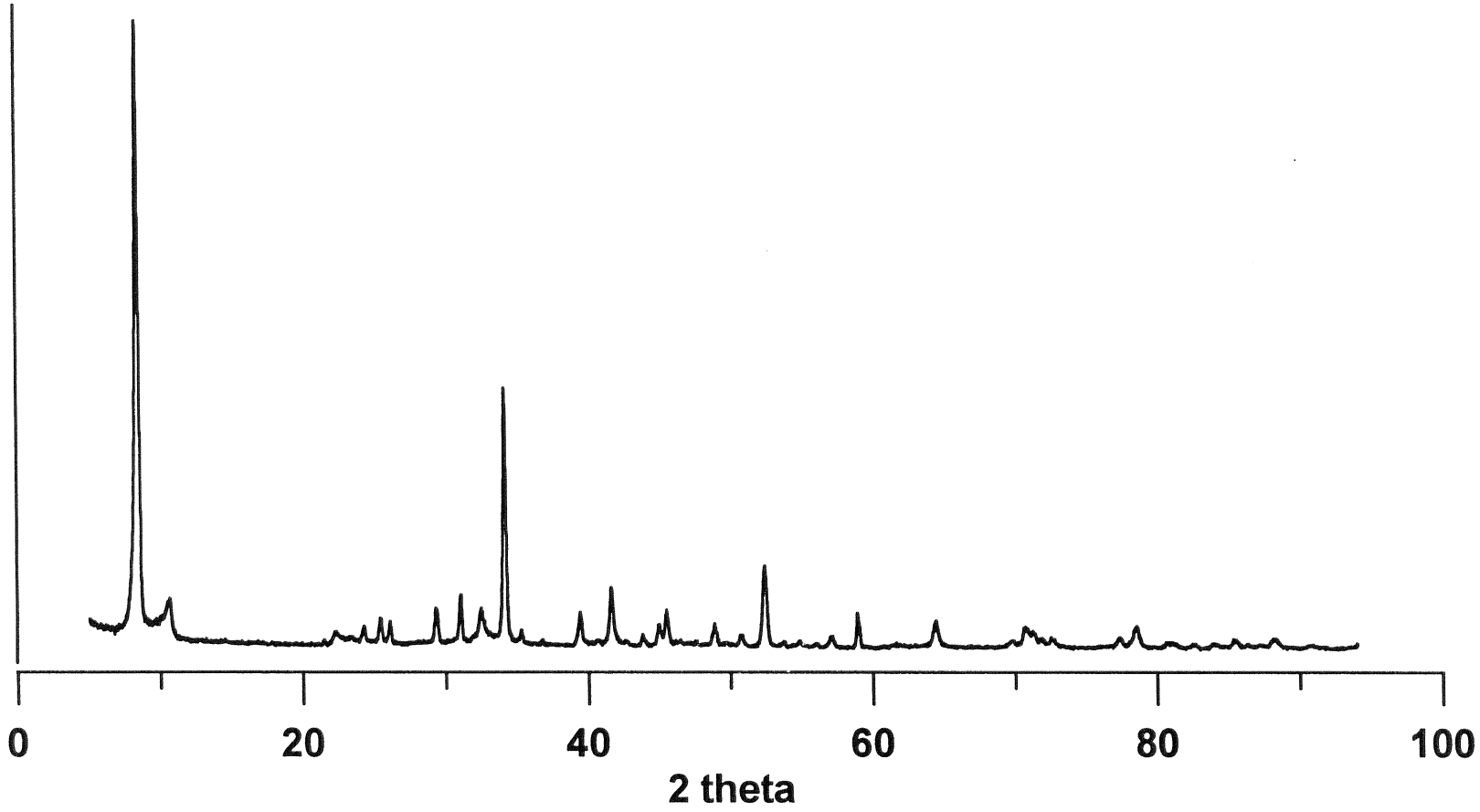


Figure 7-7.
XPD pattern of mineral from the kinetic experiment of biotite dissolution at pH 10 (M6).

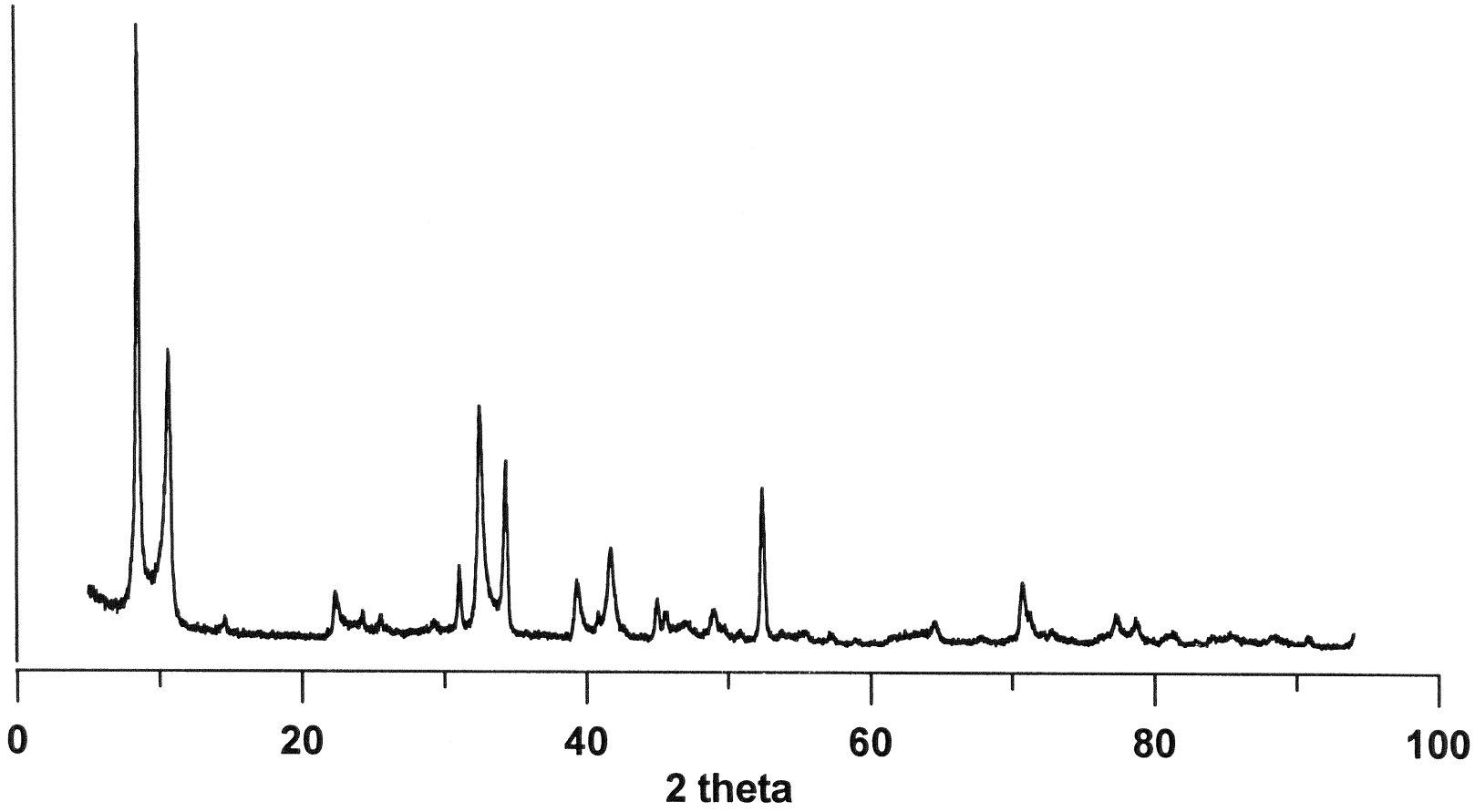


Figure 7-8.
XPD pattern of mineral from the kinetic experiment of biotite dissolution at pH 7 (M8).

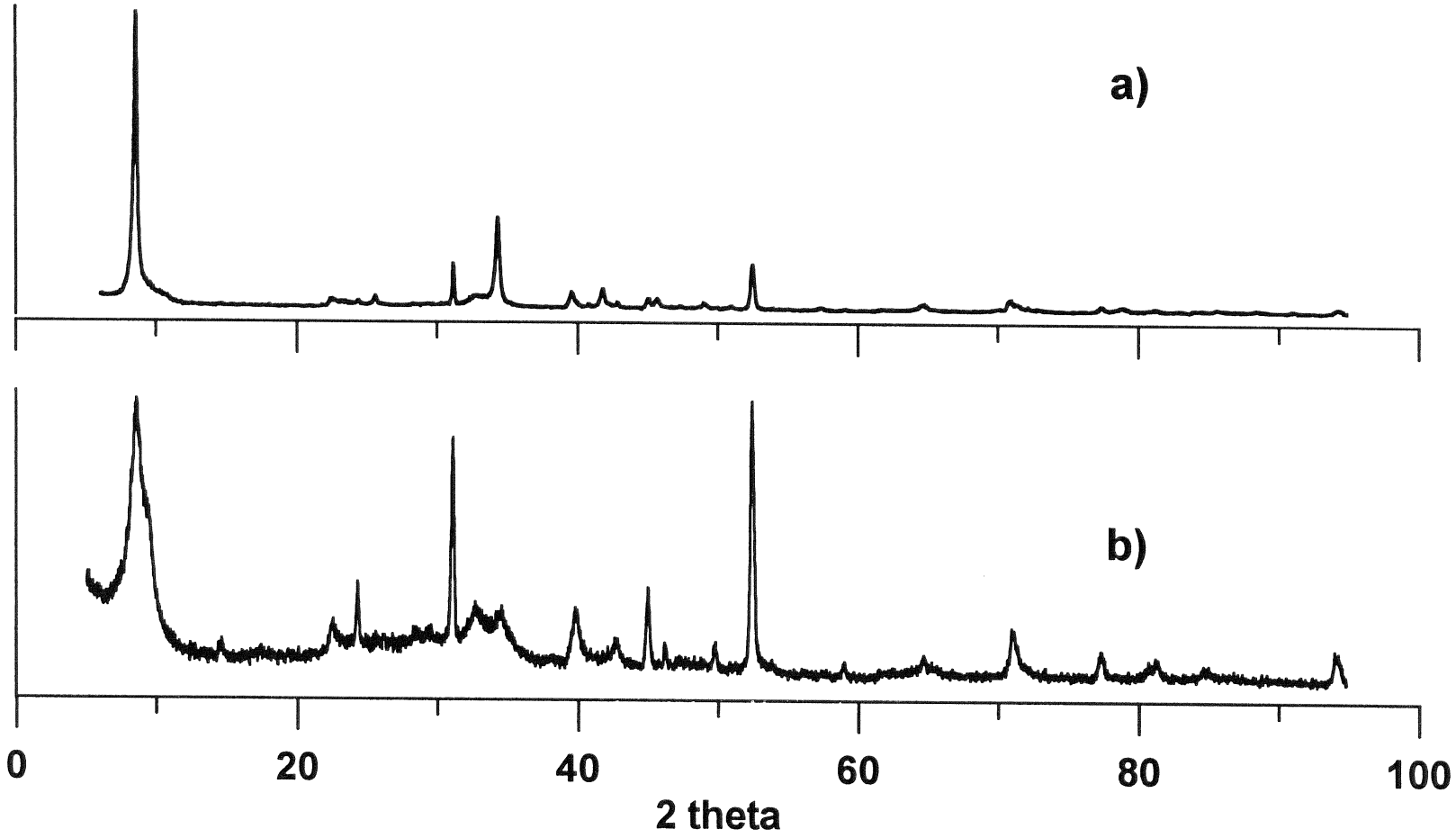


Figure 7-9.
XPD pattern of mineral from the kinetic experiment of biotite dissolution at pH2 (M10). a) darker phase b) lighter phase.

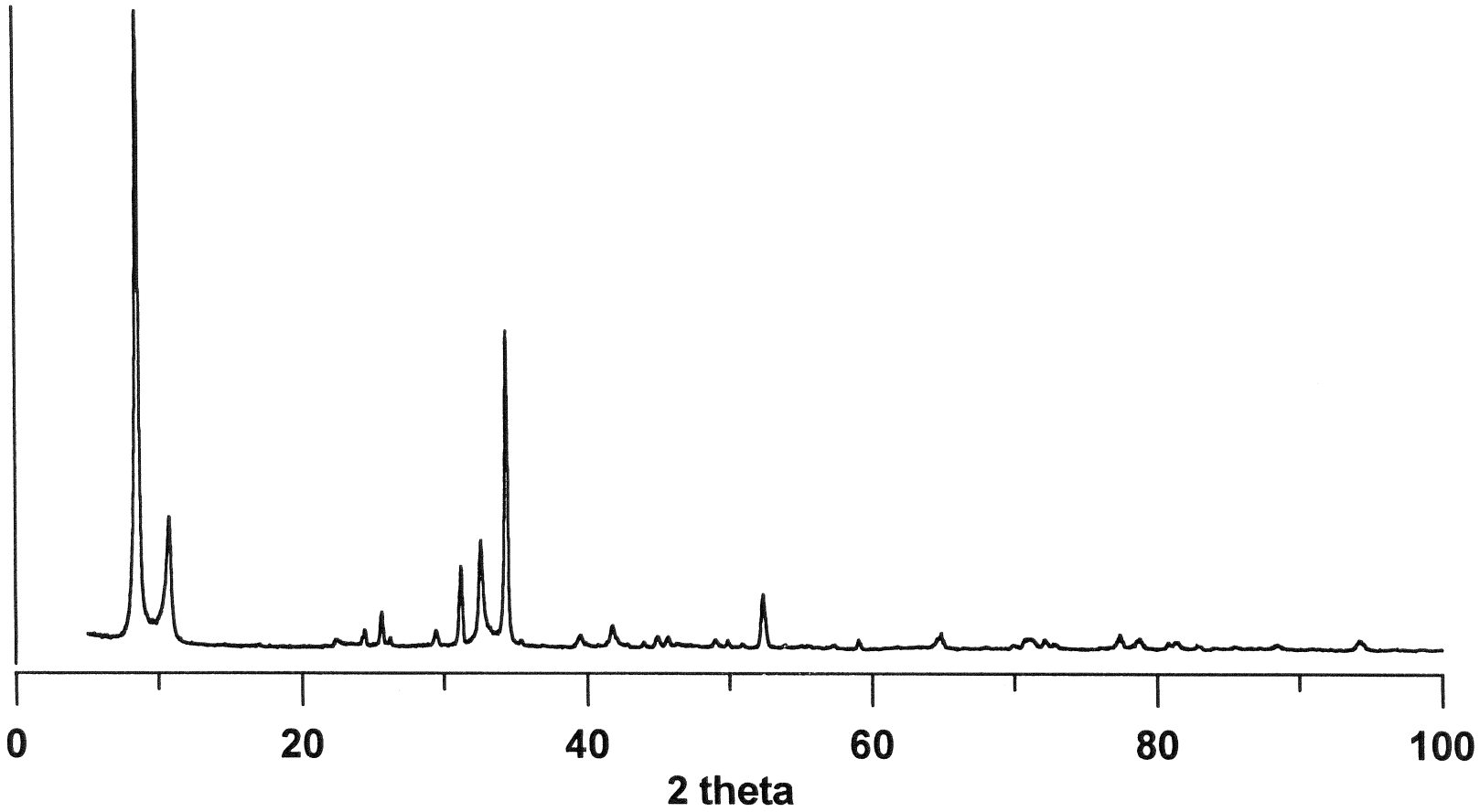


Figure 7-10.
XPD pattern of mineral from the kinetic experiment of biotite dissolution at pH 6.77 and 1% CO2 (M12).

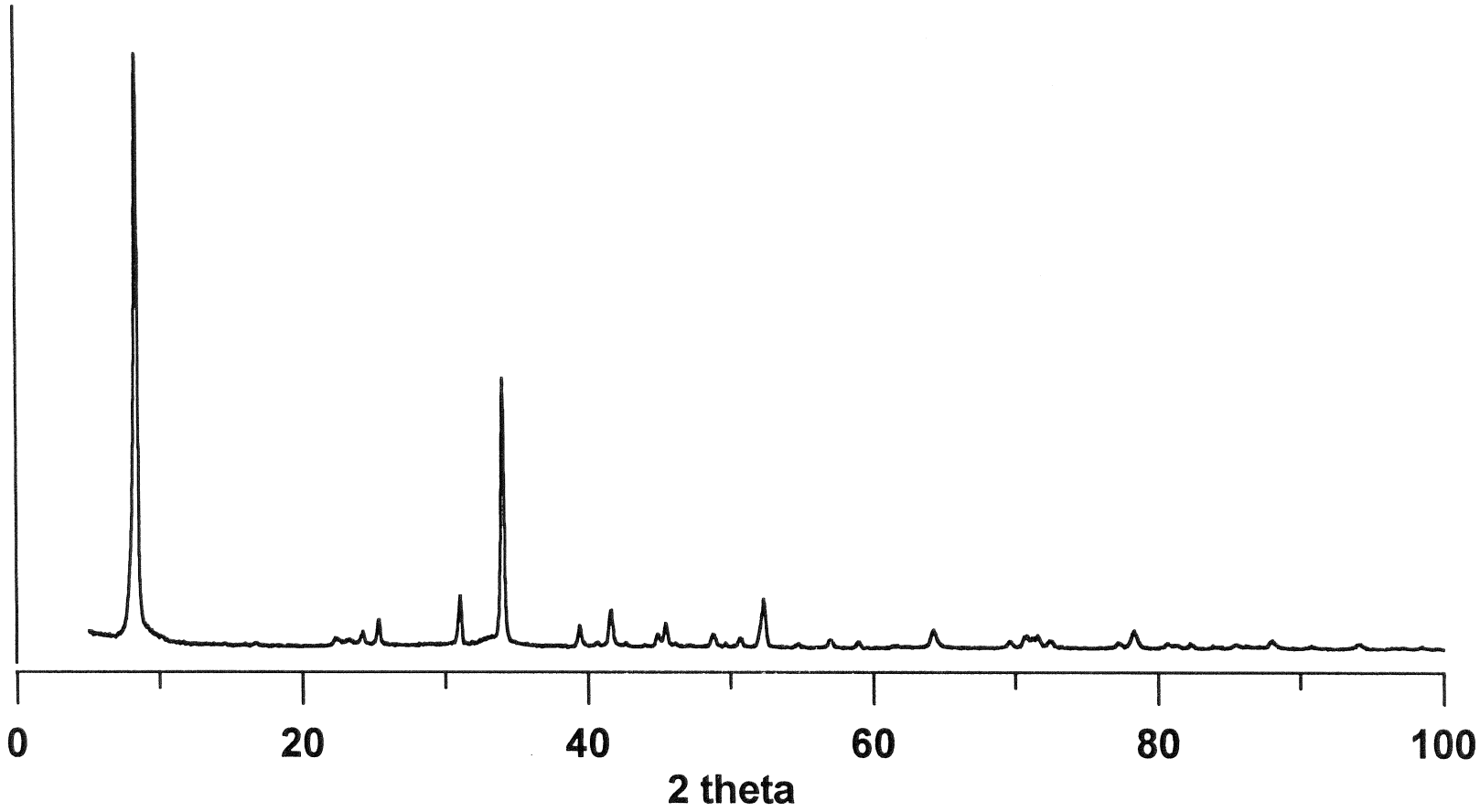


Figure 7-11.
XPD pattern of mineral from the kinetic experiment of biotite dissolution at pH 8.11 and 1% CO2 (M13).

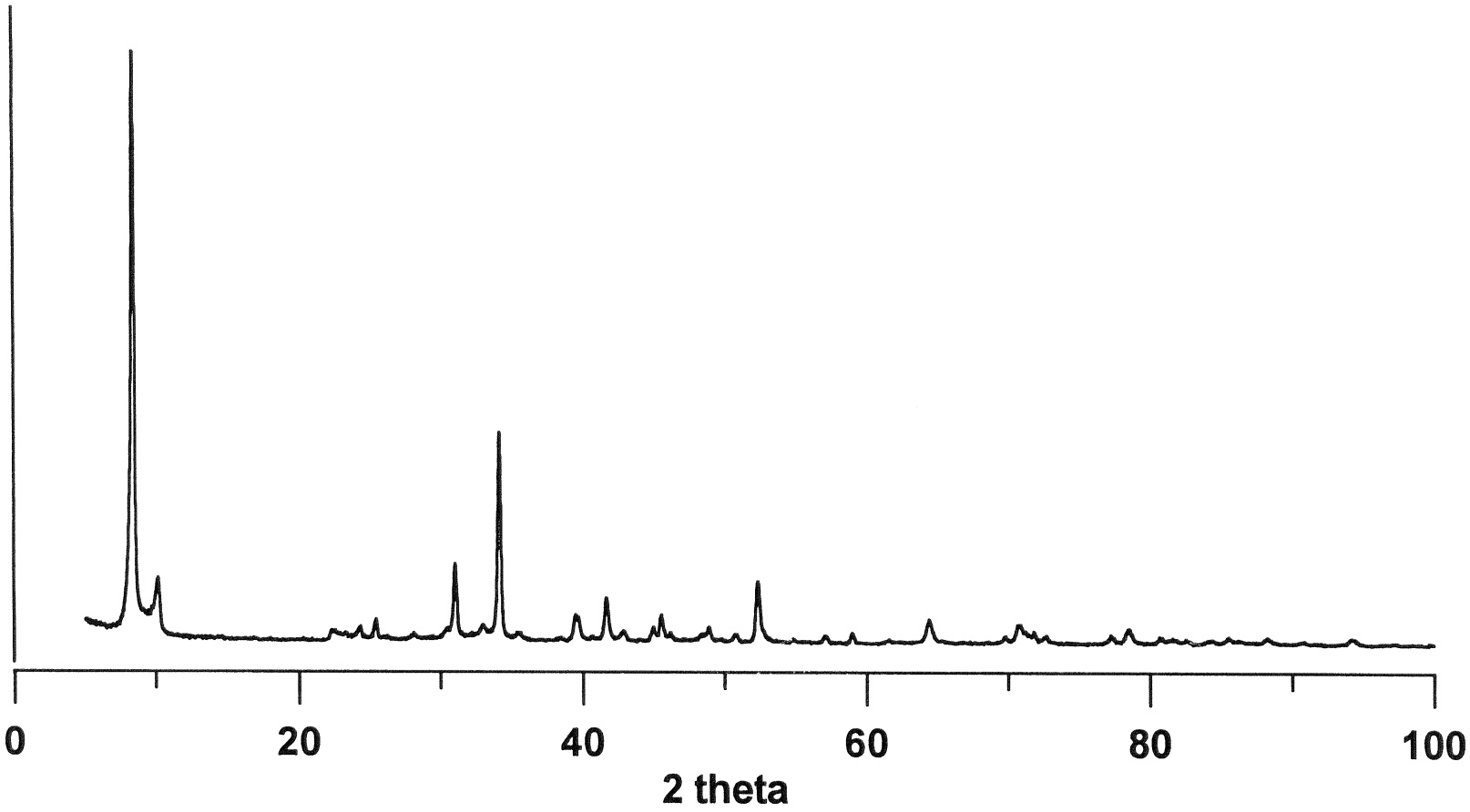


Figure 7-12.
XPD pattern of mineral from the kinetic experiment of biotite dissolution at pH 8.41 and 1% CO2 (M14).

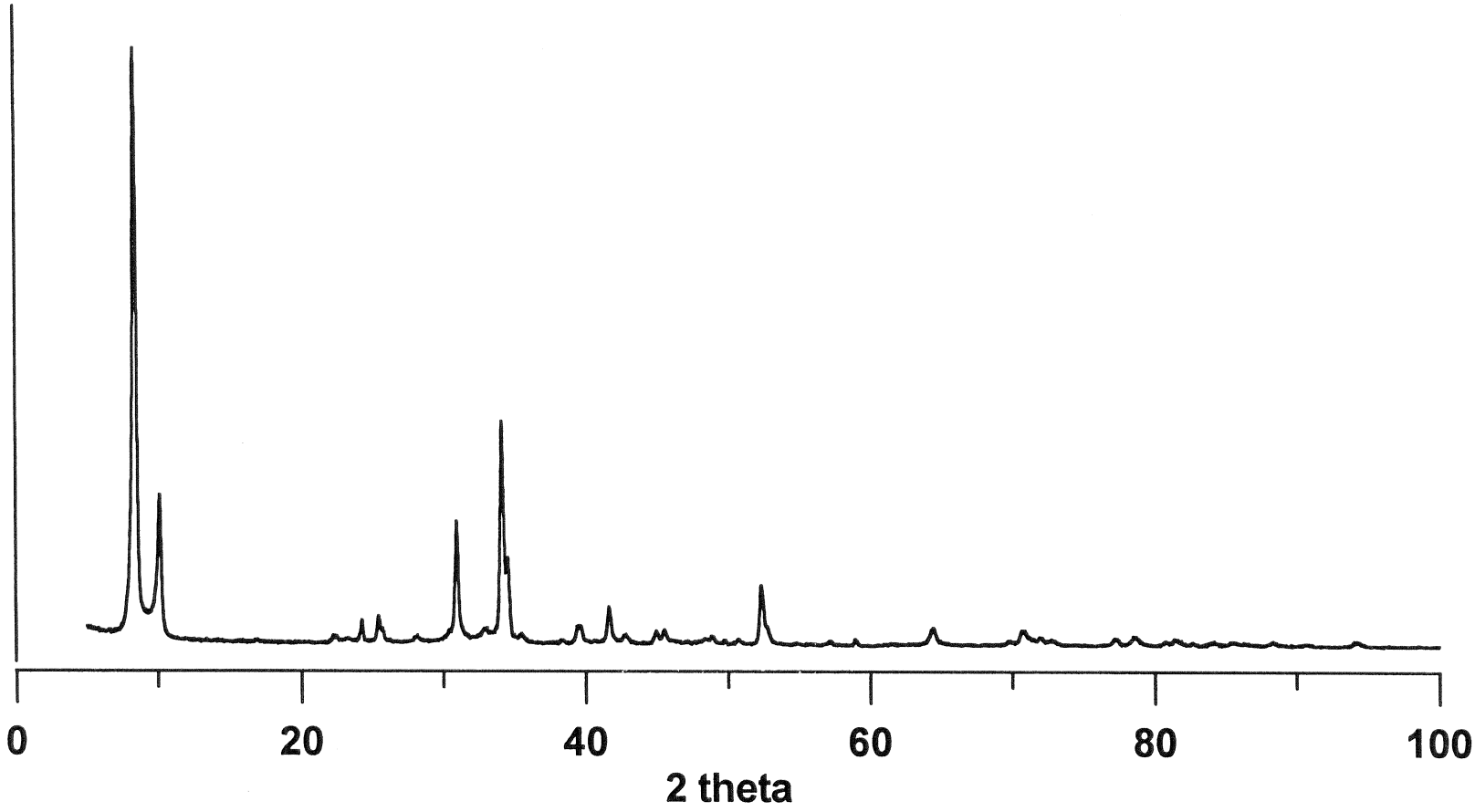


Figure 7-13.
XPD pattern of mineral from the kinetic experiment of biotite dissolution at pH 8.75 and 1% CO2 (M15).

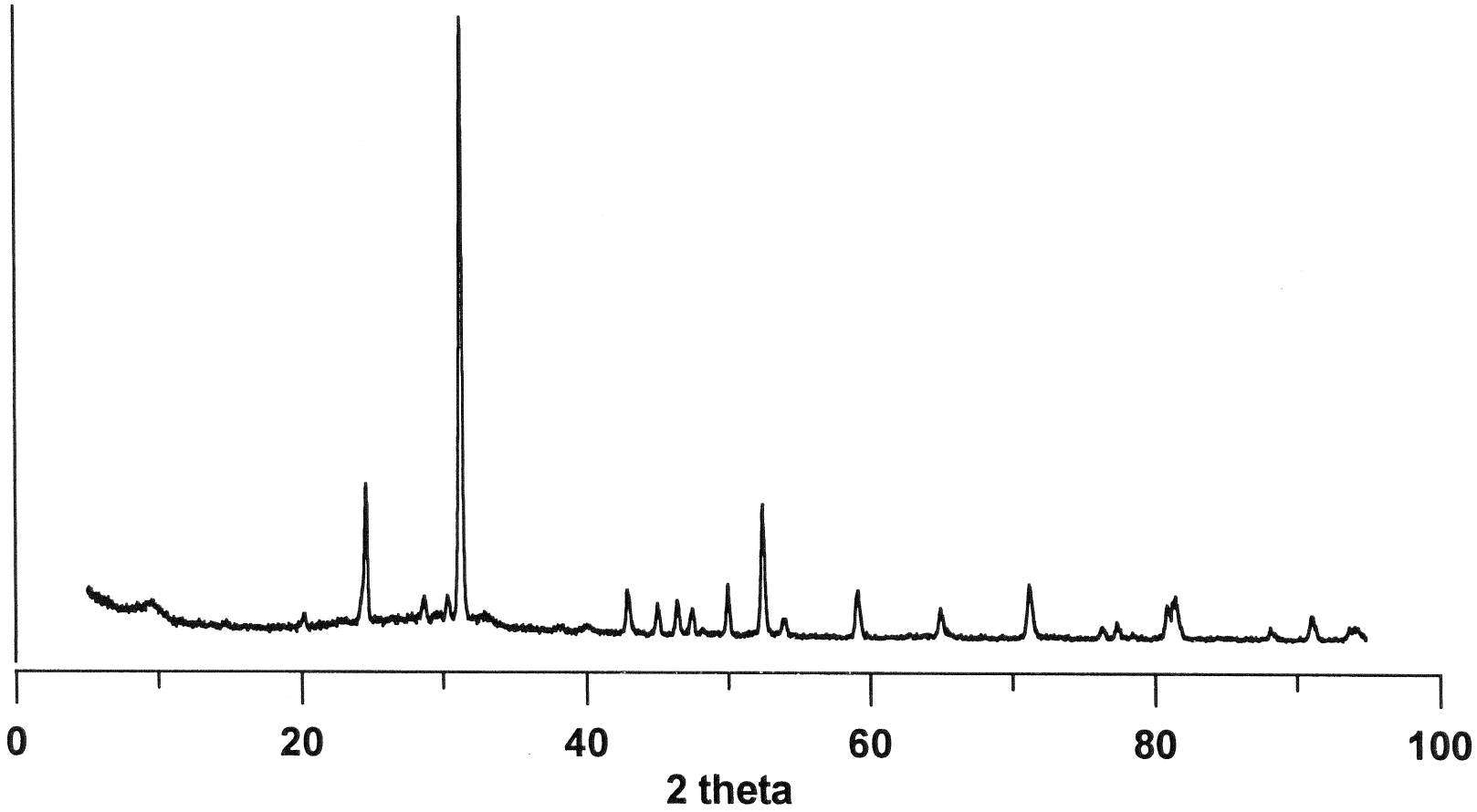


Figure 7-14.
XPD pattern of mineral from the kinetic experiment of biotite dissolution at pH <2 (M1).

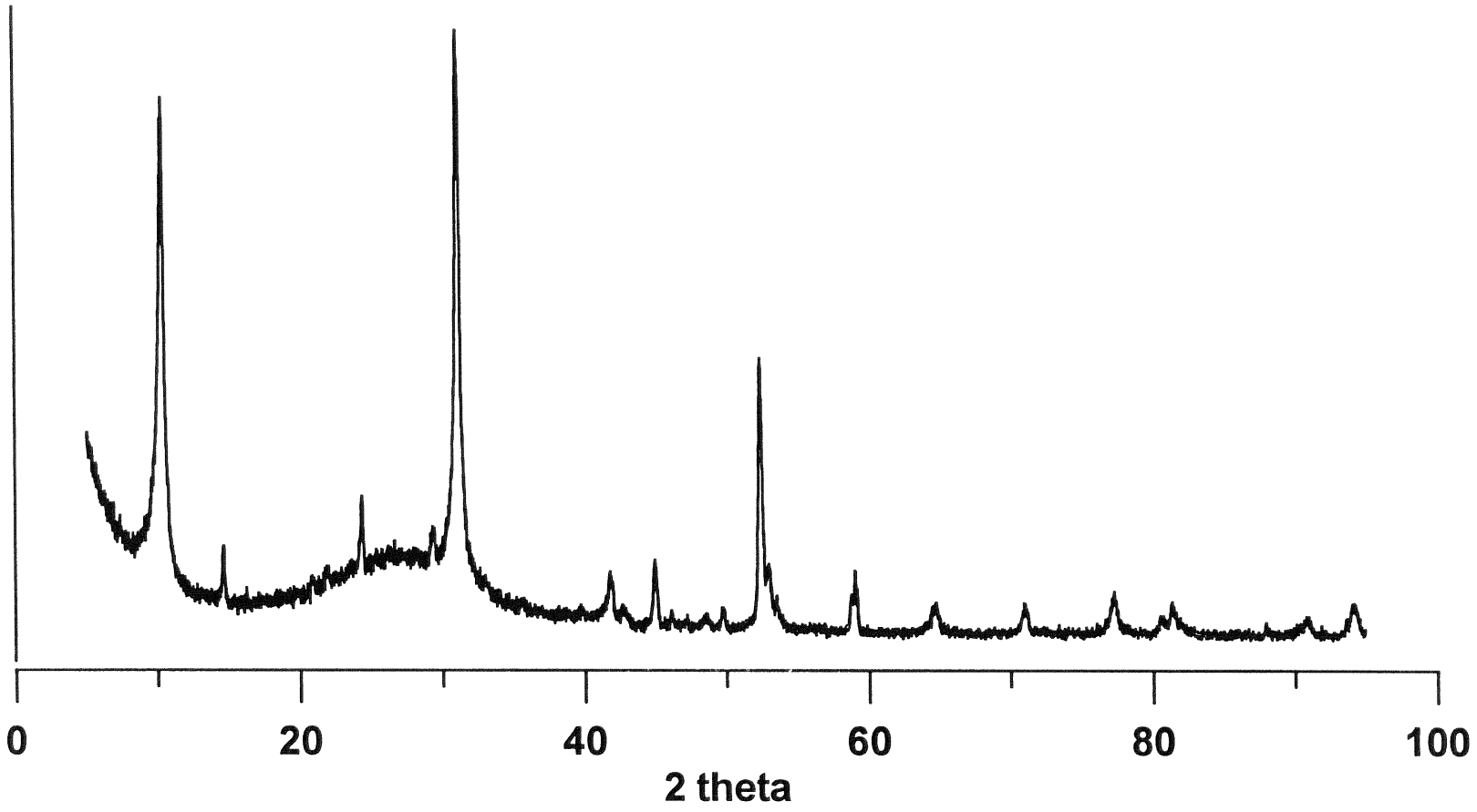


Figure 7-15.
XPD pattern of mineral from the biotite batch experiment at pH 0.3 (sample 37).

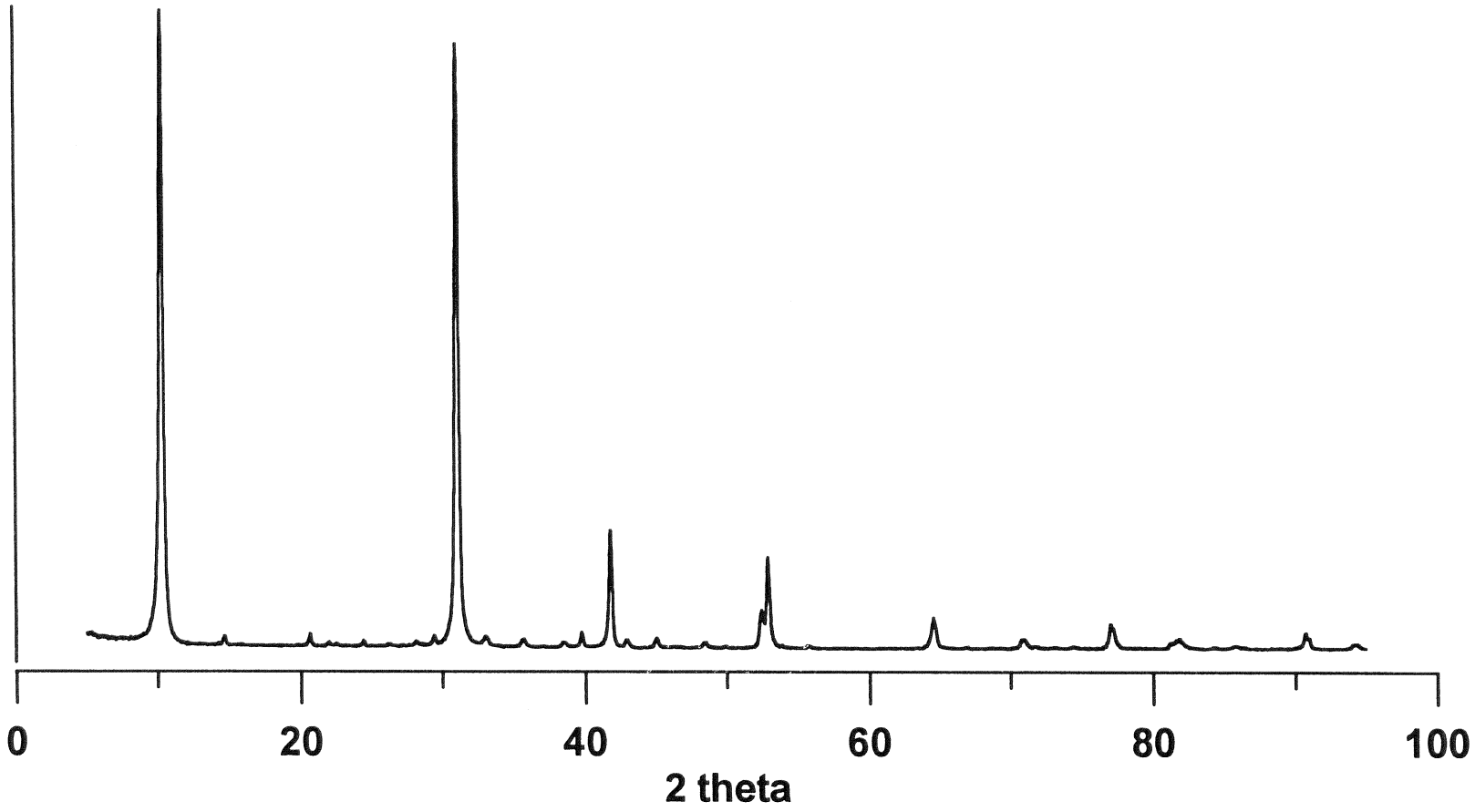


Figure 7-16.
XPD pattern of mineral from the biotite batch experiment at pH 0.64 (sample 33).

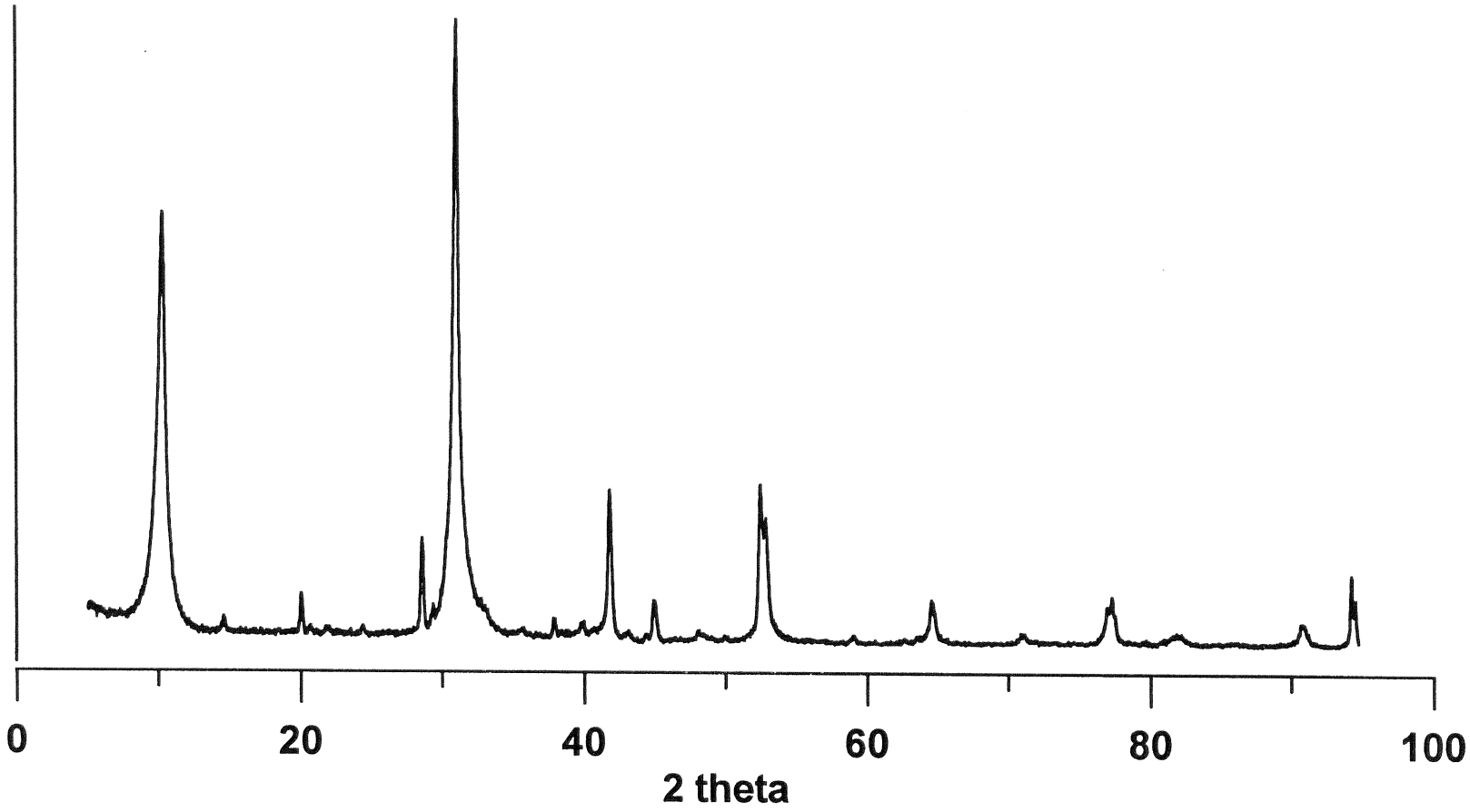


Figure 7-17.
XPD pattern of mineral from the biotite batch experiment at pH 0.82 (sample 24).

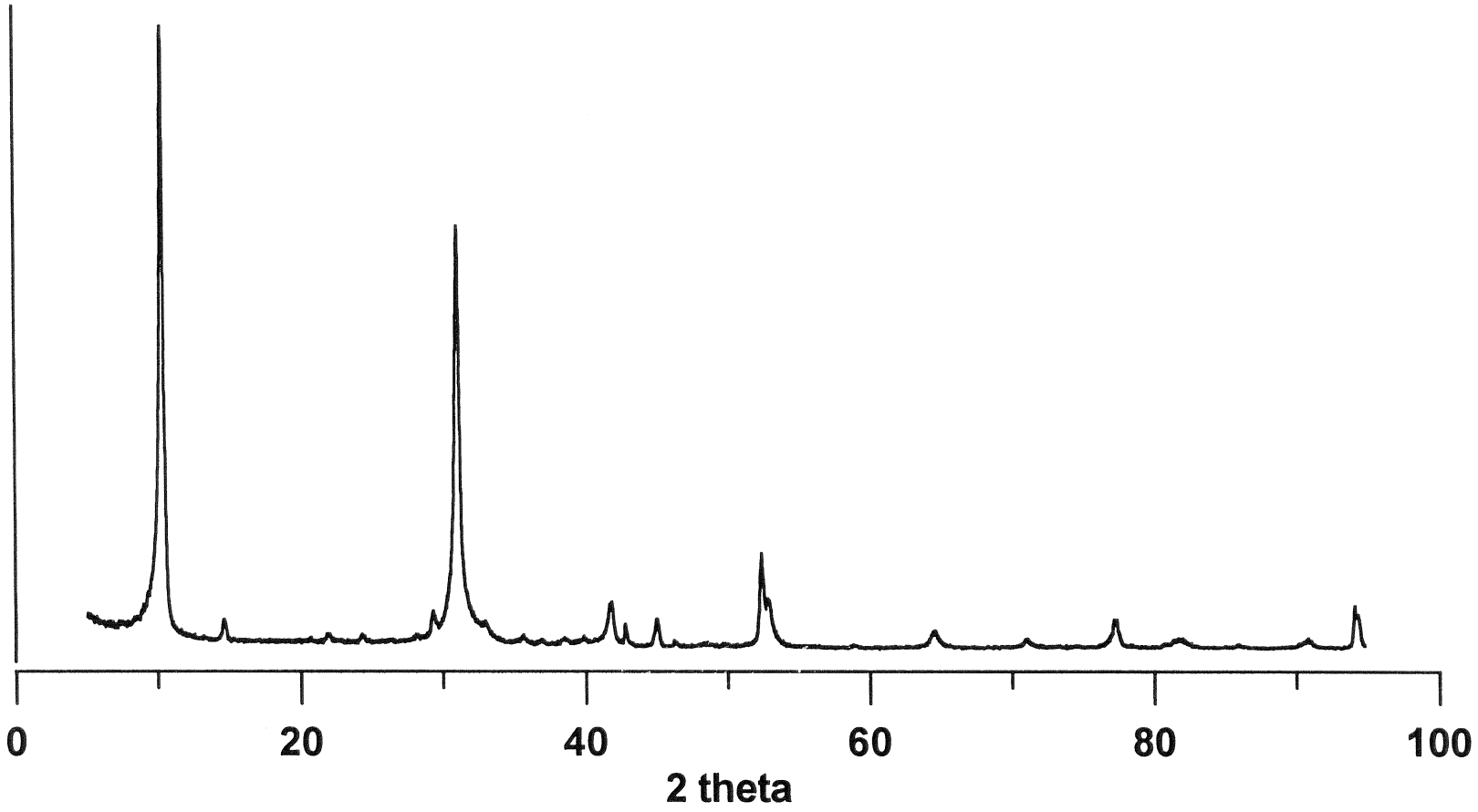


Figure 7-18.
XPD pattern of mineral from the biotite batch experiment at pH 1.18 (sample 36).

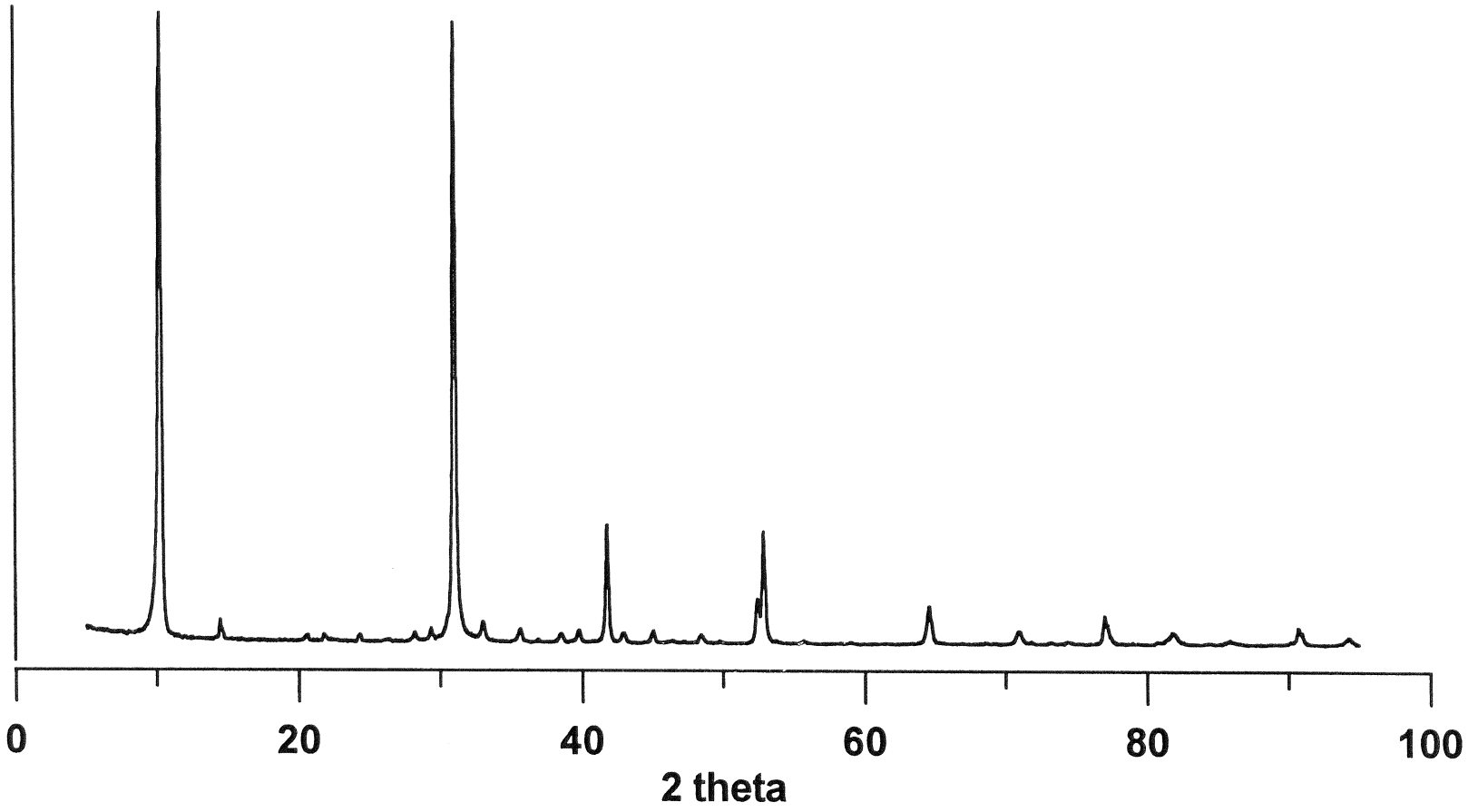


Figure 7-19.
XPD pattern of mineral from the biotite batch experiment at pH 2.34 (sample 26).

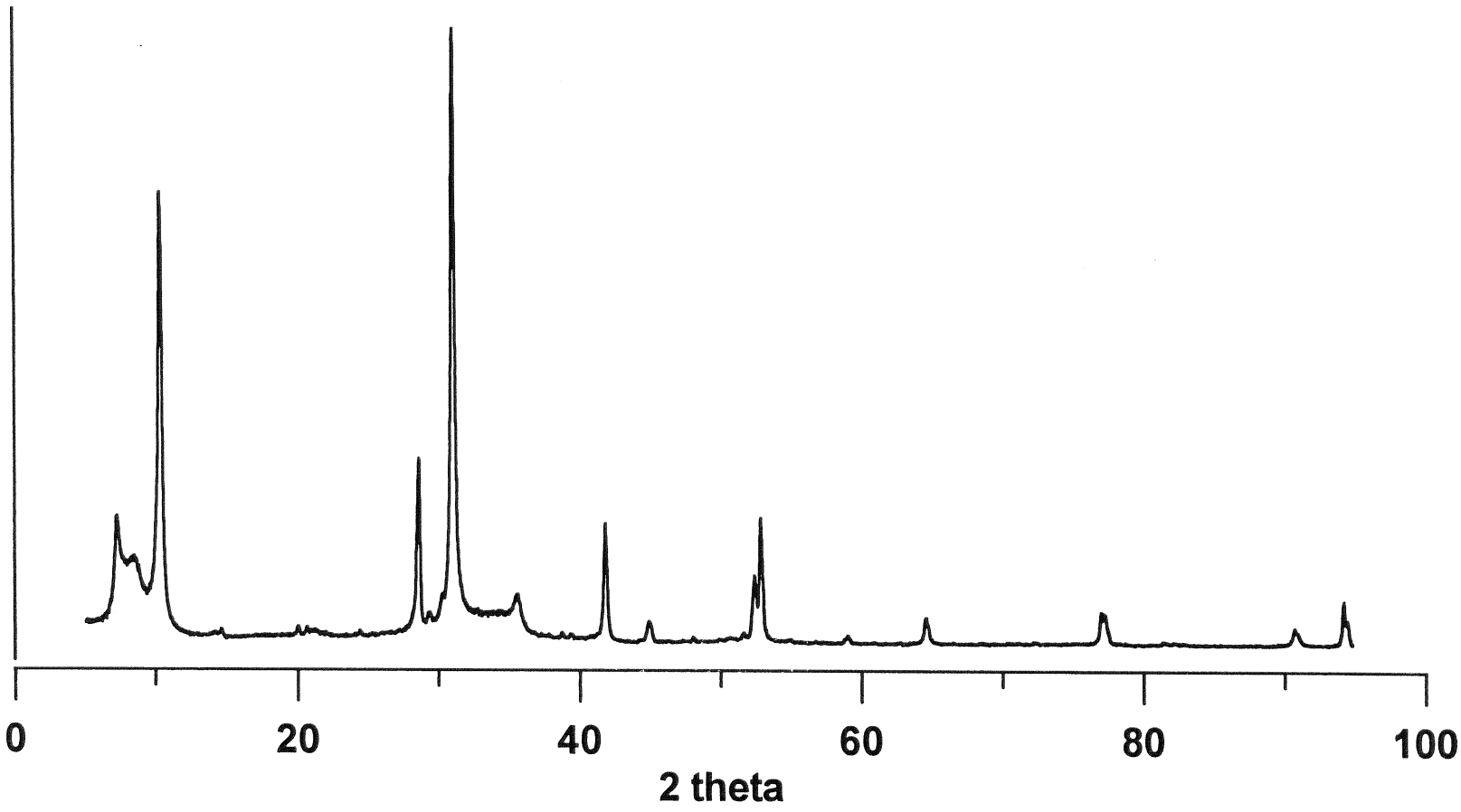


Figure 7-20.
XPD pattern of mineral from the biotite batch experiment at pH 2.57 (sample 7).

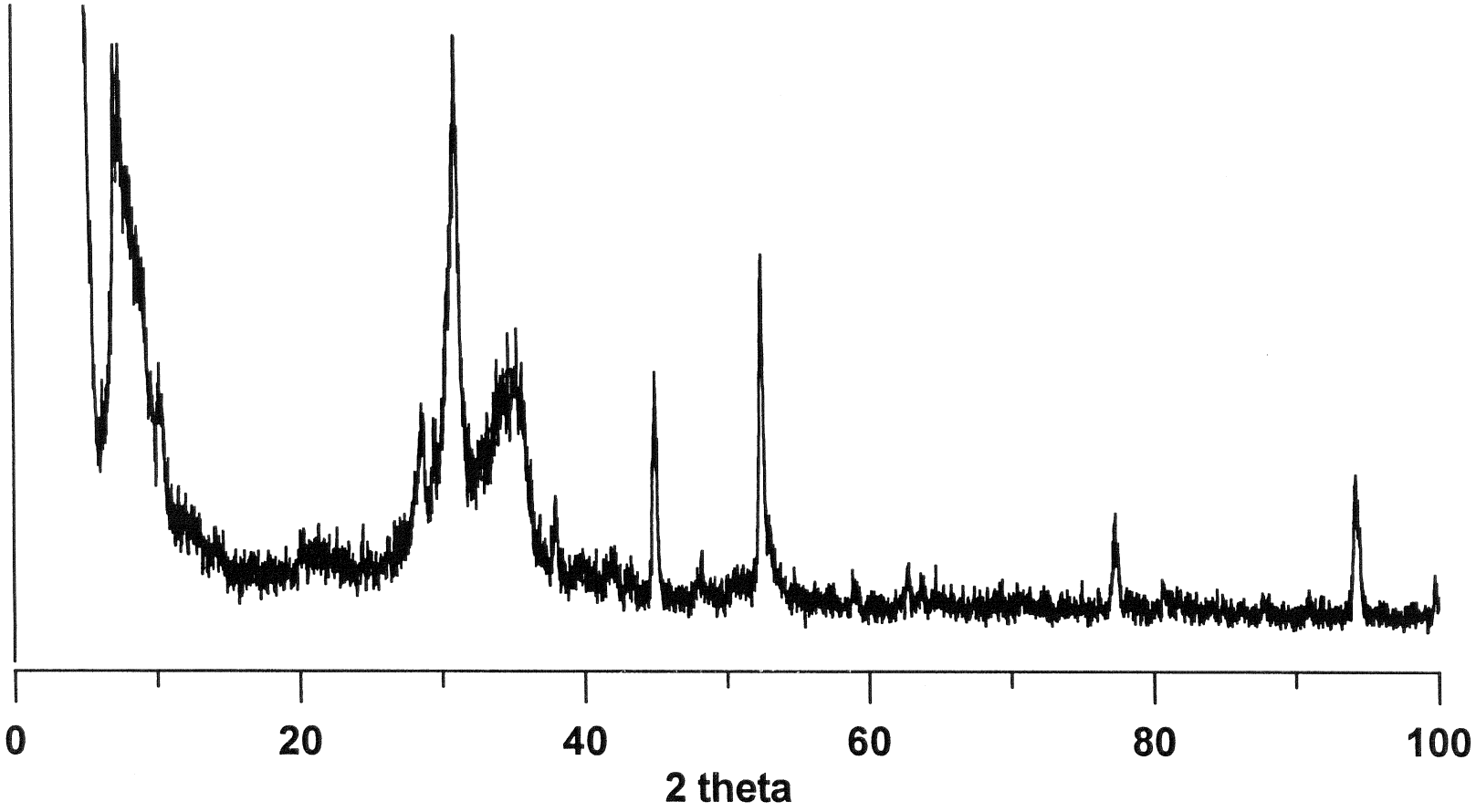


Figure 7-21.
XPD pattern of mineral from the biotite batch experiment at pH 3.9 (sample 8).

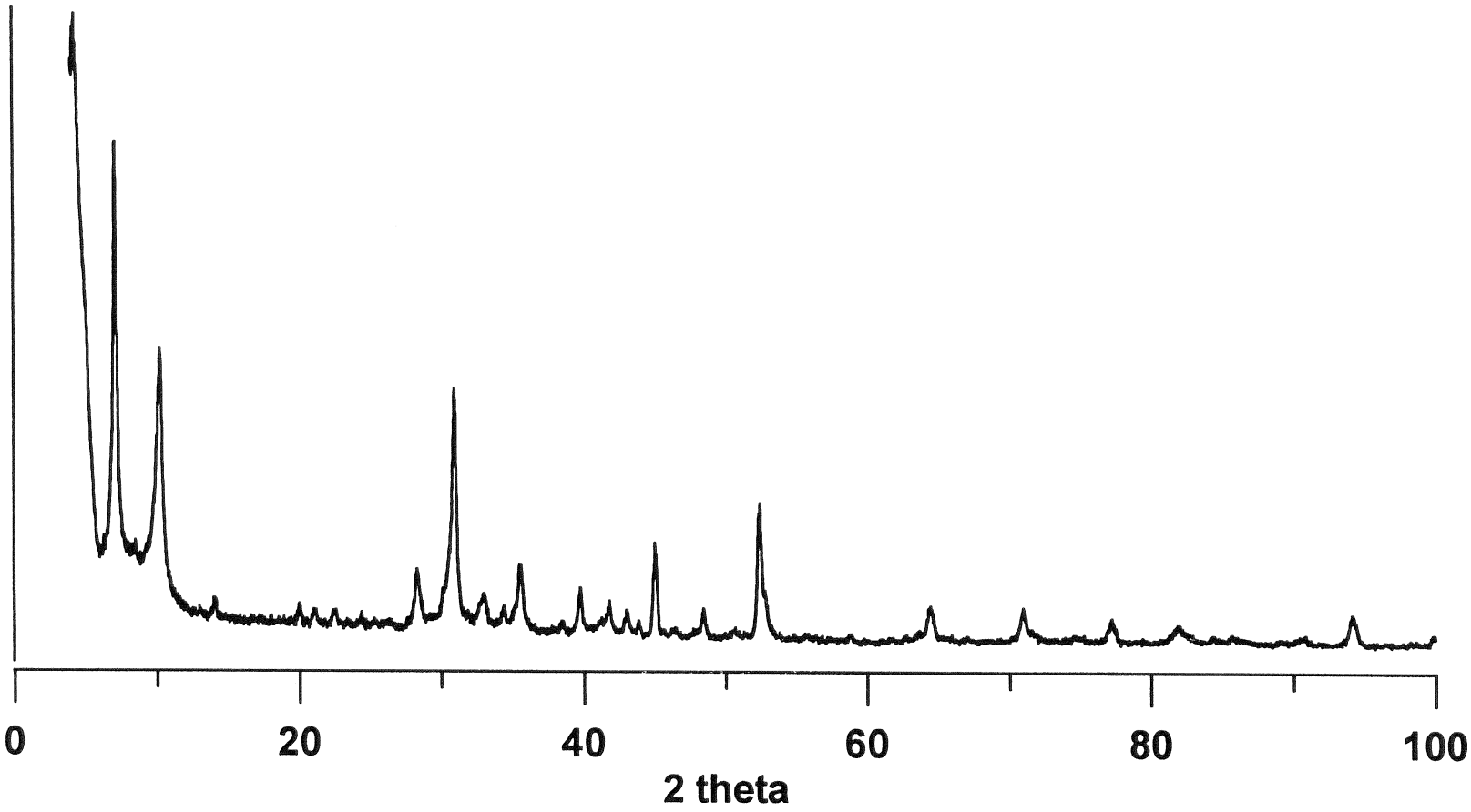


Figure 7-22.
XPD pattern of mineral from the biotite batch experiment at pH 4.58 (sample 18).

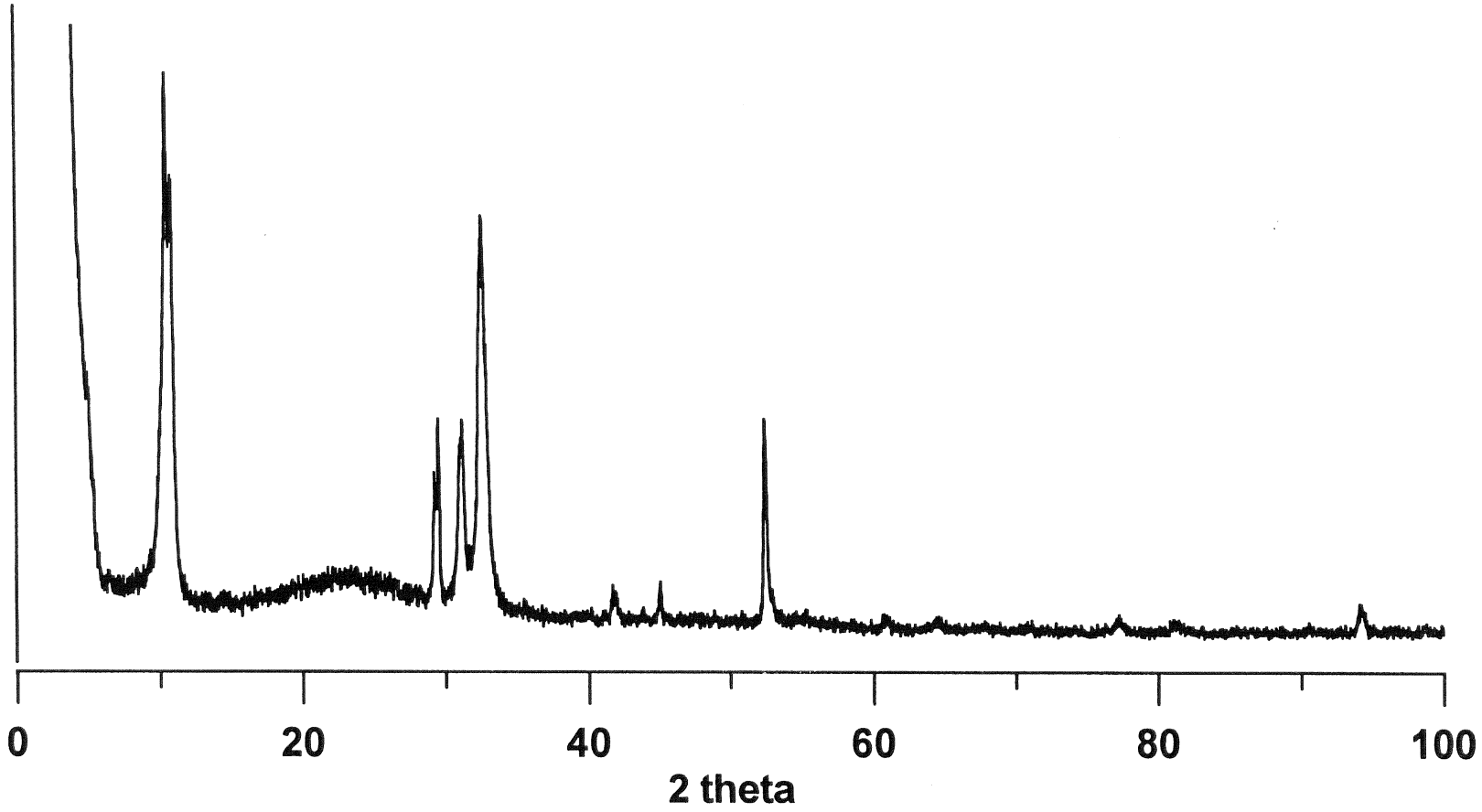


Figure 7-23.
XPD pattern of mineral from the biotite batch experiment at pH 4.78 (sample 19).

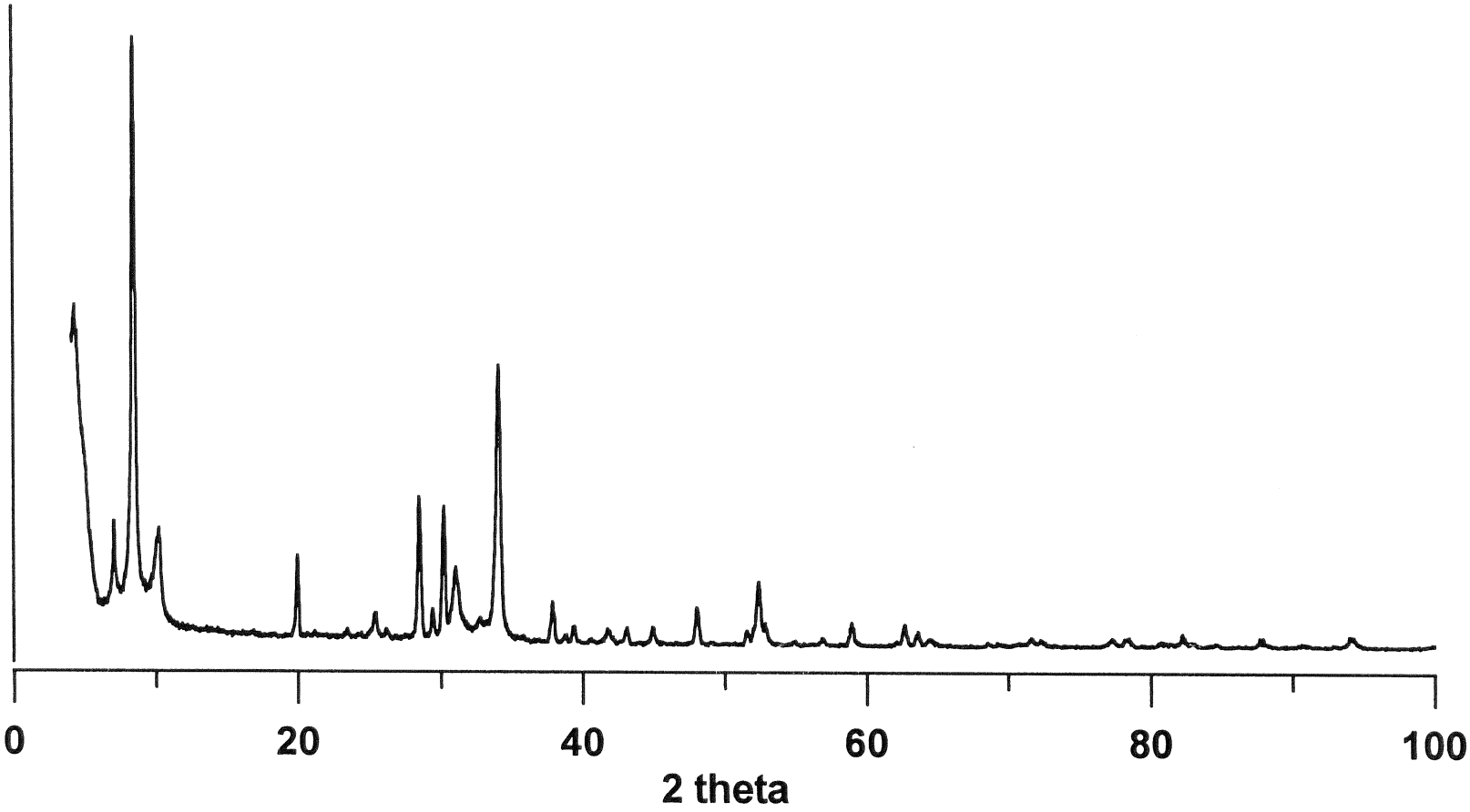


Figure 7-24.
XPD pattern of mineral from the biotite batch experiment at pH 6.73 (sample 10).

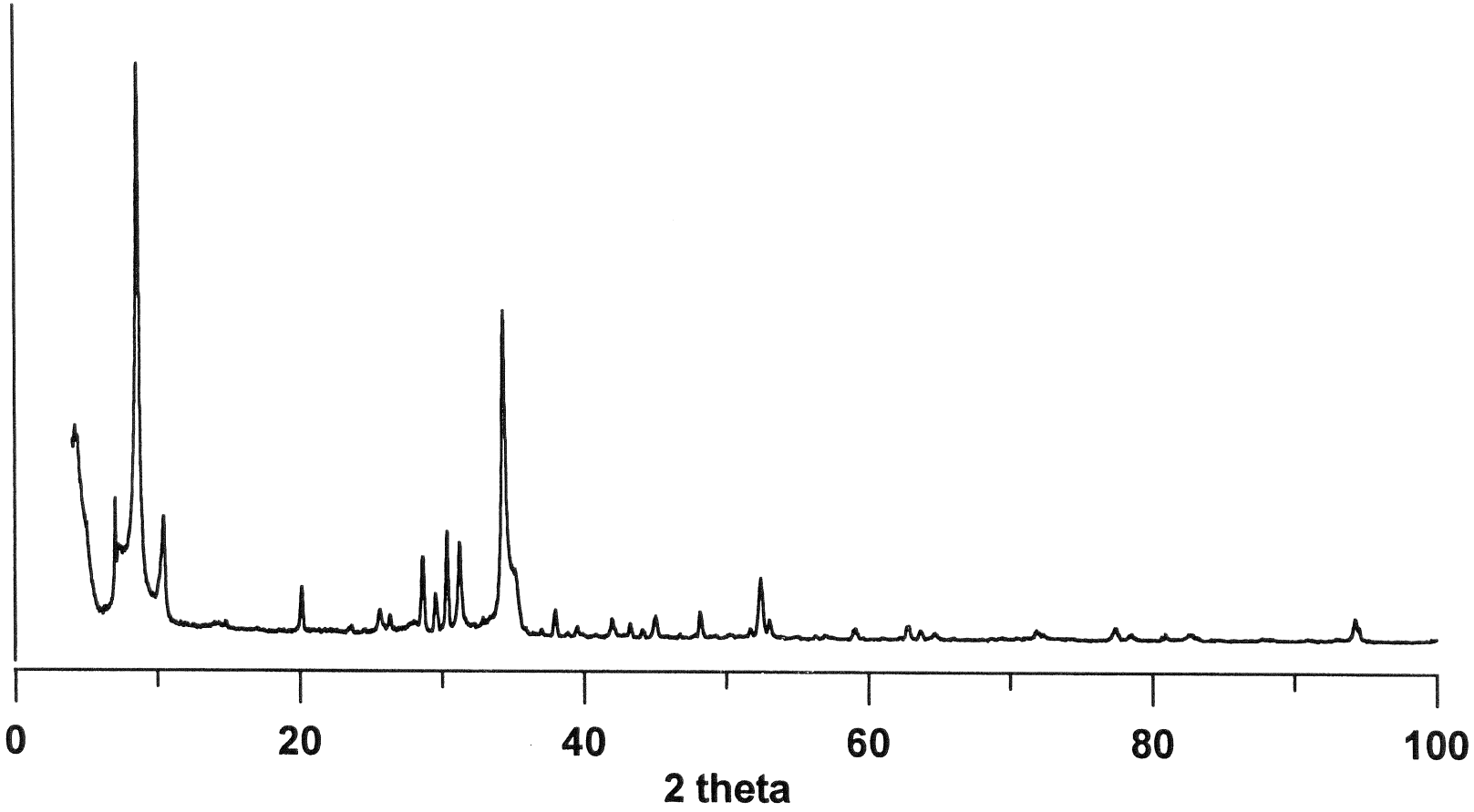


Figure 7-25.
XPD pattern of mineral from the biotite batch experiment at pH 9.43 (sample 6).

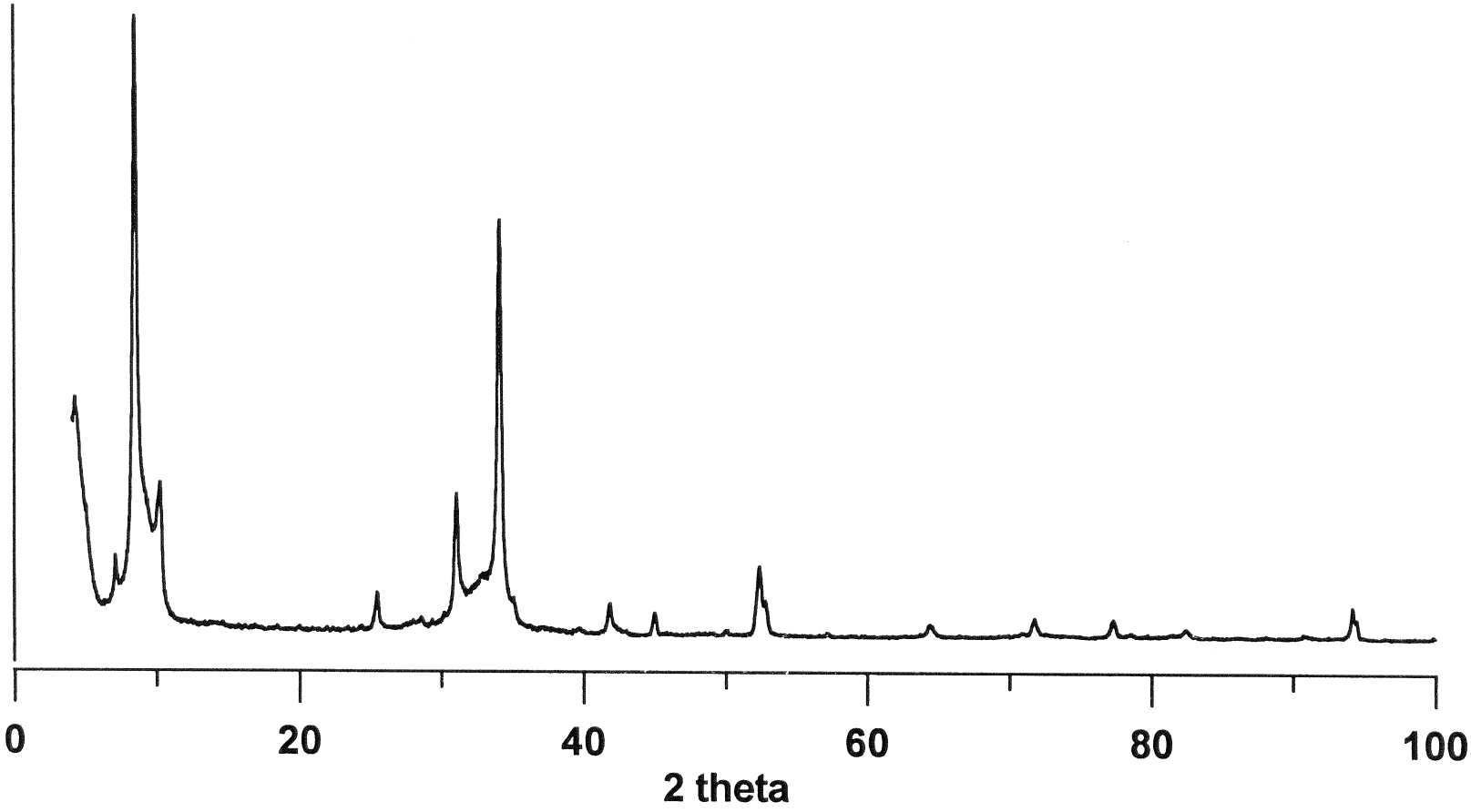


Figure 7-26.
XPD pattern of mineral from the biotite batch experiment at pH 10.67 (sample 12).

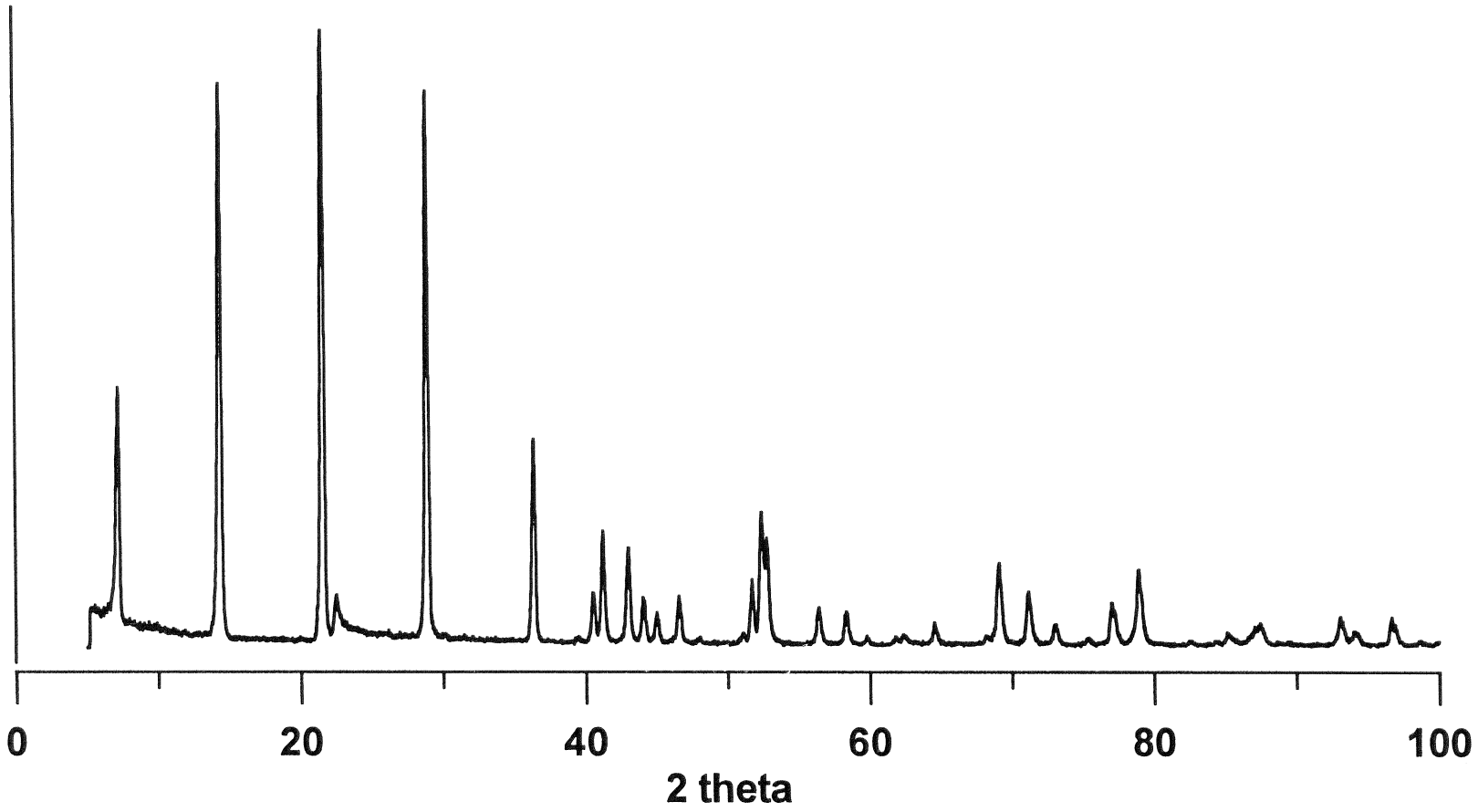


Figure 7-27.
XPD pattern of mineral from the kinetic experiment of chlorite dissolution at pH 8.18 and 1% CO2 (Ka).

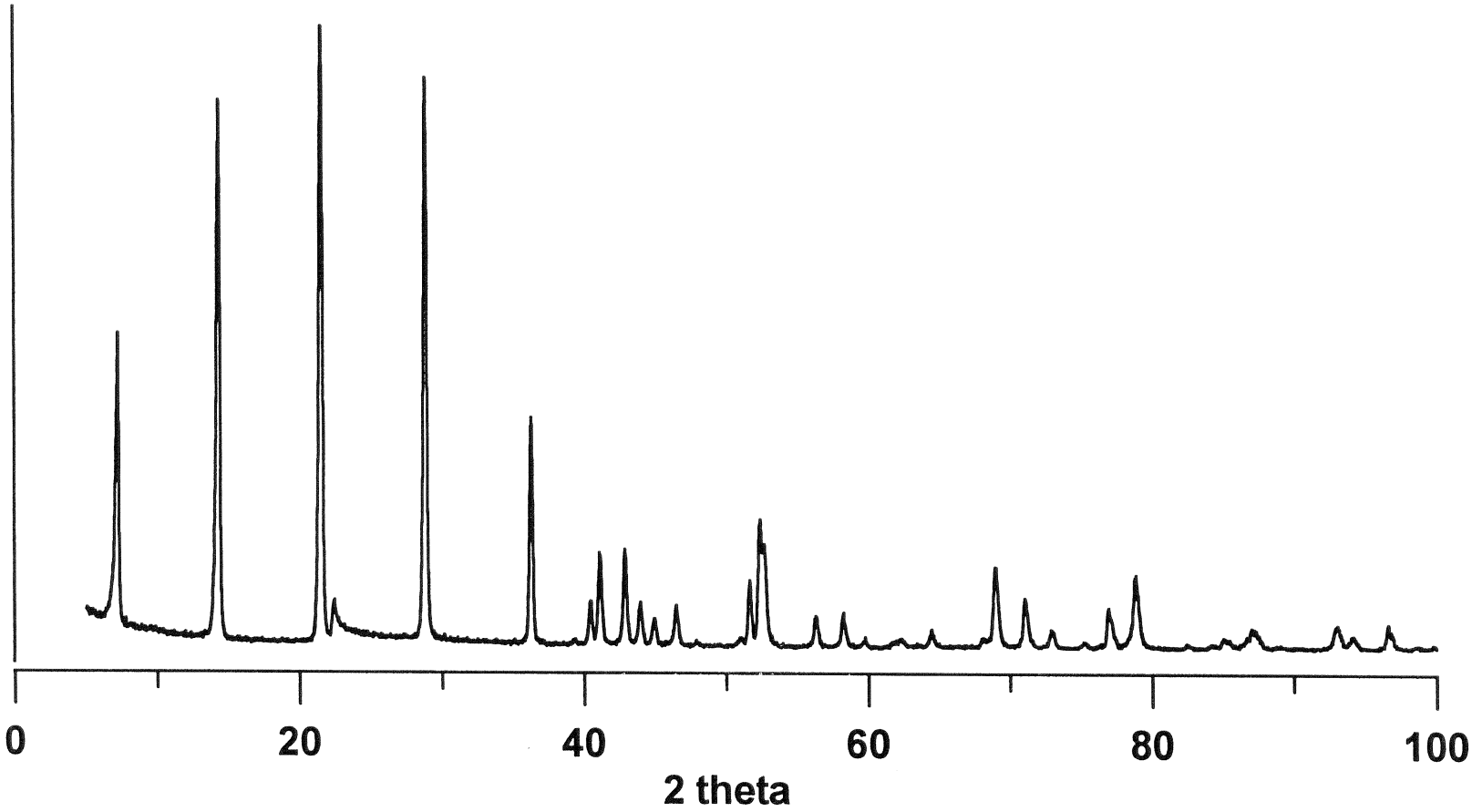


Figure 7-28.
XPD pattern of mineral from the kinetic experiment of chlorite dissolution at pH 2.60 (Kb).

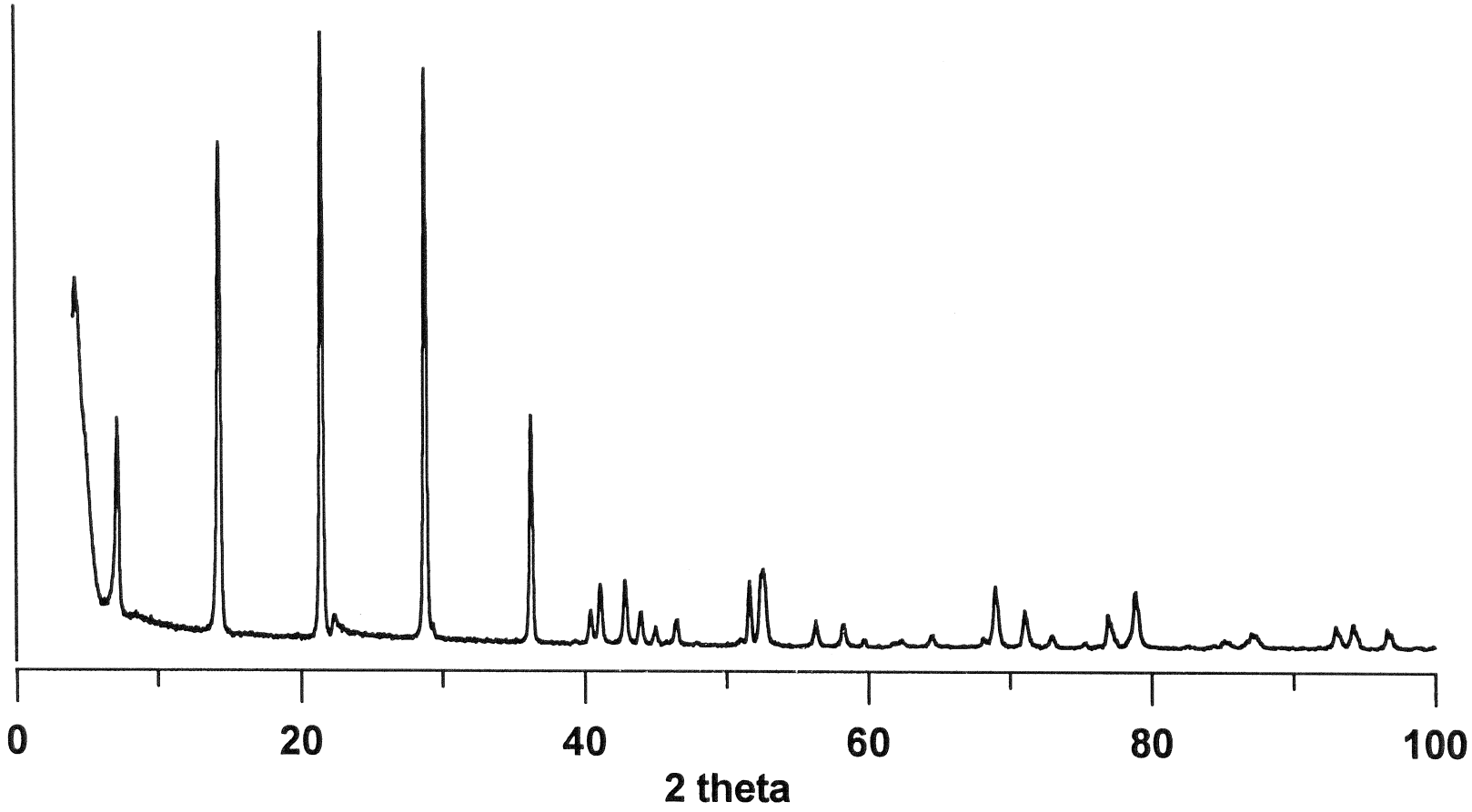


Figure 7-29.
XPD pattern of mineral from the kinetic experiment of chlorite dissolution at pH 3.8 (Kc).

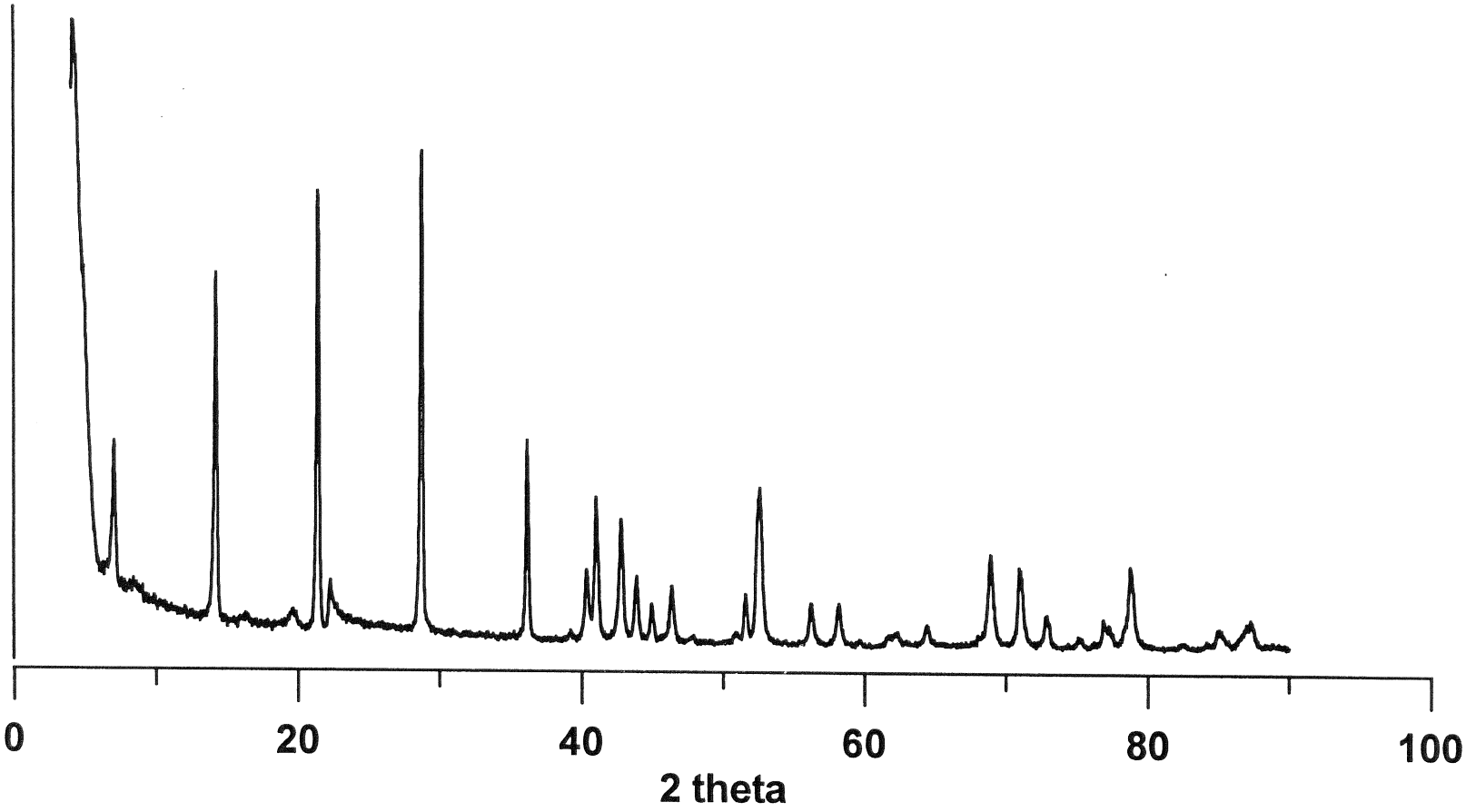


Figure 7-30.
XPD pattern of mineral from the kinetic experiment of chlorite dissolution at pH 7.12 and 100% CO2 (Kd).

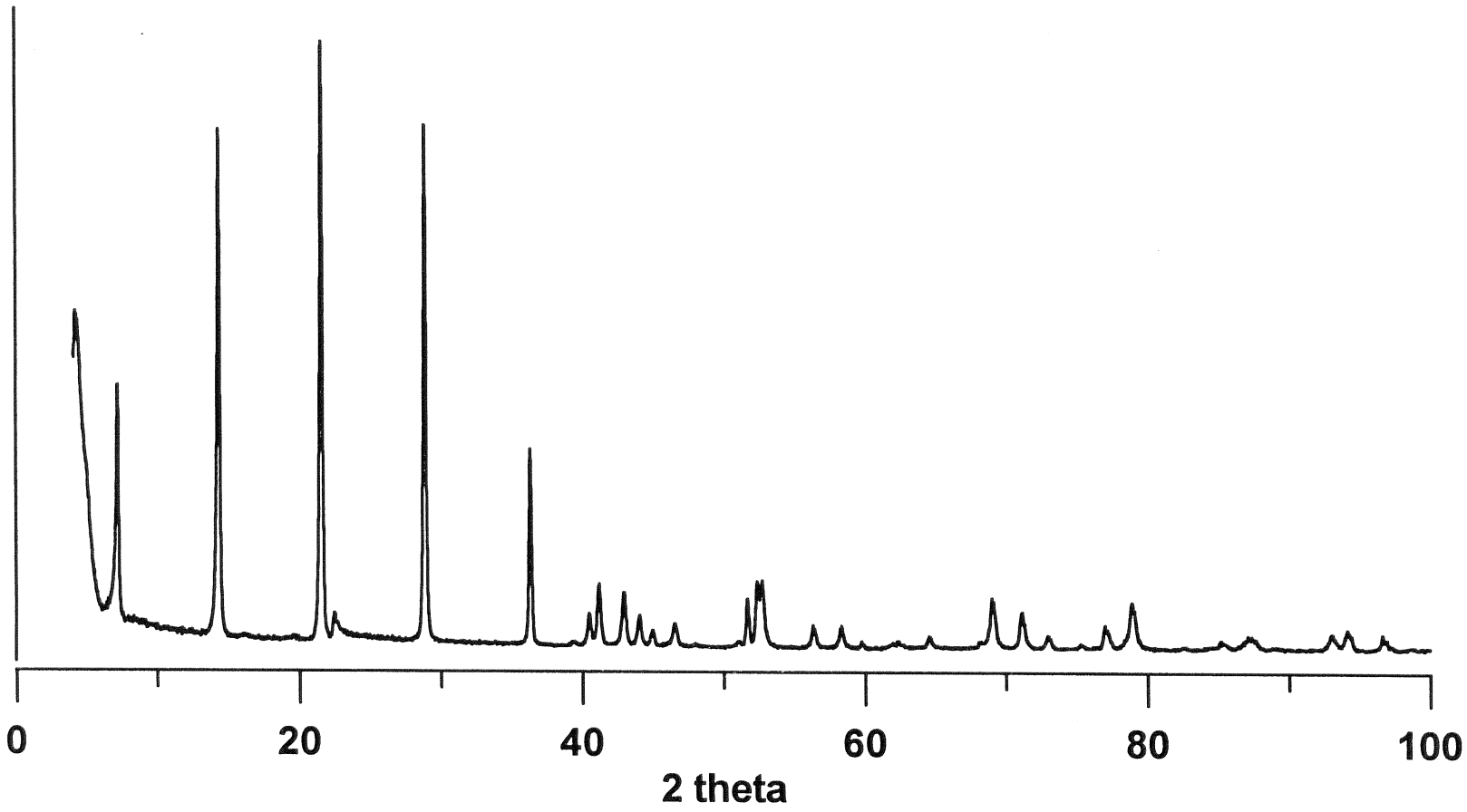


Figure 7-31.
XPD pattern of mineral from the kinetic experiment of chlorite dissolution at pH 8.92 and 100% CO2 (Ke).

# *List of SKB reports*

## Annual Reports

*1977-78*
TR 121
**KBS Technical Reports 1 – 120**
Summaries
Stockholm, May 1979

*1979*
TR 79-28
**The KBS Annual Report 1979**
KBS Technical Reports 79-01 – 79-27
Summaries
Stockholm, March 1980

*1980*
TR 80-26
**The KBS Annual Report 1980**
KBS Technical Reports 80-01 – 80-25
Summaries
Stockholm, March 1981

*1981*
TR 81-17
**The KBS Annual Report 1981**
KBS Technical Reports 81-01 – 81-16
Summaries
Stockholm, April 1982

*1982*
TR 82-28
**The KBS Annual Report 1982**
KBS Technical Reports 82-01 – 82-27
Summaries
Stockholm, July 1983

*1983*
TR 83-77
**The KBS Annual Report 1983**
KBS Technical Reports 83-01 – 83-76
Summaries
Stockholm, June 1984

*1984*
TR 85-01
**Annual Research and Development Report 1984**
Including Summaries of Technical Reports Issued during 1984. (Technical Reports 84-01 – 84-19)
Stockholm, June 1985

*1985*
TR 85-20
**Annual Research and Development Report 1985**
Including Summaries of Technical Reports Issued during 1985. (Technical Reports 85-01 – 85-19)
Stockholm, May 1986

*1986*
TR 86-31
**SKB Annual Report 1986**
Including Summaries of Technical Reports Issued during 1986
Stockholm, May 1987

*1987*
TR 87-33
**SKB Annual Report 1987**
Including Summaries of Technical Reports Issued during 1987
Stockholm, May 1988

*1988*
TR 88-32
**SKB Annual Report 1988**
Including Summaries of Technical Reports Issued during 1988
Stockholm, May 1989

*1989*
TR 89-40
**SKB Annual Report 1989**
Including Summaries of Technical Reports Issued during 1989
Stockholm, May 1990

*1990*
TR 90-46
**SKB Annual Report 1990**
Including Summaries of Technical Reports Issued during 1990
Stockholm, May 1991

*1991*
TR 91-64
**SKB Annual Report 1991**
Including Summaries of Technical Reports Issued during 1991
Stockholm, April 1992

*1992*
TR 92-46
**SKB Annual Report 1992**
Including Summaries of Technical Reports Issued during 1992
Stockholm, May 1993

*1993*
TR 93-34
**SKB Annual Report 1993**
Including Summaries of Technical Reports Issued during 1993
Stockholm, May 1994

*ISSN 0284-3757*

CM Gruppen AB, Bromma 1994